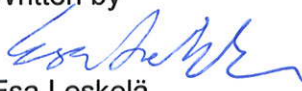
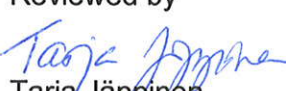





# Ultrasonic tests to compare mechanical and thermal fatigue cracks in 316L plates

Authors: Esa Leskelä, Ari Koskinen

Confidentiality: Public

Report's title Ultrasonic tests to compare mechanical and thermal fatigue cracks in 316L plates	
Customer, contact person, address SAFIR2014, The Finnish Research Programme on Nuclear Power Plant Safety 2011–2014	Order reference
Project name Monitoring of the structural integrity of materials and components in reactor circuit	Project number/Short name 77475/MAKOMON 2012
Author(s) Esa Leskelä, Ari Koskinen	Pages 70
Keywords Ultrasound, ultrasonic testing (UT), phased array testing (PA), mechanical fatigue crack, thermal fatigue crack, indication, defect	Report identification code VTT-R-00932-13
<p>Summary</p> <p>Ultrasonic indications are highly dependent on defect characteristics like roughness, crack opening, tilt and branching. In this study, thermal fatigue and mechanical fatigue defects were produced in two test specimens. These artificial defects were inspected first with conventional ultrasonic transducers with mechanised scanner and then with phased array ultrasonic techniques.</p> <p>This study was done to compare two different types of artificial defects and to test and study the influence of different reflector properties on indications. The aim was to produce new data on artificial reflectors for the needs of qualification as well as inspection.</p> <p>This work report presents the initial results of ultrasonic inspections with conventional techniques and phased array techniques. In data analysis, the signal-to-noise ratio of all defect indications has been defined. Also the length sizing of the defects has been performed. Results are presented as graphs and screen captures from the ultrasonic data.</p>	
Confidentiality	Public
Espoo 14.2.2013 Written by  Esa Leskelä Senior Scientist	
Reviewed by  Tarja Jäppinen Research Scientist	
Accepted by  Pentti Kauppinen Technology Manager	
VTT's contact address VTT Technical Research Centre of Finland, PL 1000, 02044 VTT	
Distribution (customer and VTT)	
<i>The use of the name of the VTT Technical Research Centre of Finland (VTT) in advertising or publication in part of this report is only permissible with written authorisation from the VTT Technical Research Centre of Finland.</i>	

## Preface

---

This report has been prepared in the research project Monitoring of the structural integrity of materials and components in reactor circuit. This project is a part of the SAFIR2014, the Finnish Research Program on Nuclear Power Plant Safety for years 2011 – 2014. The work was carried out at VTT Technical Research Centre of Finland. The work has been funded by the State Nuclear Waste Management Fund (VYR) and VTT.

Espoo 14.2.2013

Authors

## Contents

---

Preface.....	2
Contents.....	3
List of acronyms .....	5
1. Introduction.....	6
2. Goal.....	6
3. Test specimens.....	6
4. Limitations.....	7
5. Methods.....	7
5.1 Conventional ultrasonic testing .....	7
5.1.1 Description.....	7
5.1.2 Reference system.....	7
5.1.3 Probes .....	8
5.1.4 Coupling .....	9
5.1.5 Calibration.....	9
5.1.6 Equipment.....	9
5.1.7 Software .....	9
5.2 Phased array ultrasonic testing.....	10
5.2.1 Description.....	10
5.2.2 Reference system.....	10
5.2.3 Probes and wedges .....	11
5.2.4 Focal laws.....	12
5.2.5 Coupling .....	14
5.2.6 Calibration.....	15
5.2.7 Equipment.....	15
5.2.8 Software .....	15
5.2.9 Scan plan.....	15
5.3 Data analysis .....	15
6. Results.....	16
6.1 Conventional ultrasonic testing .....	16
6.1.1 Signal to noise ratio by technique .....	16
6.1.2 Signal-to-noise ratio by scanning direction.....	17
6.1.3 Length sizing results by technique .....	20
6.1.4 Length sizing results by scanning direction .....	22
6.2 Phased array testing.....	25
6.2.1 Signal to noise ratio by technique .....	25
6.2.2 Signal-to-noise ratio by scanning direction.....	27
6.2.3 Length sizing results by technique .....	30
6.2.4 Length sizing results by scanning direction .....	32
7. Validation of results.....	35
8. Conclusion.....	35

9. Summary .....	36
References.....	36
Appendixes .....	37
APPENDIX 1. CONVENTIONAL ULTRASONIC TESTING SCREEN CAPTURES .....	38
APPENDIX 2. PHASED ARRAY TESTING SCREEN CAPTURES .....	51

## List of acronyms

---

CIRCD	circumferential downstream
CIRCU	circumferential upstream
FSH	full screen height
ISI	in service inspection
LW	longitudinal wave
MF	mechanical fatigue
NDE	non-destructive evaluation
PA	phased array
SNR	signal-to-noise ratio
SW	shear wave
TF	thermal fatigue
TRL	transmit/receive longitudinal
TRS	transmit/receive shear
UT	ultrasonic testing
WCL	weld centre line

## 1. Introduction

Different types of artificial defects are used for qualification of inspection procedures for in-service inspections of nuclear components. To reliably evaluate the performance of a procedure, these defects have to be representative enough compared to the real service induced defects.

There are many ways to produce artificial defects in steel. Different flaws have different responses when they are inspected and it is crucial for the reliability to know how well artificial defects corresponds to the ISI defects. Fatigue defects can nowadays be produced using thermal fatigue or mechanical fatigue.

Thermal fatigue crack production is very well controlled in matter of size and opening and those cracks are very realistic option compared to the real service induced defects. Mechanical fatigue crack production is well known and widely used method and can be used to produce very realistic cracks as well.

Ultrasonic indications are highly dependent on defect characteristics like roughness, crack opening, tilt and branching. The use of different types of probes and techniques enables studying their influence in inspection performance. By investigating the specimens with destructive methods after NDE, their real size and characteristics information is reached.

## 2. Goal

This study was done to compare two different types of artificial defects and to test and study the influence of different reflector properties on indications. The aim was to produce new data on artificial reflectors for the needs of qualification as well as inspection.

## 3. Test specimens

Two different fatigue specimens were studied. Both specimens were made of austenitic stainless steel 316L (ASTM) plate with thickness of 25 mm. Specimens were butt welded from two pieces and the defects were produced on the root side along the solidification line (Figure 1). The dimensions of the defects in both specimens were targeted to be 15 mm in length and 5 mm in depth. These dimensions will be confirmed after the final destructive investigation in 2013. The crack made in the other specimen is thermal fatigue (TF) and in the other specimen there are two mechanical fatigue cracks (MF A and MF B) on the opposite side of the weld of each other.

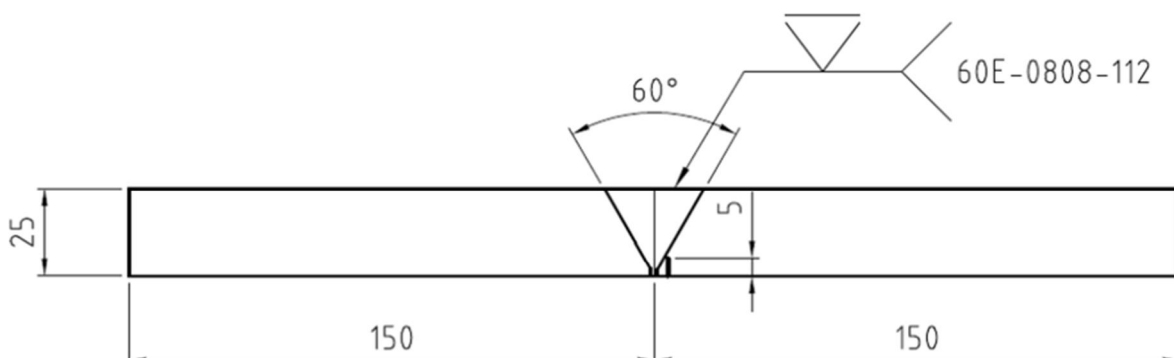


Figure 1. Schematic picture of specimen.

## 4. Limitations

---

The plate samples do not represent any specific shape of a real inspection object. The inspection of the plate samples has focused on the properties of defects of different manufacturers eliminating the effect of the shape of the inspection object.

Only one of the techniques used is based on qualified inspection procedure. This report presents only the initial results of the inspections performed for the samples. Final analysis of the UT results and comparison between two different artificial fatigue defects will be done after the destructive investigation is completed.

## 5. Methods

---

Test blocks were inspected with conventional ultrasonic and phased array techniques.

### 5.1 Conventional ultrasonic testing

#### 5.1.1 Description

In conventional ultrasonic testing, scanning was performed from weld face side using conventional transverse single transducer or longitudinal dual-element (transmit/receive) probes. Scanning was performed from both sides of the weld with motorized scanner as raster scan. Scanning step and index resolution were 1 mm. Only the defect and its surrounding areas were scanned.

#### 5.1.2 Reference system

The coordinate system used in conventional ultrasonic testing was the same as punched on the test blocks. The reference system is shown in Figure 2. Numbers 90 and 270 are the scanning directions in degrees when 0 corresponds the positive direction on x axis and 180 the negative direction on x axis.



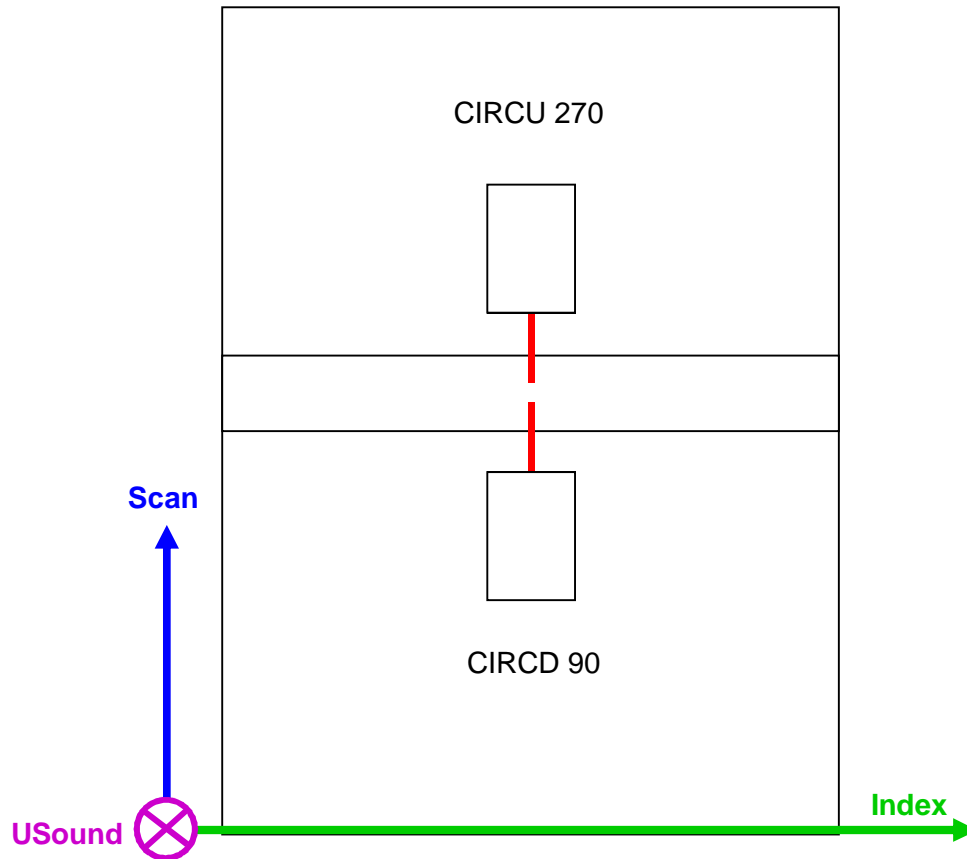


Figure 2. The reference system used in conventional ultrasonic testing.

### 5.1.3 Probes

Conventional ultrasonic testing was performed using piezoelectric probes presented in Table 1.

Table 1. Probes used in conventional ultrasonic testing.

Probe	Wavemode	Angle	Frequency (MHz)	Focus (mm)	Transducer size (mm)
MWB45-2	Transverse	45°	2	-	8x9
MWB55-2	Transverse	55°	2	-	8x9
MWB70-2	Transverse	70°	2	-	8x9
MWK45-2	Transverse	45°	2	-	8x9
MWK55-2	Transverse	55°	2	-	8x9
MWK70-2	Transverse	70°	2	-	8x9
MWK45-4	Transverse	45°	4	-	8x9
MWK55-4	Transverse	55°	4	-	8x9
MWK70-4	Transverse	70°	4	-	8x9
RTD TRL45-2	Longitudinal	45°	2	~30	2(8x14)
RTD TRL60-2	Longitudinal	60°	2	~25	2(8x14)
RTD TRL70-2	Longitudinal	70°	2	~25	2(8x14)

#### 5.1.4 Coupling

The acoustic coupling was generated by water.

#### 5.1.5 Calibration

V2 block made of austenitic stainless steel was used for time base calibration. The system sensitivity was set on a level where defect signals were not saturated to enable signal-to-noise measurement. The gain used varies between probes but scanning from both directions was carried out using the same gain.

#### 5.1.6 Equipment

Inspections using conventional ultrasonic technique were carried out using a combination of OmniScan ultrasonic device with SPIDER scanner (Figure 2) and MCDU-2 with software control by UltraVision, Figure 3.

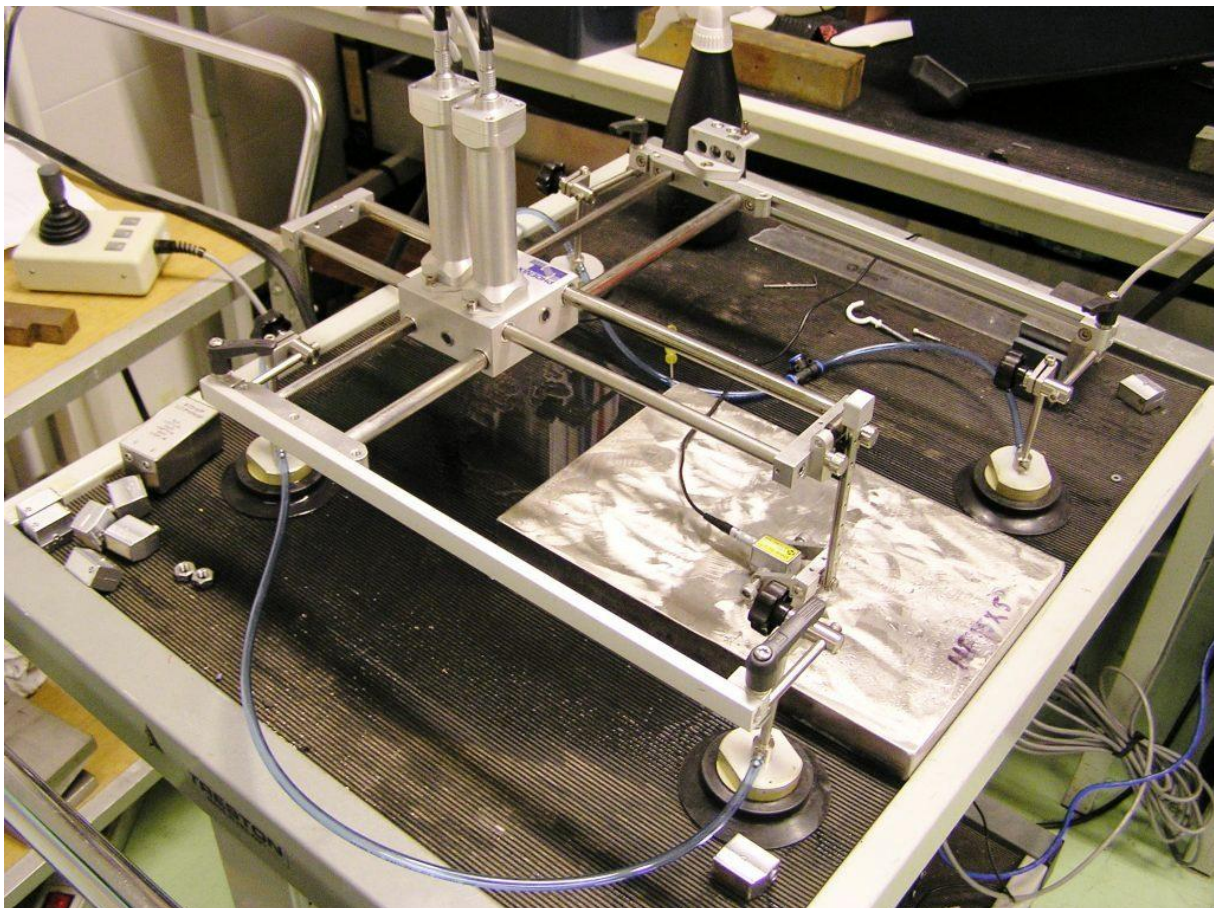


*Figure 3. Scanning of test specimen with SPIDER scanner.*

#### 5.1.7 Software

UltraVision 1.2R7 software was used for data acquisition and data analysis.

## 5.2 Phased array ultrasonic testing

### 5.2.1 Description

Phased array ultrasonic testing techniques are presented in Table 2.

*Table 2. Phased array ultrasonic techniques used in the inspection.*

Technique	Description
PA-1	Scanning from weld face side using dual matrix phased array probes with sectorial scan. Scanning was performed from both sides of the weld using manual encoded scanner with several scan lines along the weld. Technique is qualified to be used in in-service inspections of piping welds in nuclear power plants in the USA. Procedure: Zetec OmniScanPA01 rev. C.
PA-2	Scanning from weld face side using single linear phased array probes with sectorial scan. Scanning with resolution of 1 mm was performed from both sides of the weld using manual encoded scanner with several scan lines with index resolution of 5 mm.
PA-3	Scanning from weld face side using single linear phased array probe with linear electronic scan. Scanning with resolution of 1 mm was performed from both sides of the weld using manual encoded scanner with several scan lines with index resolution of 10 mm
PA-4	Scanning from weld face side using single linear phased array probe with sectorial scan. The aim was to generate inner surface creeping wave. Scanning was performed from both sides of the weld using automated scanner with several scan lines with index resolution of 5 mm. Three different wave types are generated [2]: <ul style="list-style-type: none"> <li>- <b>Direct sectorial scan longitudinal wave: 60° - 89°</b> refracted longitudinal wave.</li> <li>- <b>Shear wave (30-70-70):</b> Along with the 70° longitudinal wave, a 30° shear wave is generated. This wave shear hits the back surface of the test piece and some of the wave energy will be reflected as a 70° longitudinal signal. The "mode-converted" 70° wave will strike the reflector face and then propagate back to the transducer. This round trip signal is also known as a "30-70-70" signal to denote the angle of each portion of the triangular soundpath.</li> <li>- <b>ID Creeping Wave:</b> This wave mode is essentially a subsurface longitudinal wave which propagates along the inner surface of the test piece.</li> </ul>

### 5.2.2 Reference system

The y coordinate in the coordinate system used in phased array ultrasonic tests deviates from the one marked on the test blocks. The index zero location was set in the weld centre line (WCL). The reference system is presented in Figure 4.

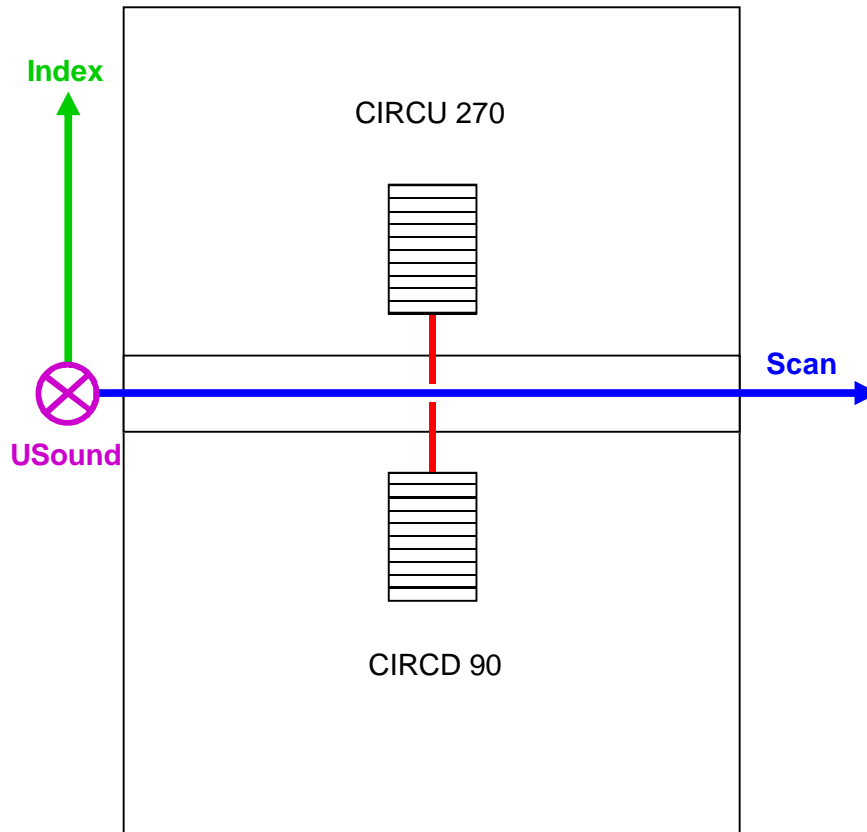


Figure 4. The reference system used in phased array ultrasonic testing.

### 5.2.3 Probes and wedges

Phased array ultrasonic testing was performed using probes and wedges presented in Table 3. Figure 5. shows an example of scanning with technique PA-4.

Table 3. Probes and wedges used in phased array testing.

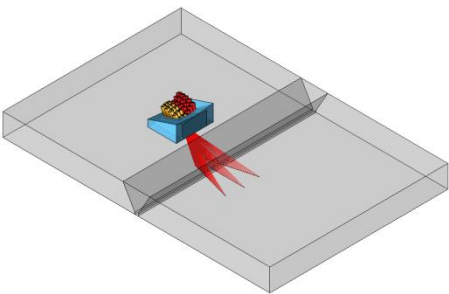
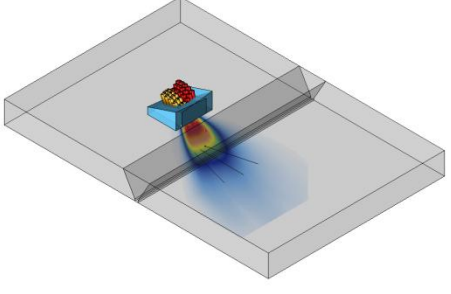
Technique	Probe	Wedge	Wavemode	Angles	Frequency (MHz)	Focus (mm)	Aperture (mm)
PA-1	1.5M5x3E17.5-9	ADUX576A	Transverse	40° - 70°	1.5	25 TD	2x(9x17.5)
	1.5M5x3E17.5-9	ADUX582A	Longitudinal	40° - 70°	1.5	25 TD	2x(9x17.5)
PA-2	2L16A10	SA10-N55S	Transverse	40° - 70°	2.25	25 TD	9.6x10
	5L32A11	SA11-N55S	Transverse	40° - 70°	5	25 TD	11.4x10
PA-3	5L32A11	SA11-N55S	Transverse	45°, 55°, 70°	5	25 TD	11.4x10
PA-4	5L16A10	SA10-N60L	Longitudinal	60° - 89°	5	50 HP	9.6x10



Figure 5. Scanning with technique PA-4.

#### 5.2.4 Focal laws

Focal laws were generated using Zetec's Advanced PA Calculator 1.2R7 and Zetec's UltraVision 3.3R4. Examples of sound beam simulations are presented in Figures 6–9.

	
<p>PA-1 technique: 3D ray tracing showing the skew angles <math>-15^\circ</math>, <math>0^\circ</math> and <math>+15^\circ</math> with LW.</p>	<p>PA-1 technique: 3D sound beam simulation showing the skew angles <math>-15^\circ</math>, <math>0^\circ</math> and <math>+15^\circ</math> LW.</p>

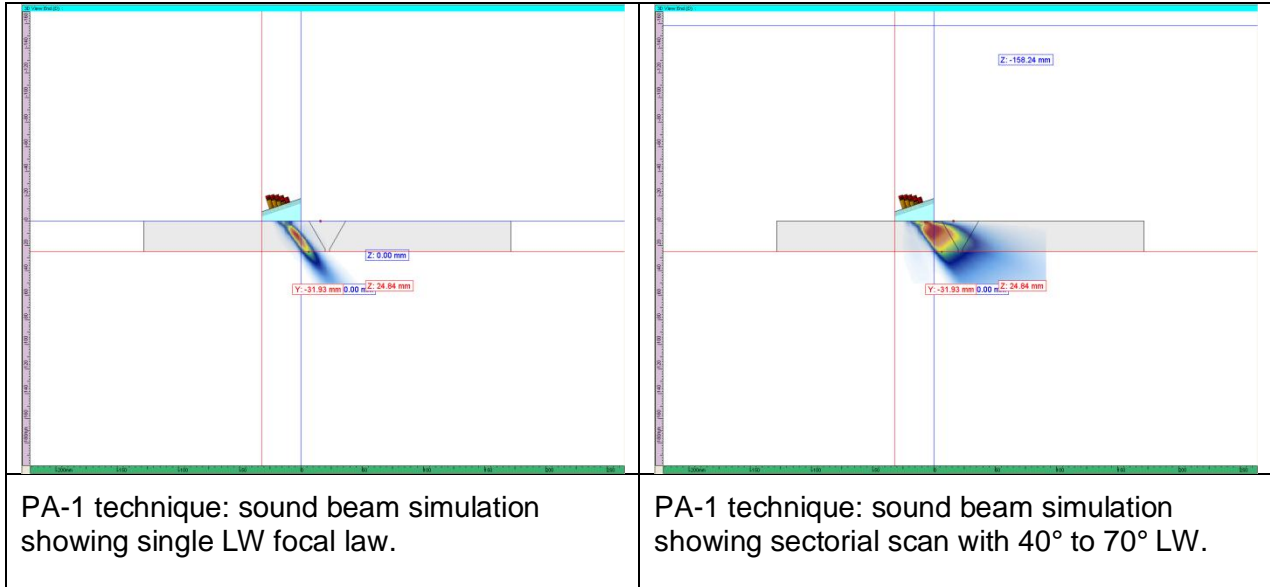


Figure 6. Examples of sound beam simulations for PA-1 technique.

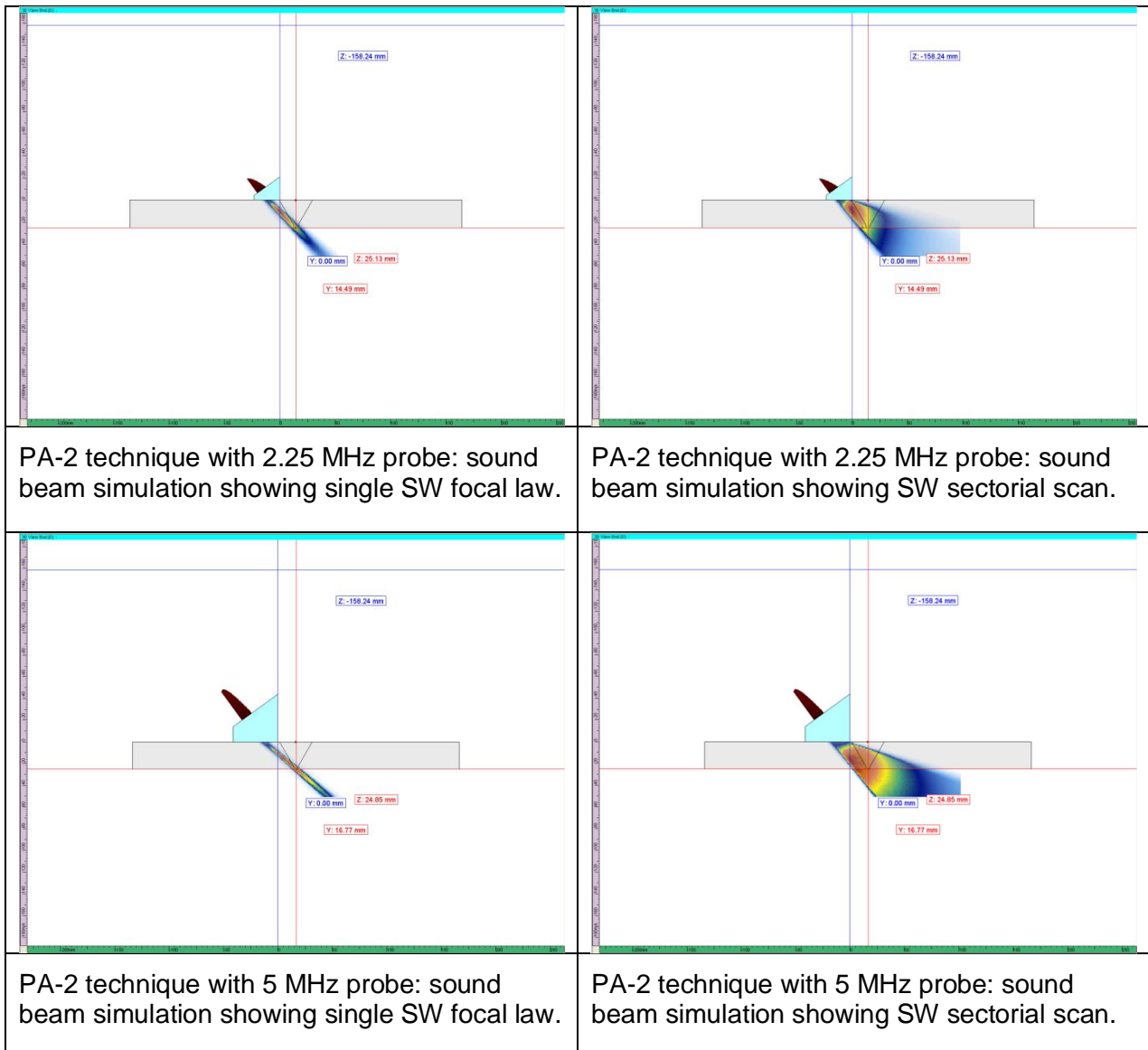


Figure 7. Examples of sound beam simulations for PA-2 technique.

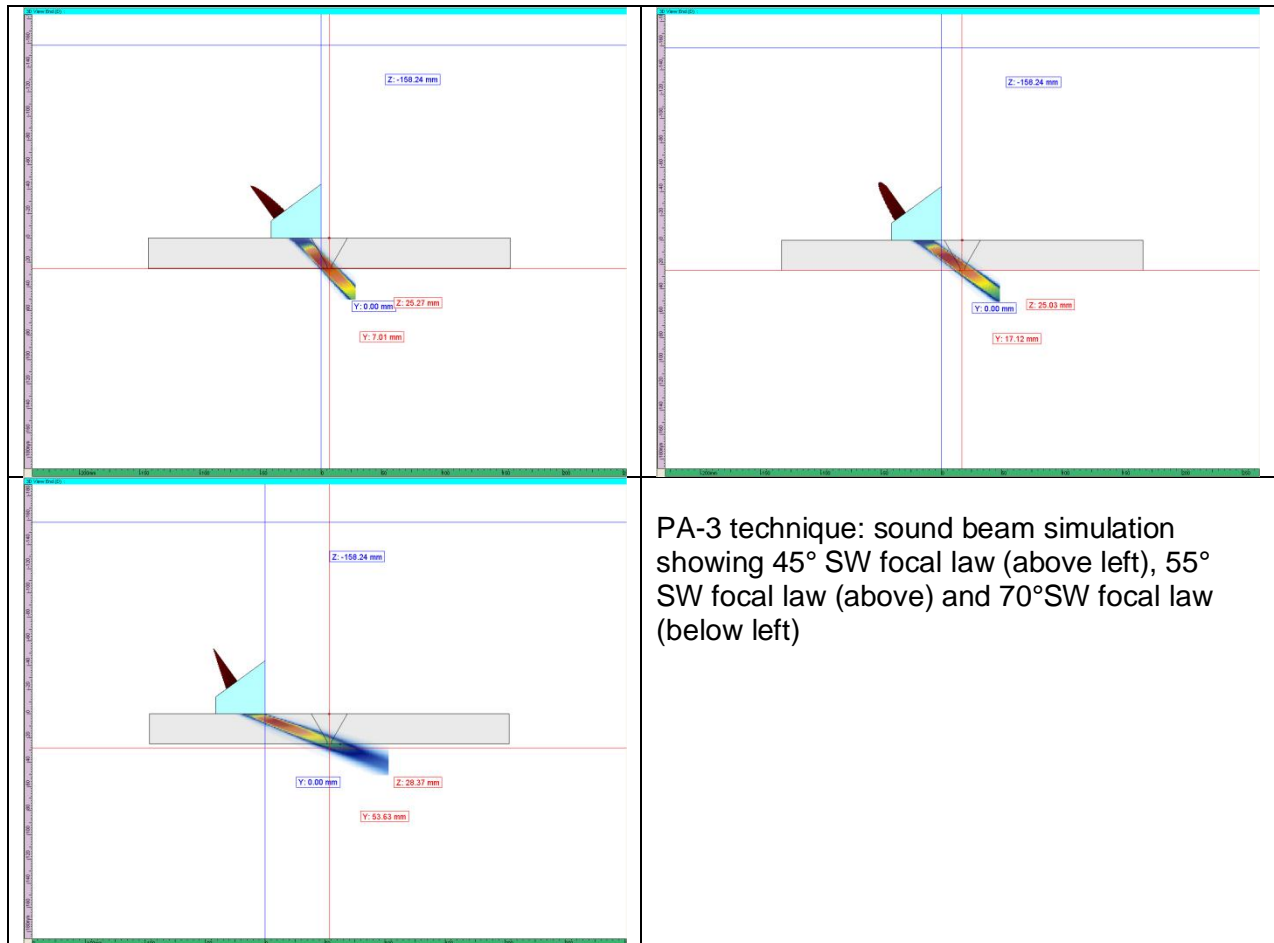


Figure 8. Examples of sound beam simulations for PA-3 technique.

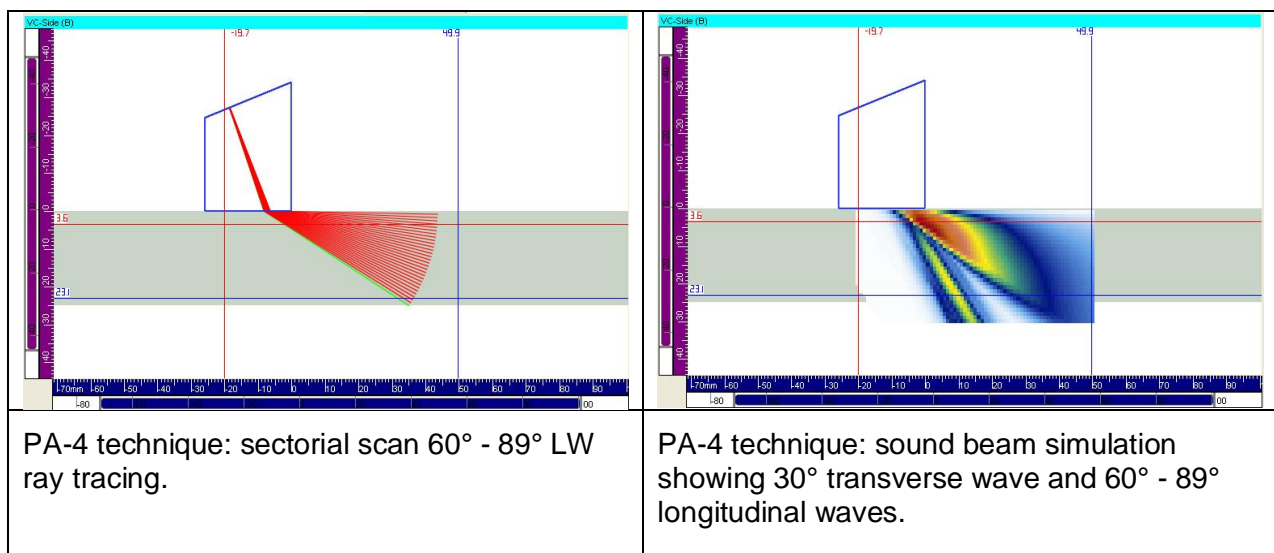


Figure 9. Examples of sound beam simulations for PA-4 technique.

### 5.2.5 Coupling

The acoustic coupling was generated by water and mixture of water and gel.

### 5.2.6 Calibration

V2 block made of austenitic stainless steel was used for time base calibration. The system sensitivity was set on a level where defect signals were not saturated. The gain for each technique was the same regardless of the scanning direction. In technique PA-1, the average noise level was set to 5–10 % of FSH as stated in the procedure [1].

### 5.2.7 Equipment

Phased array testing with techniques PA-1 and PA-4 was performed using OmniScan 16/128PR with software control by UltraVision. PA testing with techniques PA-2 and PA-3 was performed using Dynaray Lite 64/64PR. Scanning was performed by Zetec's Manual Pipe Scanner except in technique PA-4 where motorized scanner SPIDER was used.

### 5.2.8 Software

Both UltraVision 1.2R7 and UltraVision 3.3R4 were used for data acquisition and data analysis.

### 5.2.9 Scan plan

In technique PA-1 a specific scan plan according to procedure [1] was used, Table 4. In other techniques, scanning was performed so that ~50 % overlap between the electronic scan lines was achieved.

Table 4. Scanning sequences for phased array technique PA-1.

SCANNING SEQUENCES CIRCUMFERENTIAL FLAWS												
Focal law group	Beam Offset	MinTB	MaxTB	# Data Points	Scan			Index			# Lines	Done ? (OK / NA)
	A:55.0 Sk:000 (mm)				Start	End	Resol.	Start	End	Resol.		
CIRCD_TRS_90	-13,8	91,4	114,2	800	0,0	210,0	1,0	-33,7	-16,0	17,7	2	
CIRCU_TRS_270	-13,8	91,4	114,2	800	0,0	210,0	1,0	16,0	33,7	17,7	2	
CIRCD_TRL_90	-13,1	91,4	114,2	480	0,0	210,0	1,0	-34,4	10,6	15,0	4	
CIRCU_TRL_270	-13,1	91,4	114,2	480	0,0	210,0	1,0	-10,6	34,4	15,0	4	

## 5.3 Data analysis

First the data was processed with analysis program. A volumetric merge combining all data points from A-scans was generated. In PA-3 technique, data from different angles 45°, 55°, 70° was evaluated separately.

Hysteresis correction was performed for conventional ultrasonic data due to systematic ~2–3 mm difference between two adjacent scan lines in the index direction. The cause for difference was mechanical.

To define signal-to-noise ratio first the highest amplitude of defect indication was measured. After that the average noise level in the surrounding area of the defect was measured. Signal to-noise ratio was defined in percentages and in decibels. Values in this report are presented in percentages.

Also the length of defect indications was measured. The technique used was full amplitude drop according to procedure [1].

In the results, the defects are categorized by scanning direction. The categorizing of the defects by scanning direction is shown in Table 5. Near side corresponds to scanning from the defect side, far side corresponds to scanning through the weld.



Table 5. Defect categorizing by the scanning direction.

Defect	Scanning direction	
	CIRCD 90	CIRCU 270
MF 15X5 A	near side	far side
MF 15X5 B	far side	near side
TF 15X5	near side	far side

## 6. Results

The screenshots showing B-, C- and D-scans from conventional ultrasonic testing are presented in Appendix 1 and from phased array data in Appendix 2. In this report the screenshots are usually presented without additional gain.

### 6.1 Conventional ultrasonic testing

#### 6.1.1 Signal to noise ratio by technique

Signal-to-noise ratios of all three defects inspected by conventional transverse probes are presented in Figure 10 and by longitudinal TRL probes in Figure 11.

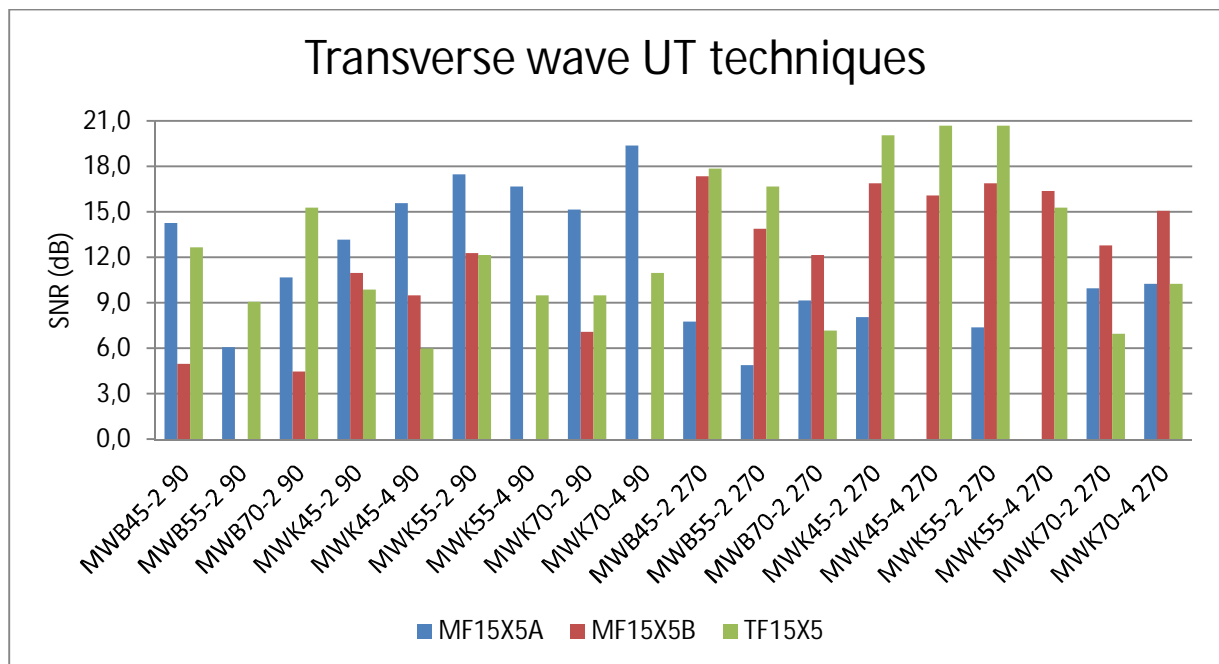


Figure 10. Signal-to-noise ratio of all defects with transverse wave UT techniques.

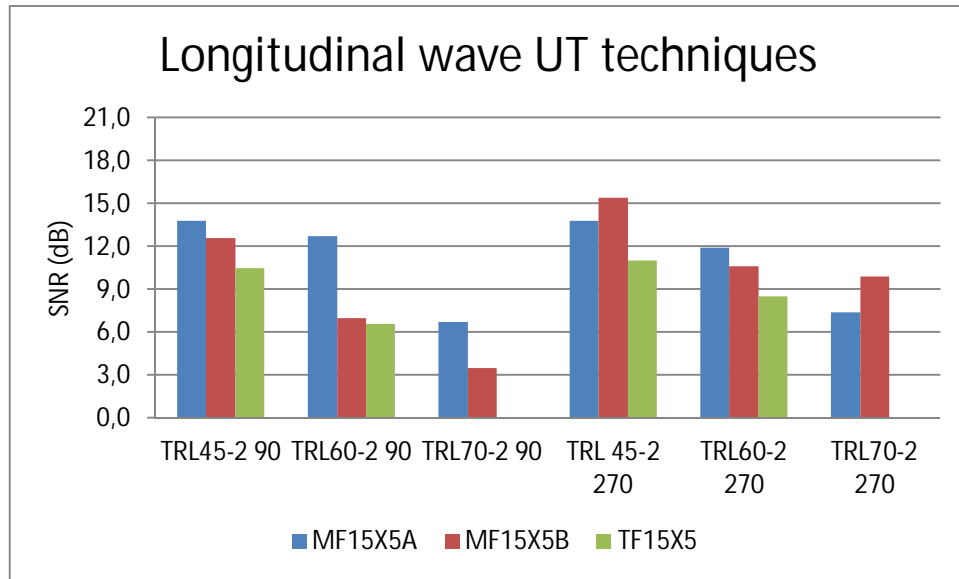


Figure 11. Signal-to-noise ratio of all defects with longitudinal wave UT techniques.

### 6.1.2 Signal-to-noise ratio by scanning direction

Signal-to-noise ratios of each defect scanned from two different directions are presented in Figures 12–17.

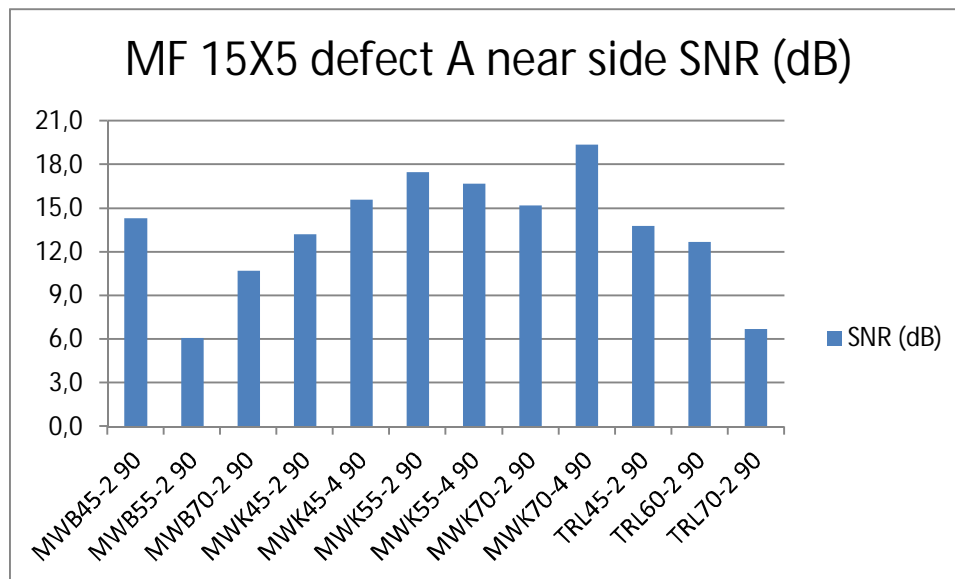


Figure 12. Signal-to-noise ratio of defect MF15X5 A scanned from near side of the defect.

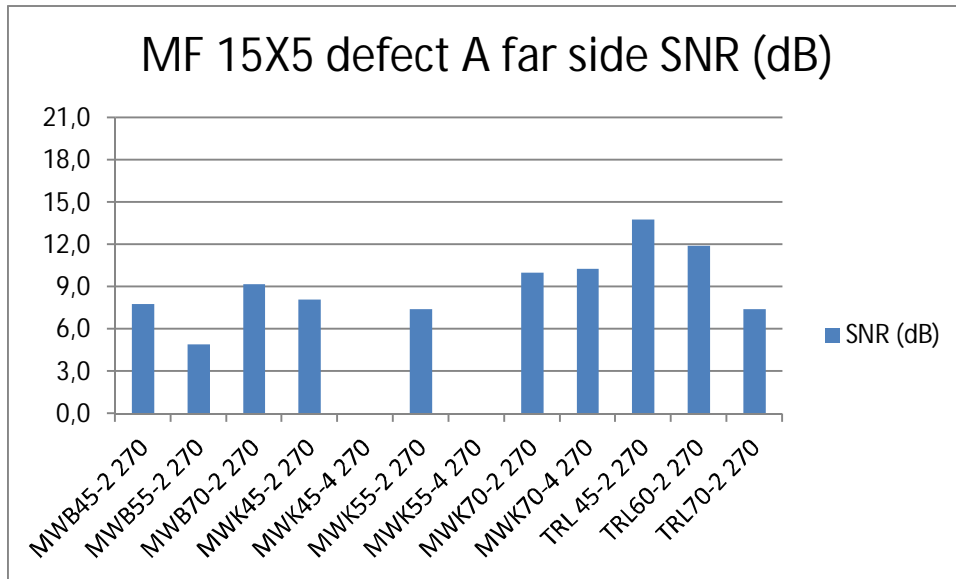


Figure 13. Signal-to-noise ratio of defect MF15X5 A scanned from far side of the defect.

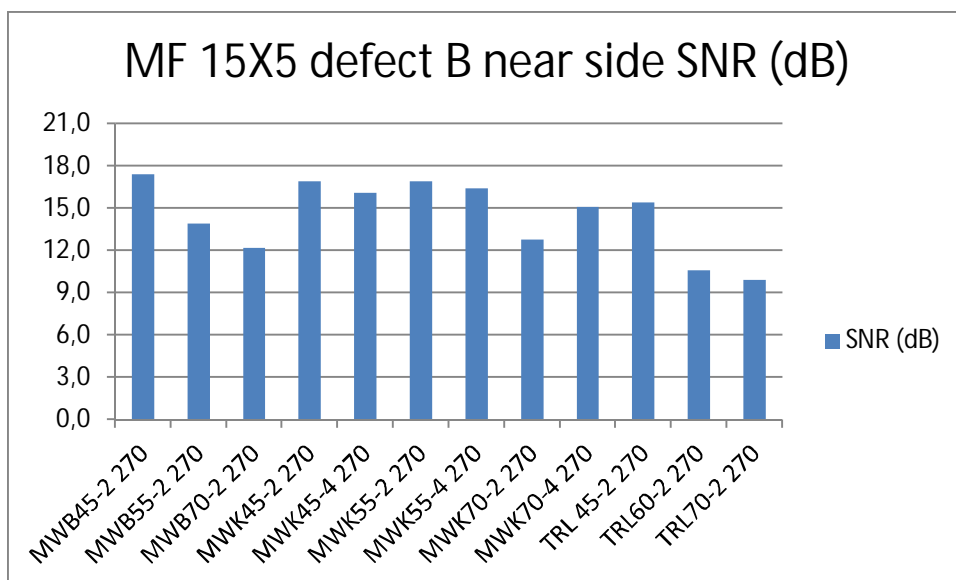


Figure 14. Signal-to-noise ratio of defect MF15X5 B scanned from near side of the defect.

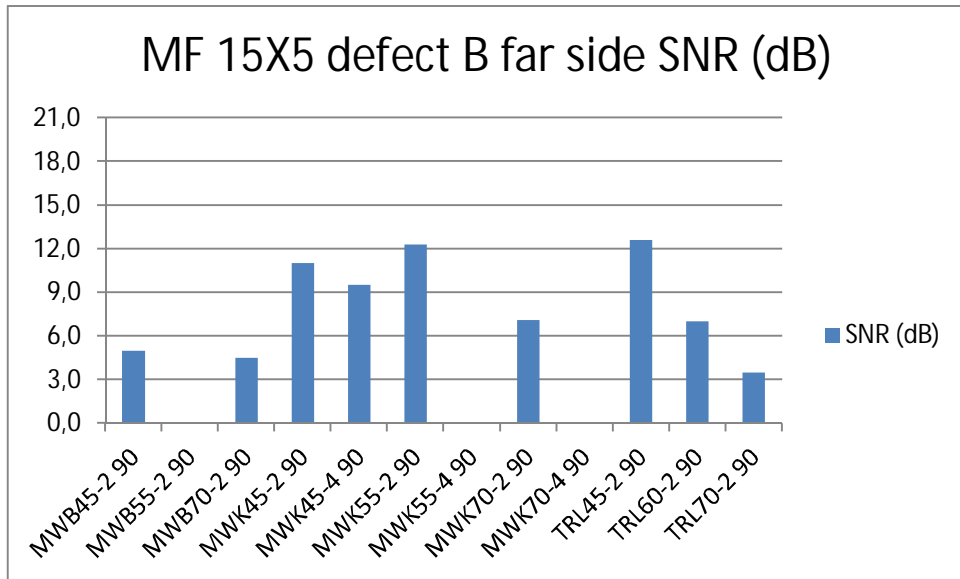


Figure 15. Signal-to-noise ratio of defect MF15X5 A scanned from far side of the defect.

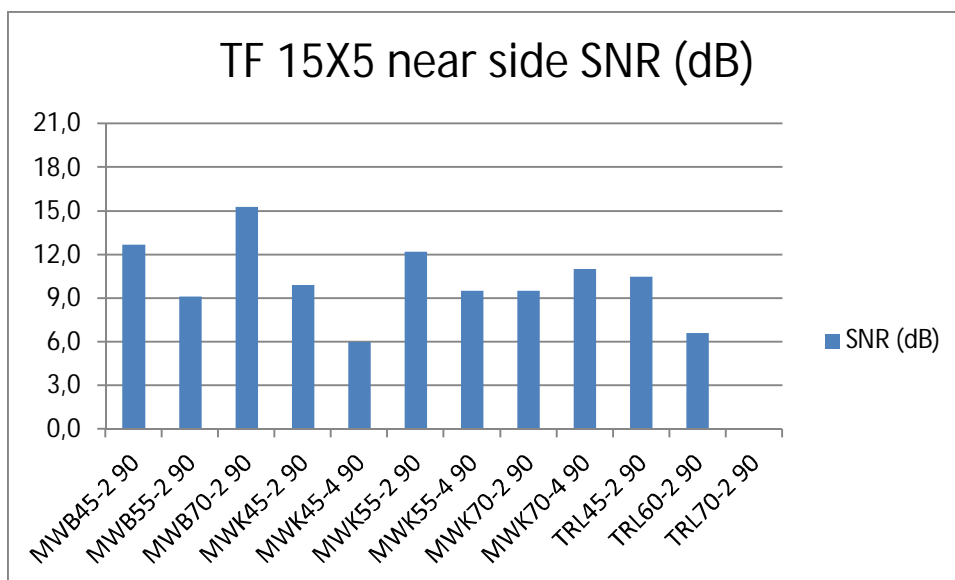


Figure 16. Signal-to-noise ratio of defect TF15X5 scanned from near side of the defect.

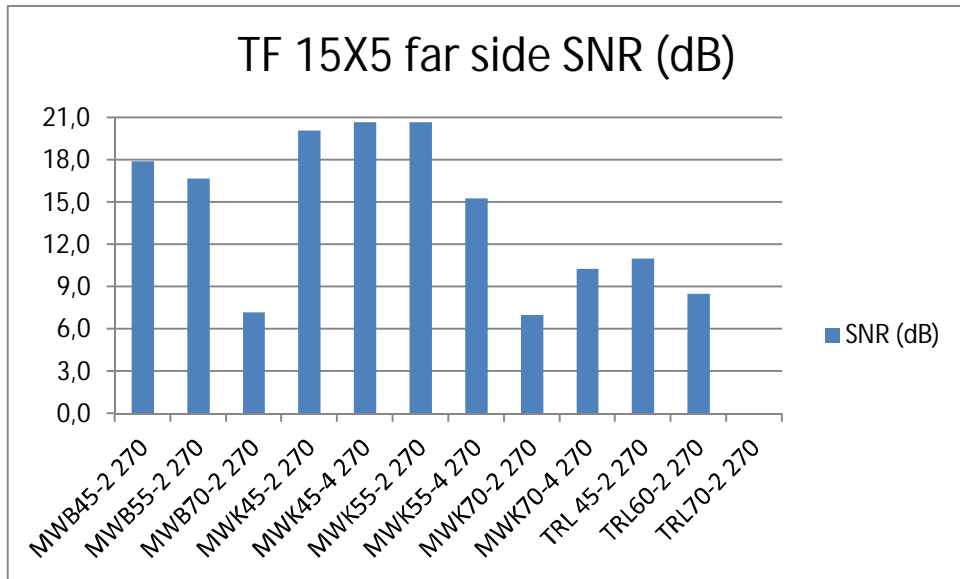


Figure 17. Signal-to-noise ratio of defect TF15X5 scanned from far side of the defect.

### 6.1.3 Length sizing results by technique

Defect length sizing results with transverse ultrasonic techniques are shown in Figure 18 and with longitudinal wave techniques in Figure 19.

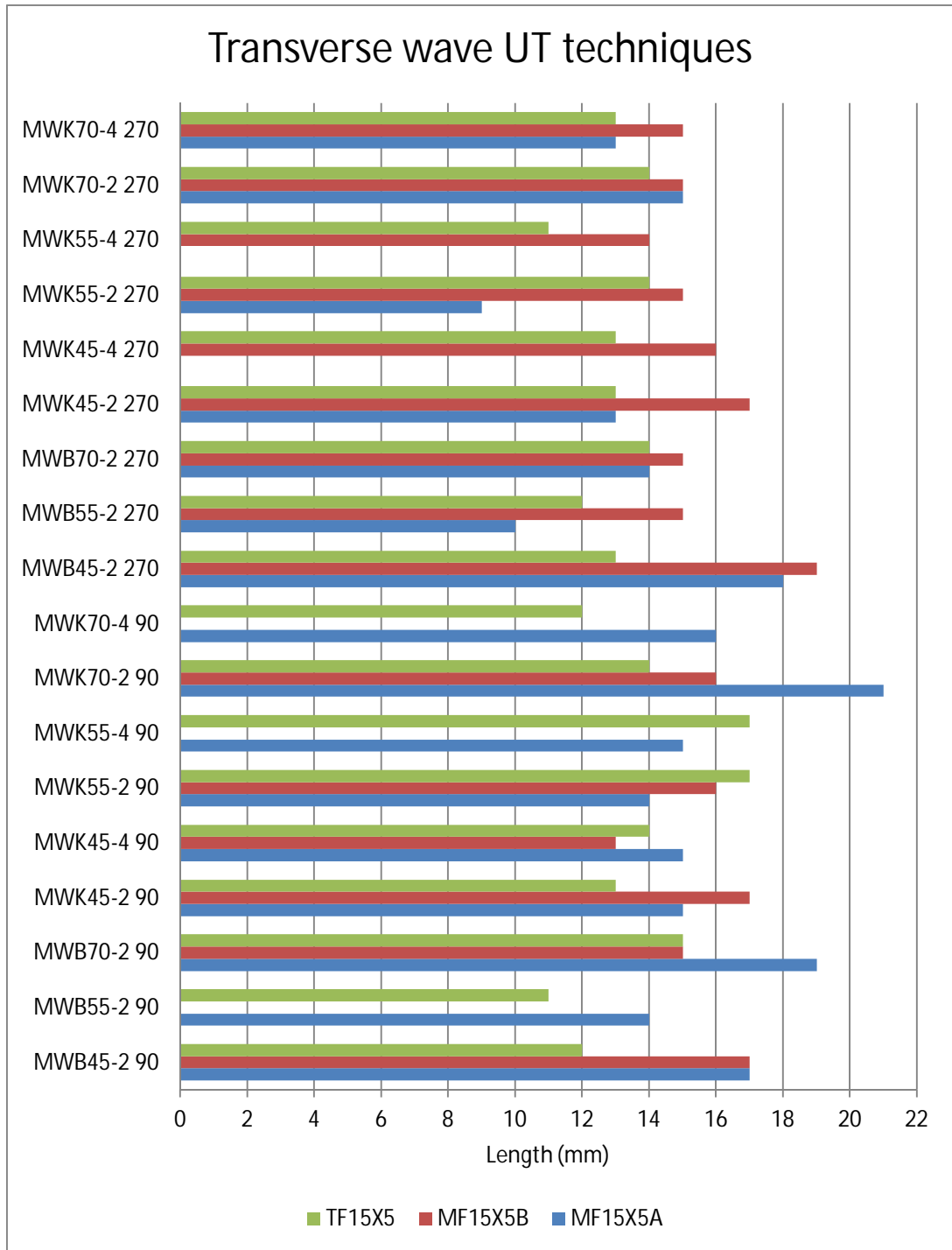


Figure 18. Length sizing results of all defects scanned with transverse wave ultrasonic techniques.

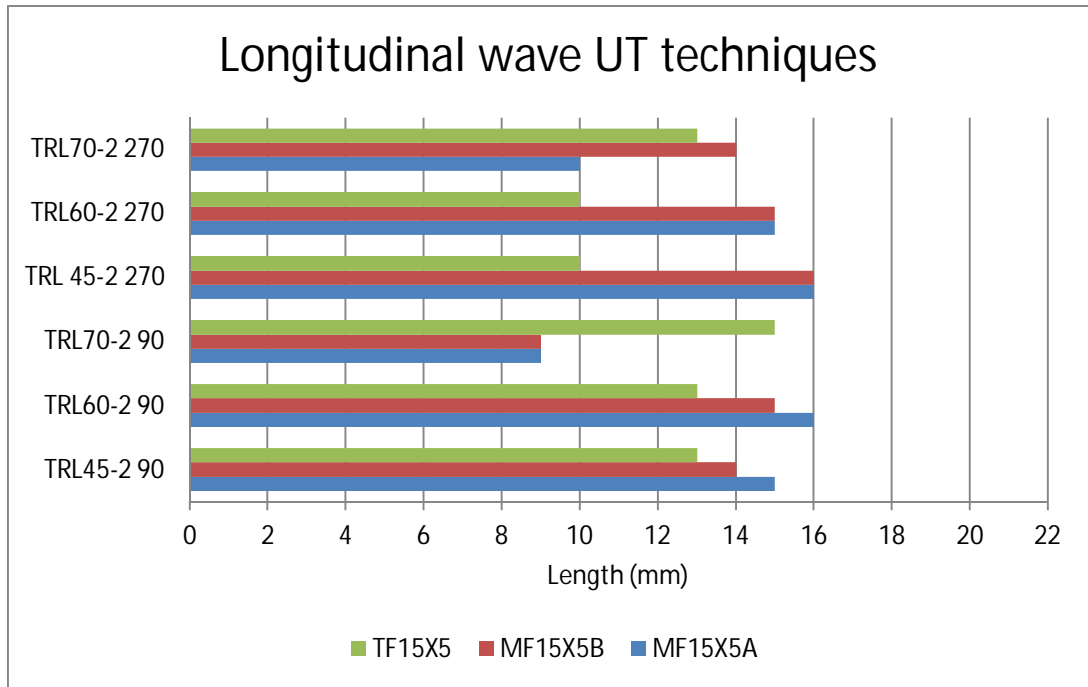


Figure 19. Length sizing results of all defects scanned with longitudinal wave ultrasonic techniques.

6.1.4 Length sizing results by scanning direction

Defect length sizing results for each defects from both scanning directions are shown in Figures 20–25.

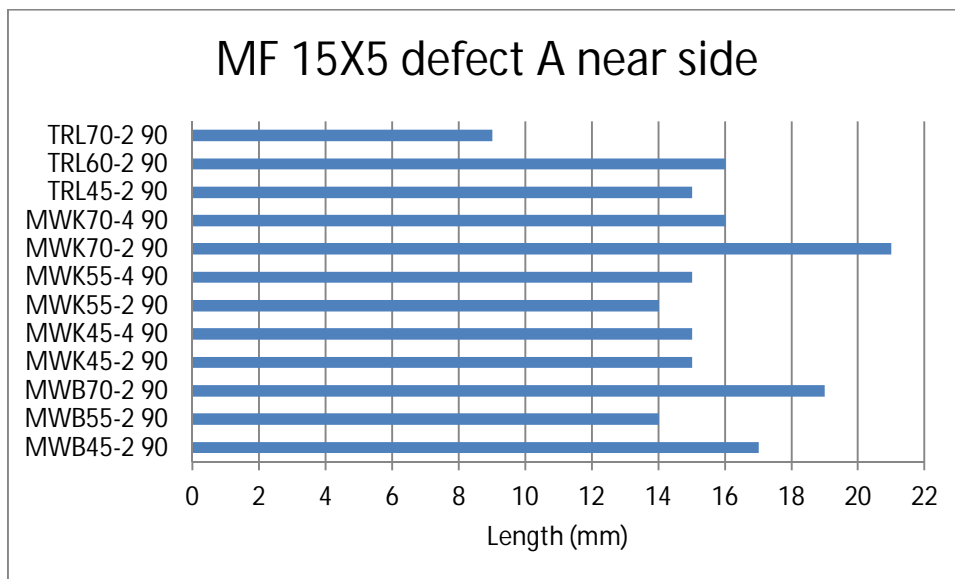


Figure 20. Length sizing results of defect MF15X5 A scanned from near side of the defect.

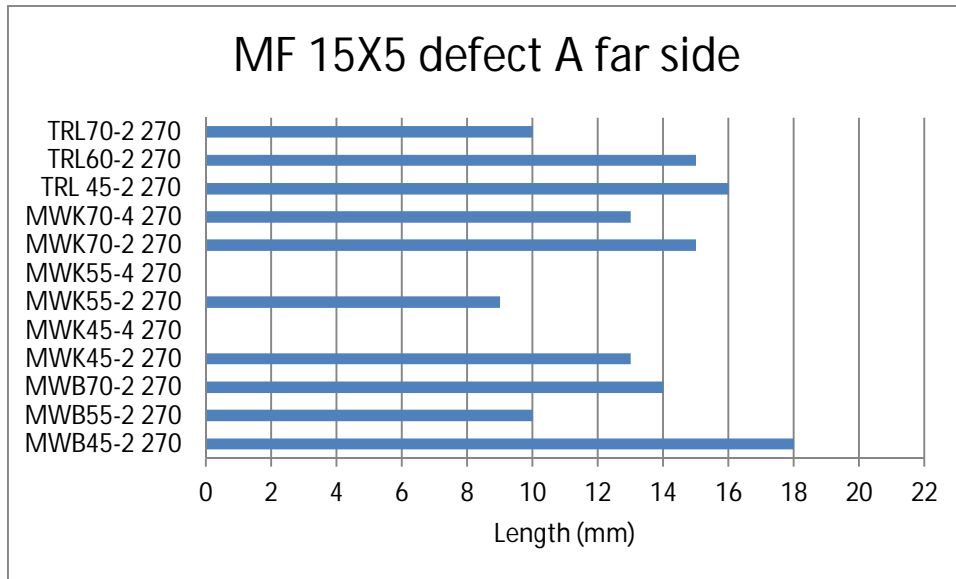


Figure 21. Length sizing results of defect MF15X5 A scanned from far side of the defect.

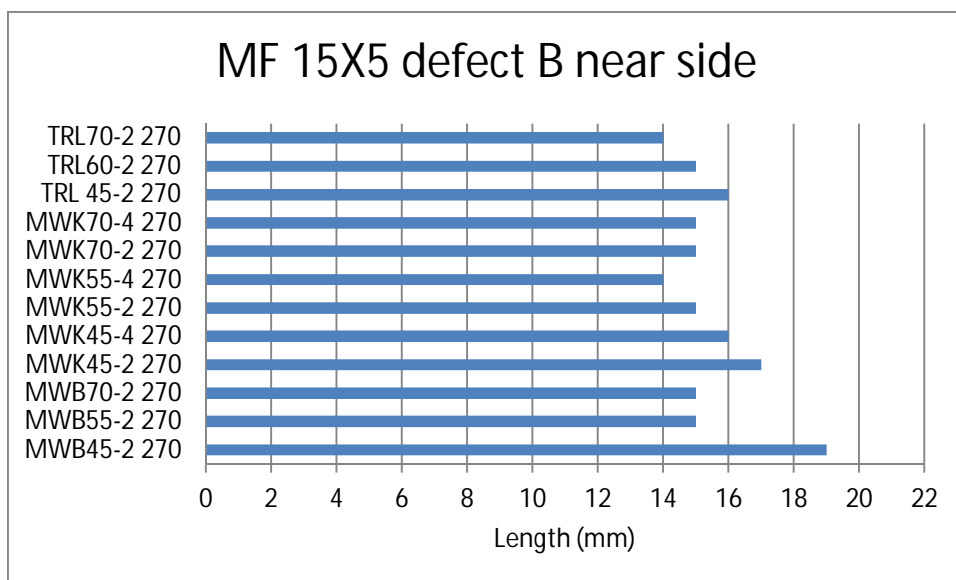


Figure 22. Length sizing results of defect MF15X5 B scanned from near side of the defect.



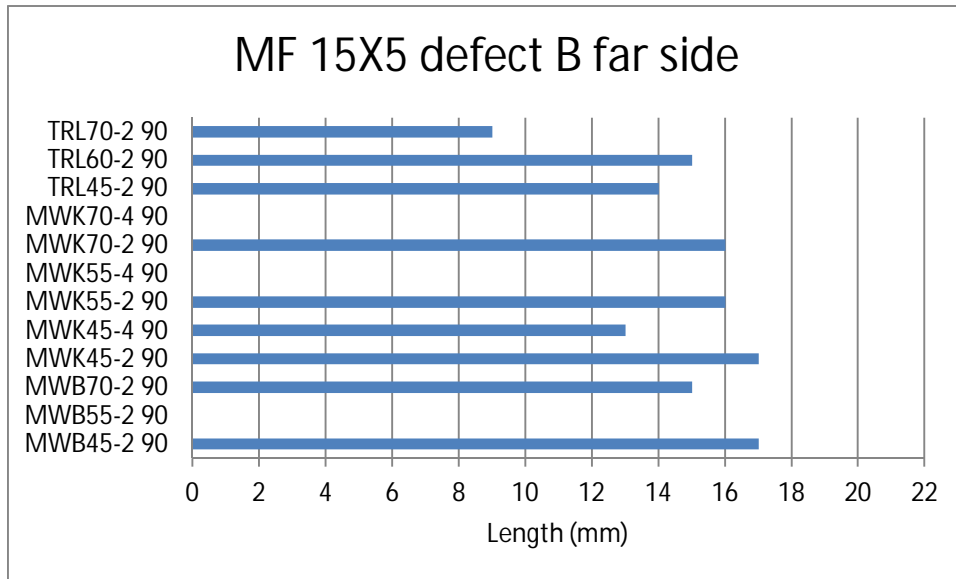


Figure 23. Length sizing results of defect MF15X5 B scanned from far side of the defect.

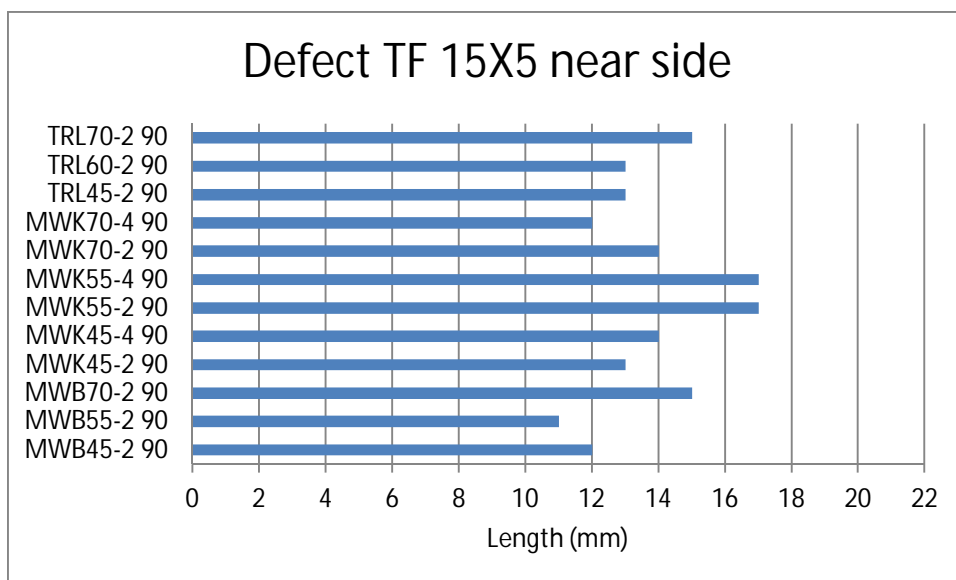


Figure 24. Length sizing results of defect TF15X5 scanned from near side of the defect.

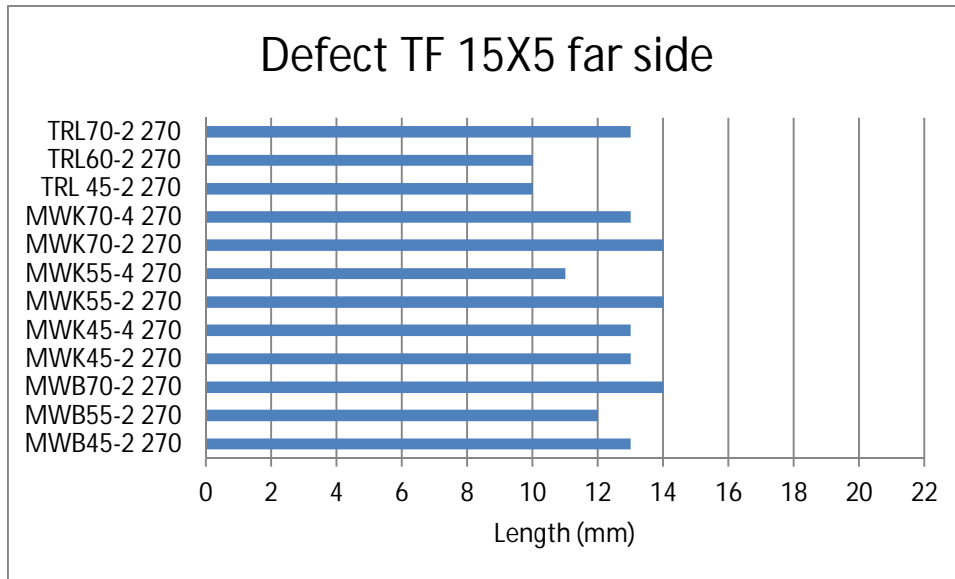


Figure 25. Length sizing results of defect TF15X5 scanned from near side of the defect.

## 6.2 Phased array testing

### 6.2.1 Signal to noise ratio by technique

Signal-to-noise ratios of all three defects inspected by phased array techniques PA-1, PA-2, PA-3 and PA-4 are shown in Figures 26–28.

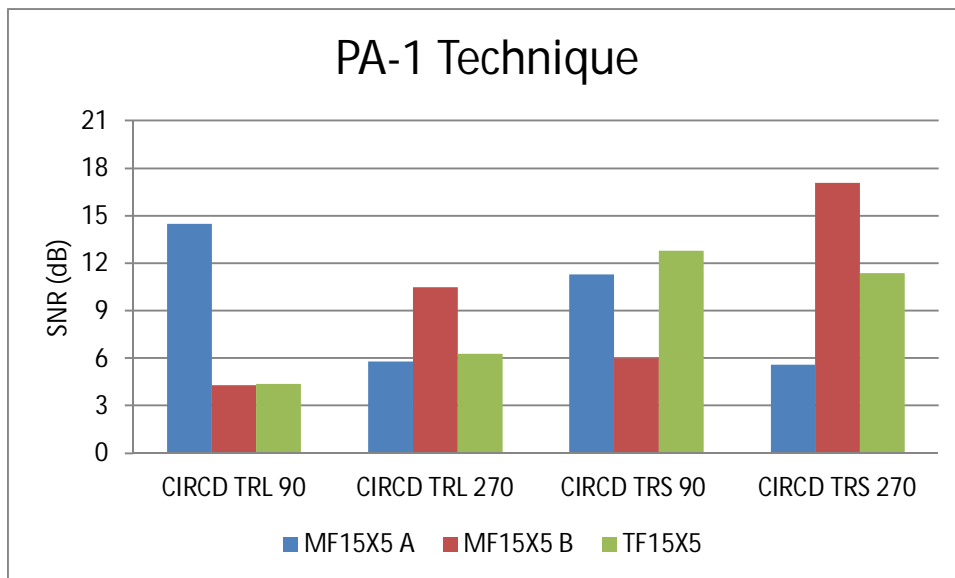


Figure 26. Signal-to-noise ratio of all defects inspected with PA-1 technique.

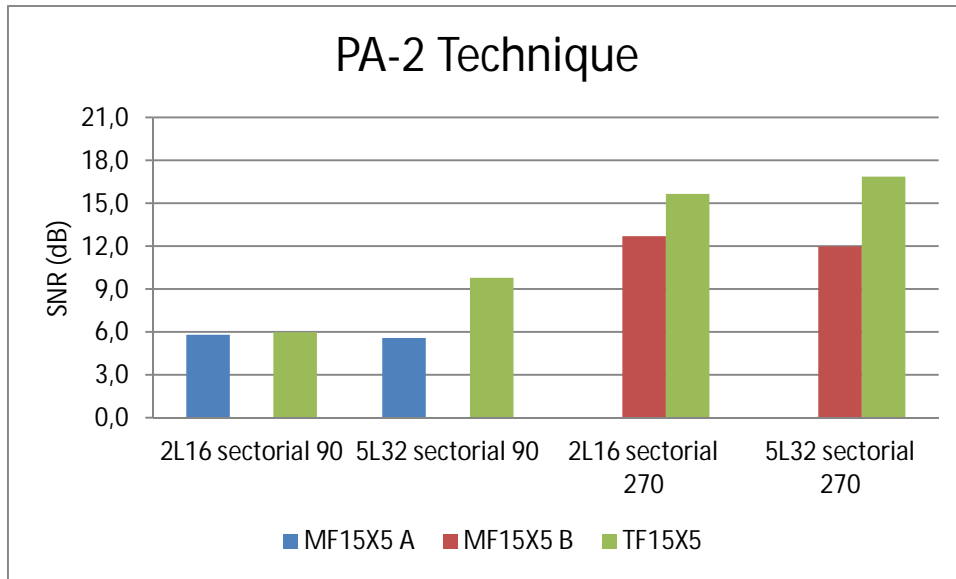


Figure 27. Signal-to-noise ratio of all defects scanned with PA-2 technique.

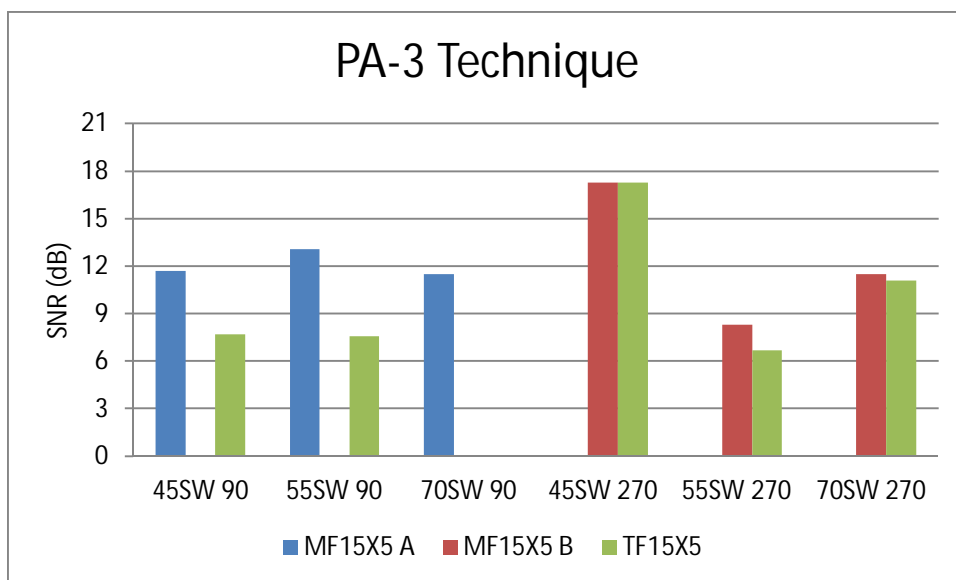


Figure 28. Signal-to-noise ratio of all defects with PA-3 technique.

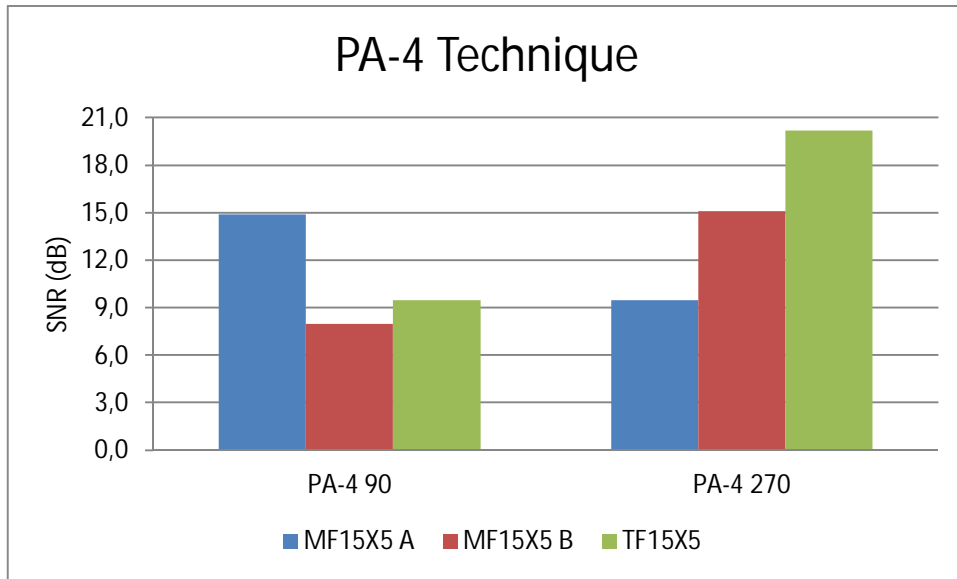


Figure 29. Signal-to-noise ratio of all defects with PA-4 technique.

### 6.2.2 Signal-to-noise ratio by scanning direction

Signal-to-noise ratio of each defect scanned from both directions is shown in Figures 30–35.

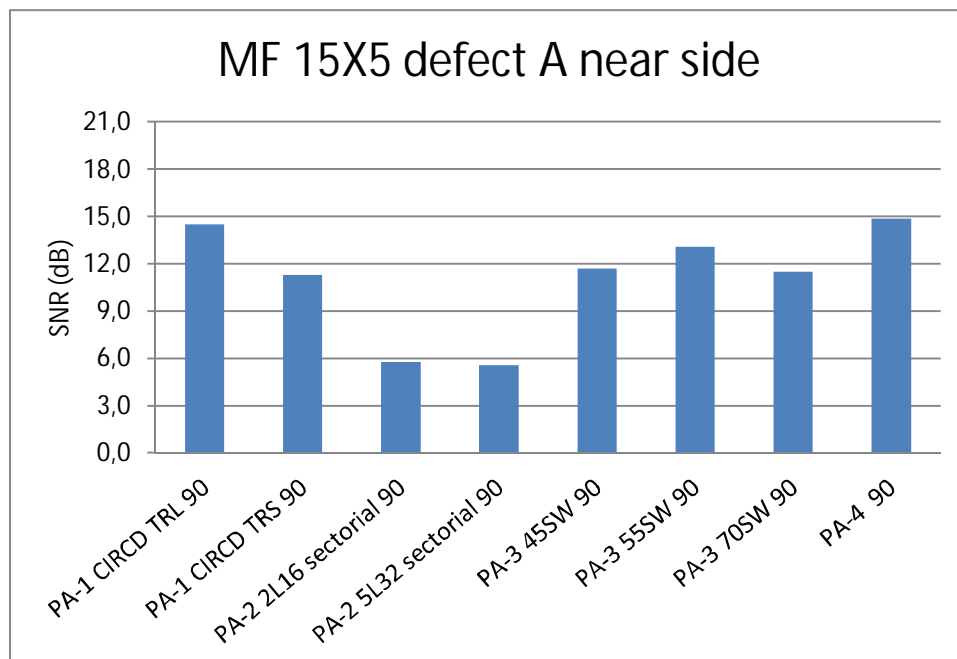


Figure 30. Signal-to-noise ratio of defect MF15X5 A scanned from near side of the defect.

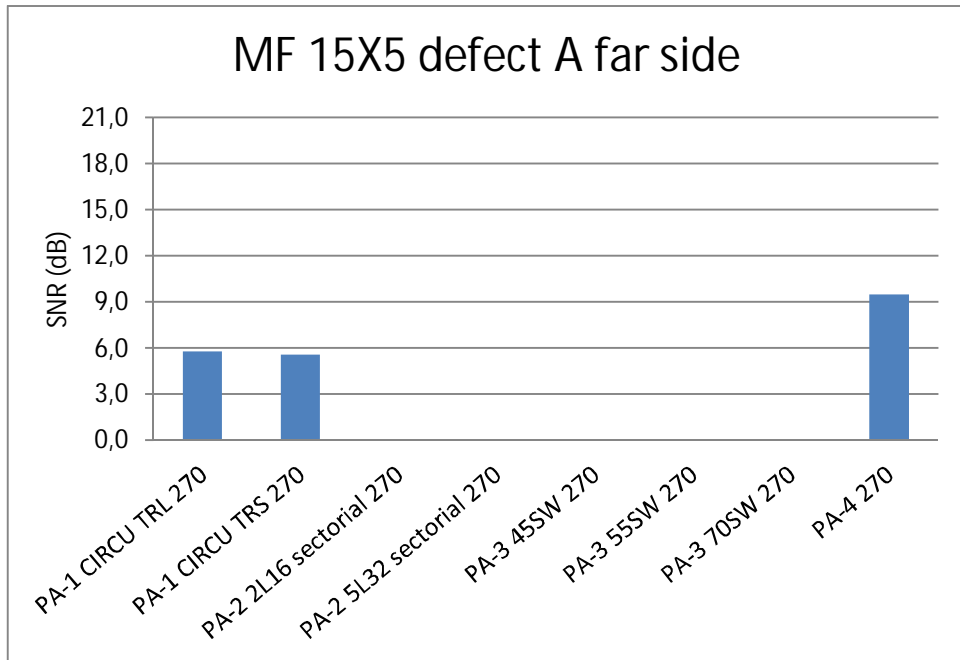


Figure 31. Signal-to-noise ratio of defect MF15X5 A scanned from far side of the defect.

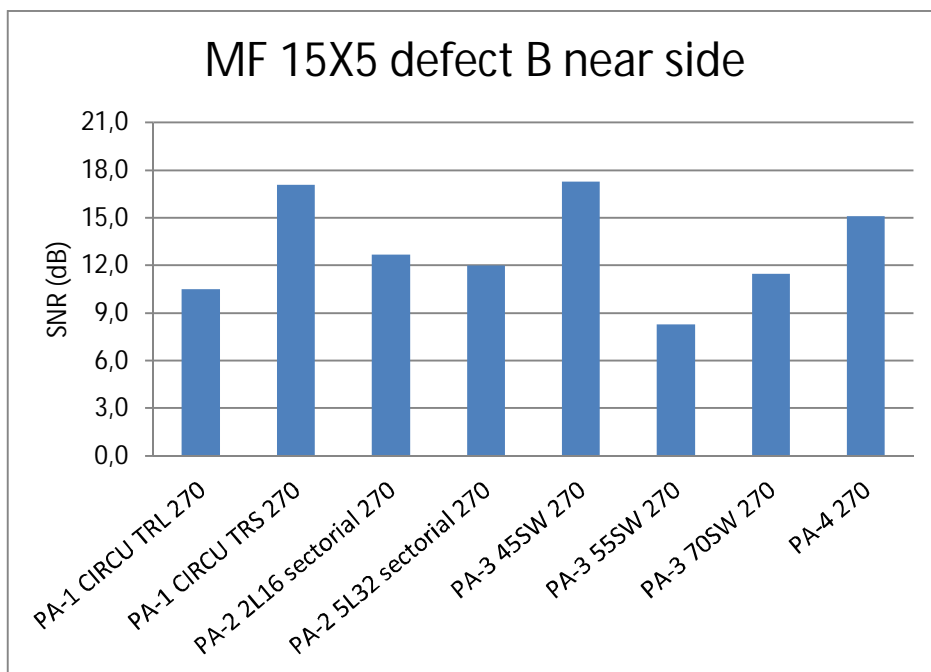


Figure 32. Signal-to-noise ratio of defect MF15X5 B scanned from near side of the defect.

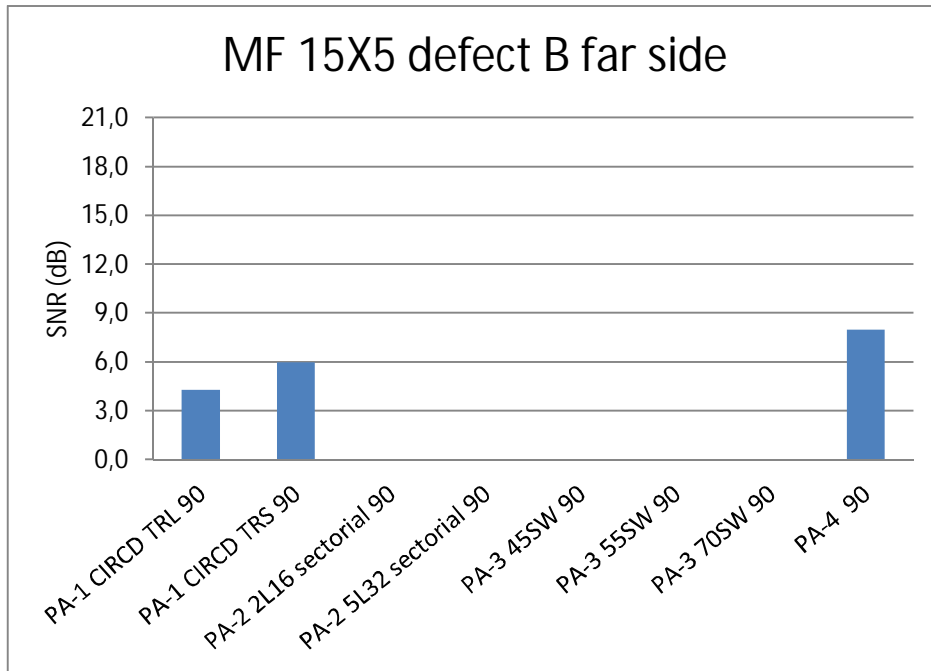


Figure 33. Signal-to-noise ratio of defect MF15X5 B scanned from far side of the defect.

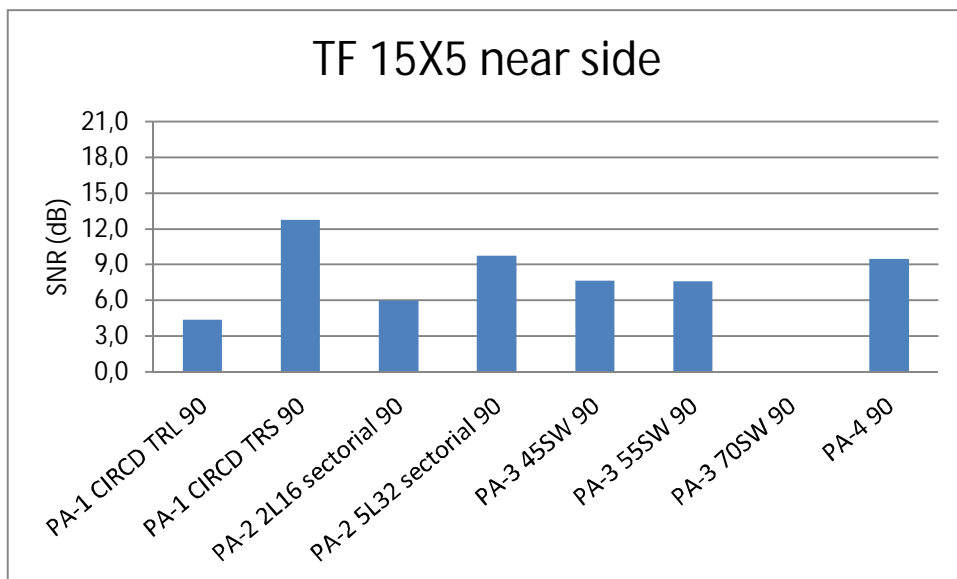


Figure 34. Signal-to-noise ratio of defect TF15X5 scanned from near side of the defect.

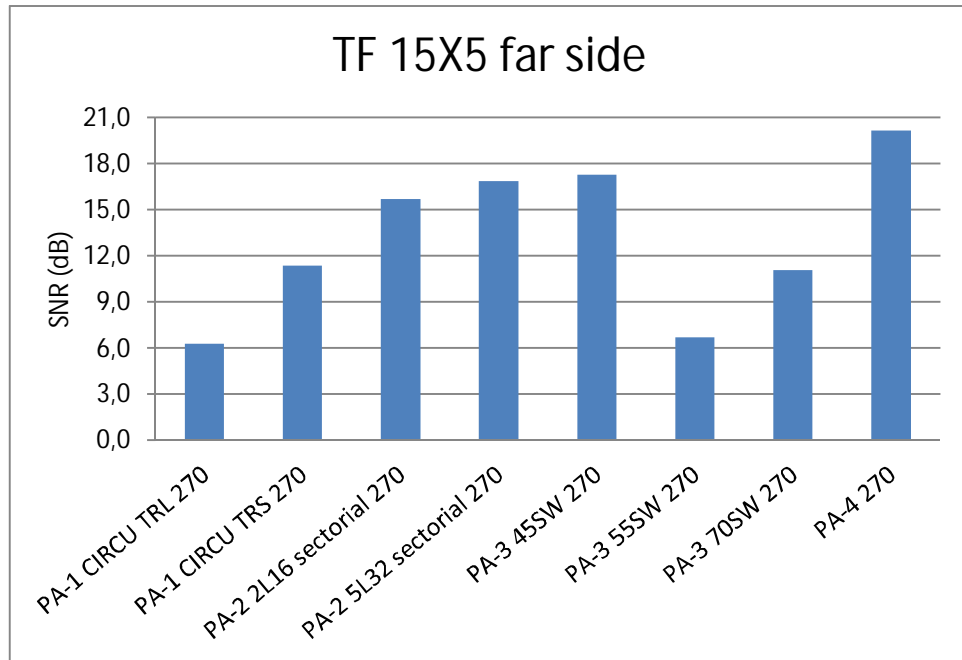


Figure 35. Signal-to-noise ratio of defect TF15X5 scanned from far side of the defect.

### 6.2.3 Length sizing results by technique

Results of defect length measurement with different techniques are shown in Figures 36–39.

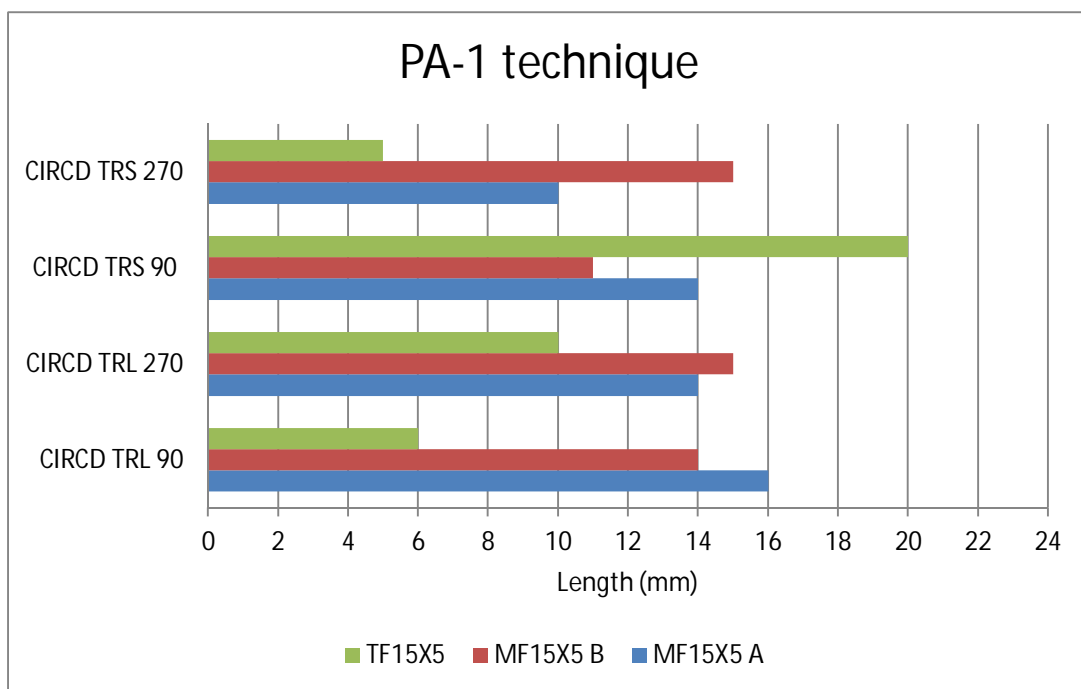


Figure 36. Length sizing results of all defects inspected with PA-1 technique.

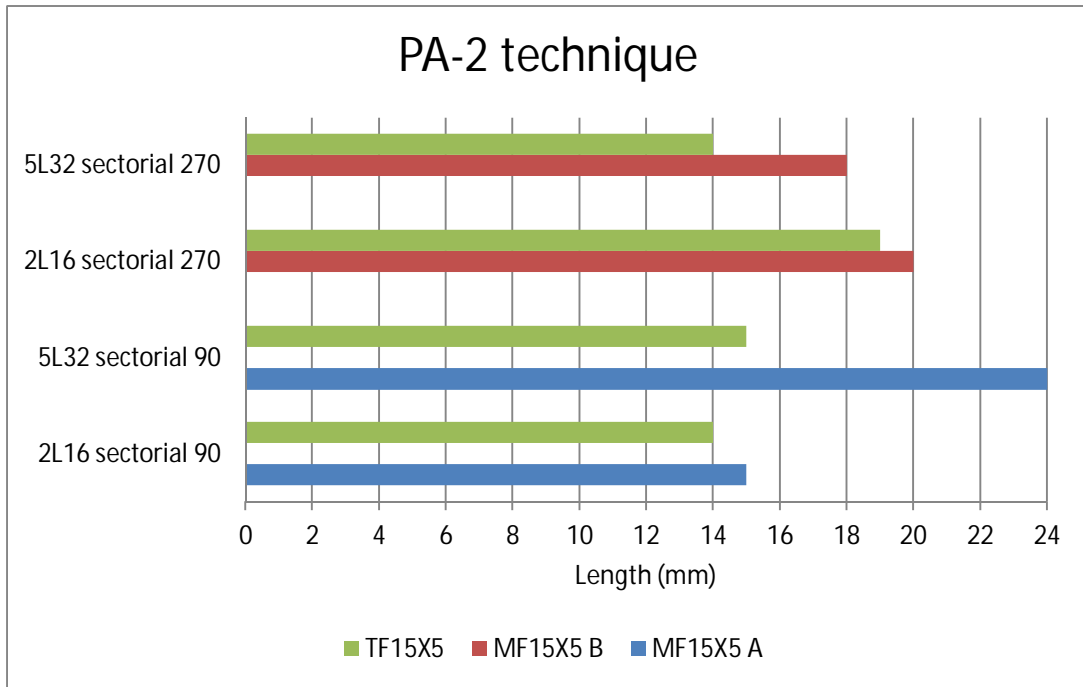


Figure 37. Length sizing results of all defects scanned with PA-2 technique.

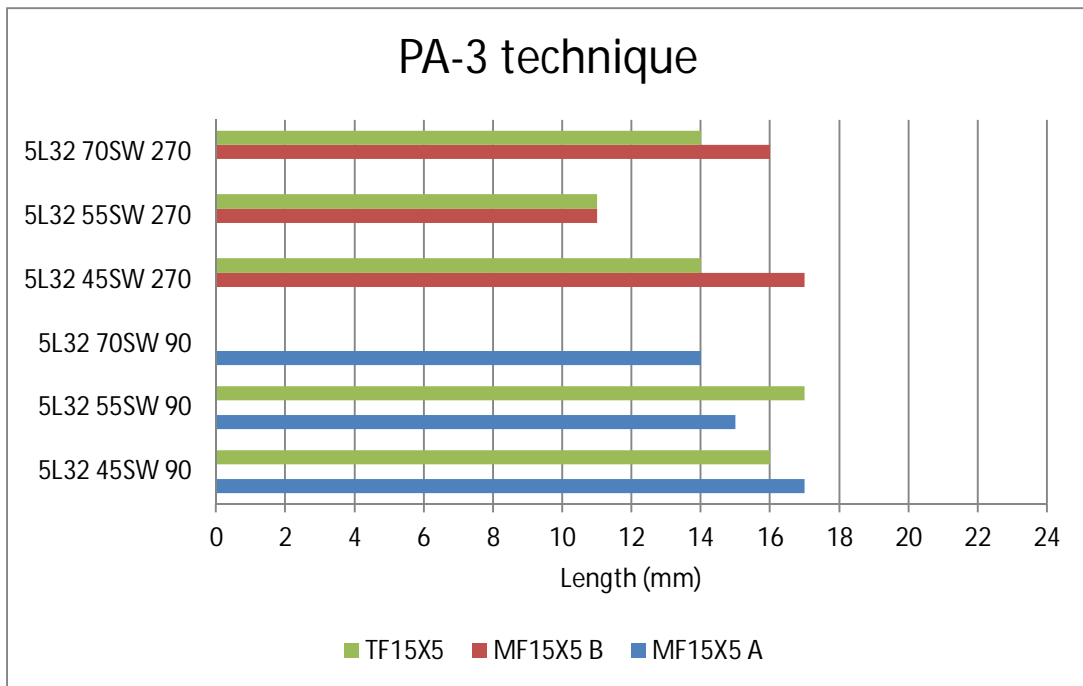


Figure 38. Length sizing results of all defects scanned with PA-3 technique.



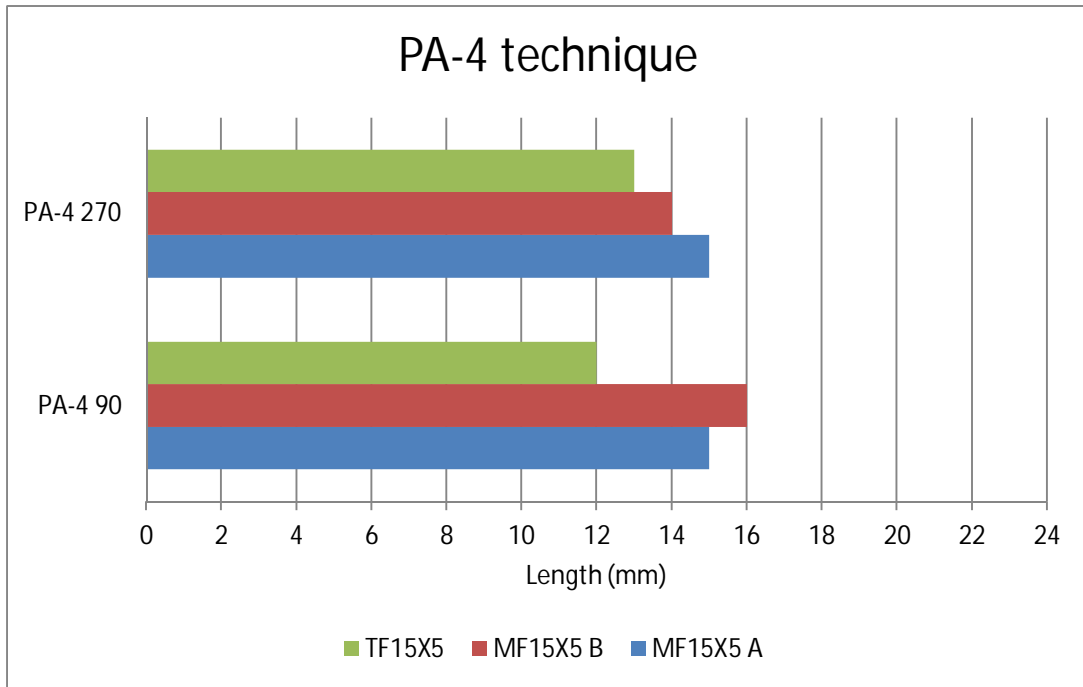


Figure 39. Length sizing results of all defects scanned with PA-4 technique.

#### 6.2.4 Length sizing results by scanning direction

Defect length sizing results for each defects from both scanning directions are shown in Figures 40–45.

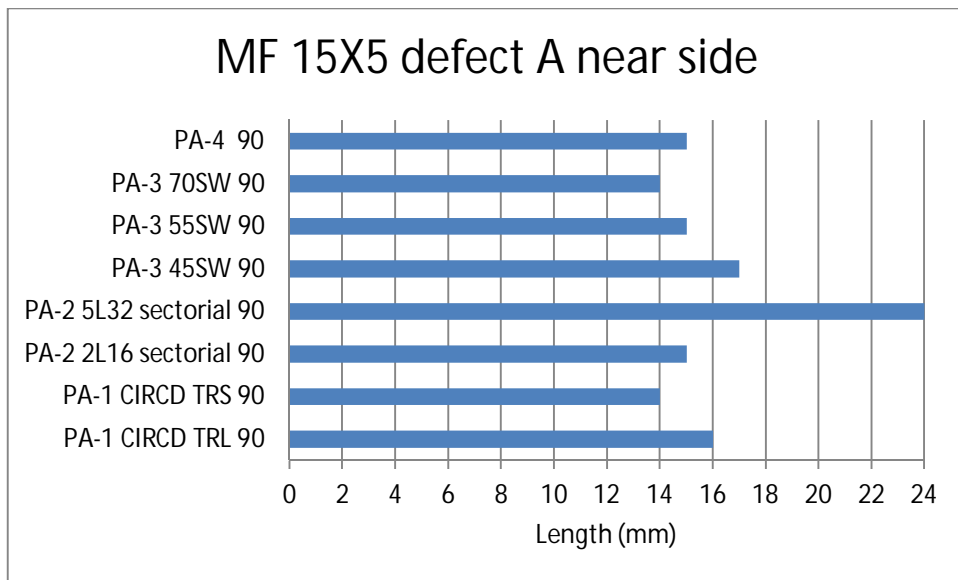


Figure 40. Length sizing results of defect MF15X5 A scanned from near side of the defect.

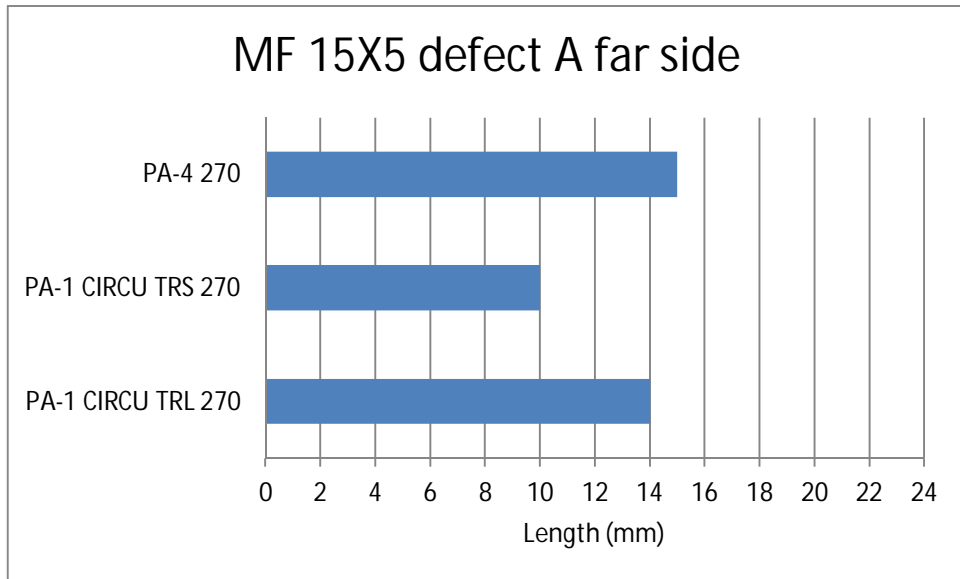


Figure 41. Length sizing results of defect MF15X5 A scanned from far side of the defect.

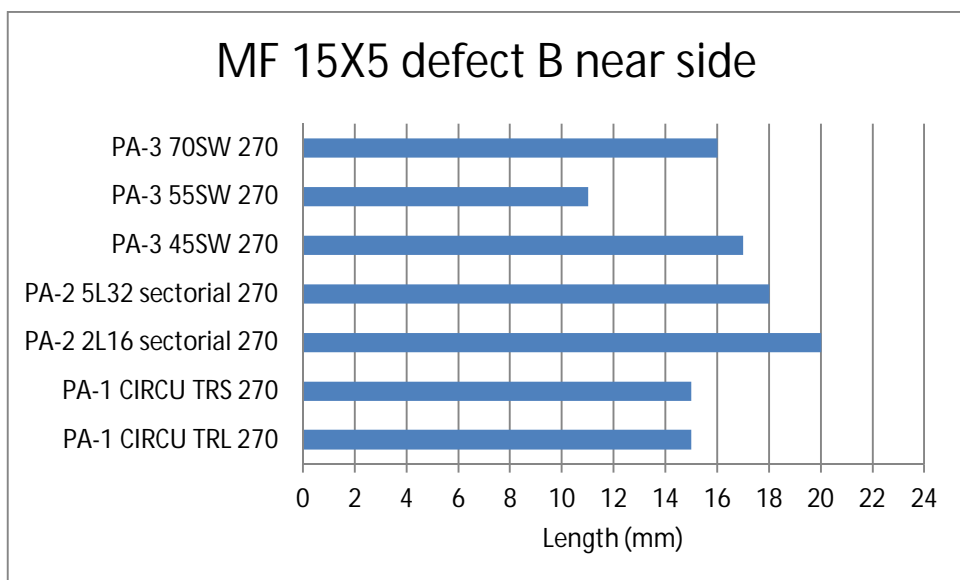


Figure 42. Length sizing results of defect MF15X5 B scanned from near side of the defect.

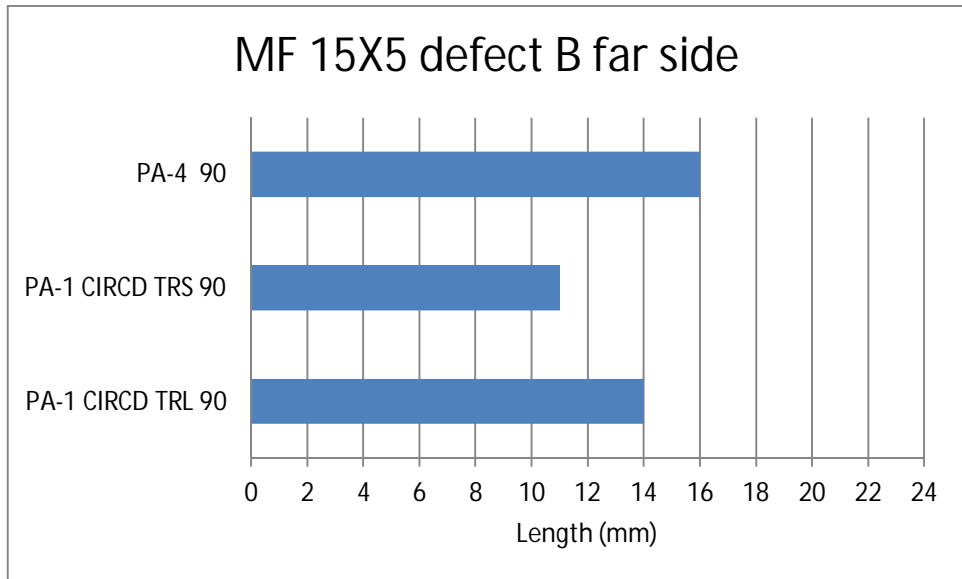


Figure 43. Length sizing results of defect MF15X5 B scanned from far side of the defect.

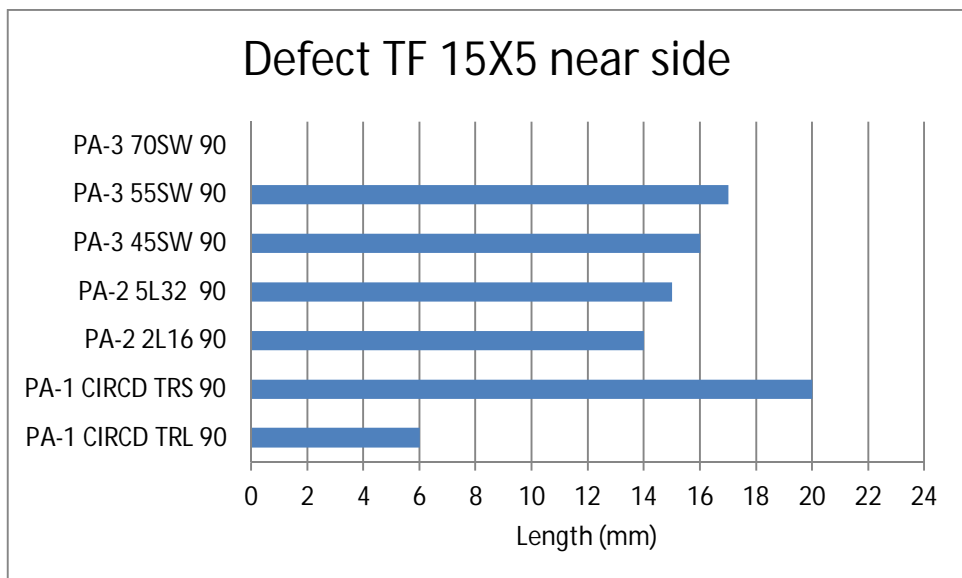


Figure 44. Length sizing results of defect TF15X5 scanned from near side of the defect.

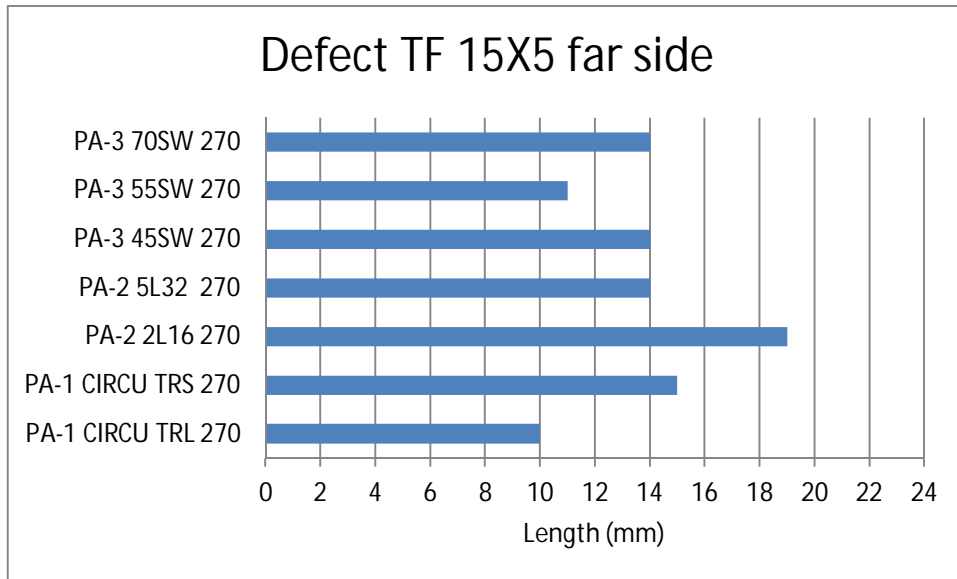


Figure 45. Length sizing results of defect TF15X5 scanned from far side of the defect.

## 7. Validation of results

Repeatability of testing is very important in ultrasonic testing. Mechanizing and automation was used as much as possible to minimize the influence of variance in scanning movement. After time base calibration, a series of measurements was carried out without changing settings except gain. Set ups were saved and the same set ups were used in possible re-scanning.

The maximum amplitude of defect indication is an absolute value and there is a minor risk for deviation caused by human factor in data analysis. The average noise measurement is more complicated variable and dependent on interpretation of the data. In this study, all noise measurements were performed as similarly as possible to minimize the variation between data.

Full amplitude drop as defect length sizing method seems to perform well for material in question. However, the noise level measurement required in that technique gives also a possibility for different interpretation depending on data analyst.

Due to grinding of the weld, there is some variety in the surface roughness and the shape of the surface of test specimens which may have some influence to acoustic contact and incidence angle.

## 8. Conclusion

In inspection of mechanical fatigue cracks with conventional single crystal probes the scanning direction near/far side of the defect usually has a clear influence on SNR. In case of thermal fatigue crack the SNR with several probes seems to be better when scanned from far side of the defect.

With conventional longitudinal TR technique the 45 degree probe SNR was rather high regardless of scanning direction. When probe angle increases the SNR decreases significantly and with 70 degree probe defect TF was missed from both scanning directions.

Usually the SNR is higher with MWK probes (piezocomposite crystal) when scanning from defect side. When scanning from opposite side of the defect MWK probes don't have such benefit. When scanned from defect side the SNR results of defect MF15X5 A are more uniform than results of defect MF15X5 B. In case of thermal fatigue crack SNR with smaller angle probes is better when scanned from far side regardless of the probe type.

The procedure for phased array technique PA-1 performed well and defects were detected from both scanning directions. The difference between mechanical fatigue defects was that MF15X5A received the highest SNR value with longitudinal wave PA probe, whereas MF15X5B received the highest SNR value with transverse wave PA probe. With TF15X5 defect the two highest SNR values were detected with transverse wave PA probe and surprisingly the highest SNR value for TF15X5 defect was detected when inspection was performed through the weld.

Only PA-1 and PA-4 techniques were able to detect mechanical fatigue defects from far side. Thermal fatigue defect was detected from both sides. It seems that there is no significant difference in SNR between the two different frequencies when inspection was performed from the defect side. In PA-3 technique tests almost similar results were obtained as in PA-2 tests. With 70 degree angle and inspecting through the weld, TF15X5 defect was not detected.

The results of length sizing will be compared to true state information after destructive testing of defects.

More detailed analysis and more tests are needed. Testing will be carried out using scanning acoustic microscope (SAM), time of flight diffraction (TOFD) and eddy current testing. Final analysis of the NDE results and comparison between two different artificial fatigue defects will be done after the destructive investigation is completed.

## 9. Summary

---

Two test blocks welded of austenitic stainless steel 316L (ASTM) plates with thickness of 25 mm were inspected with different ultrasonic methods. One of the specimens contained a thermal fatigue crack and the other contained two mechanical fatigue cracks. This work report presents the initial results from the inspections with conventional and phased array ultrasonic techniques.

All defects were scanned from both sides of the weld and data stored. The data was then analysed and signal-to-noise ratio of defect indications measured. Also length sizing of the defects was performed.

Final analysis and comparison of the results will be performed after destructive testing of the samples.

## References

---

1. Zetec\_OmniScanPA\_01\_revC.doc. Procedure for Encoded, Manually Driven, Phased Array Ultrasonic Flaw Detection and Length Sizing in Ferritic and Wrought Austenitic Piping Welds. Zetec Inc., Canada, 2006.
2. Russ Minkwitz. Detection and Sizing Techniques of ID Connected Cracking. Olympus Corporation. <http://www.olympus-ims.com/en/applications/detection-sizing-techniques-id-connected-cracking/> (accessed 12 Feb, 2013).

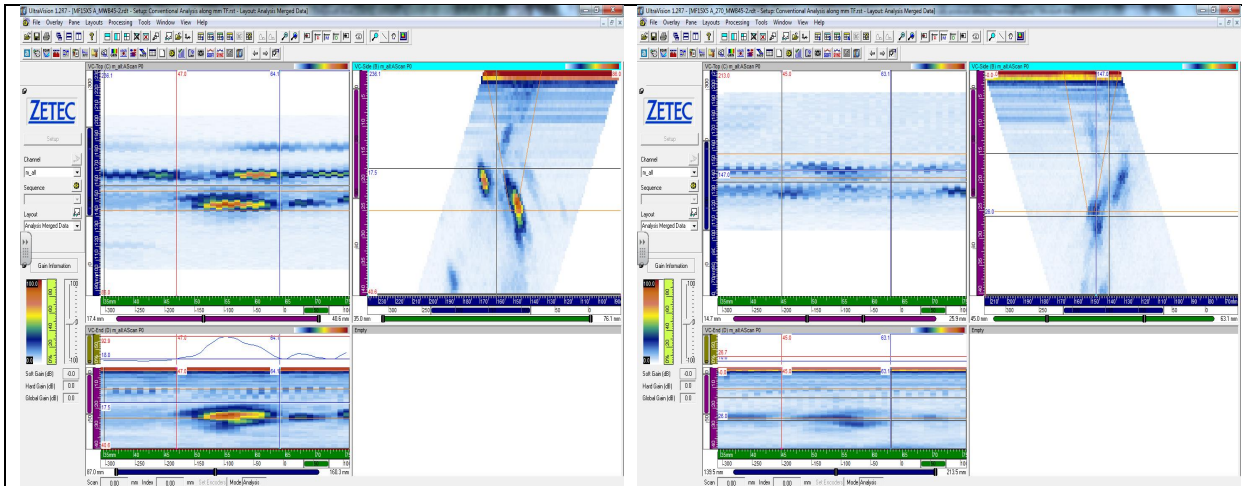
## Appendixes

---

1. Conventional ultrasonic testing screen captures
2. Phased array testing screen captures

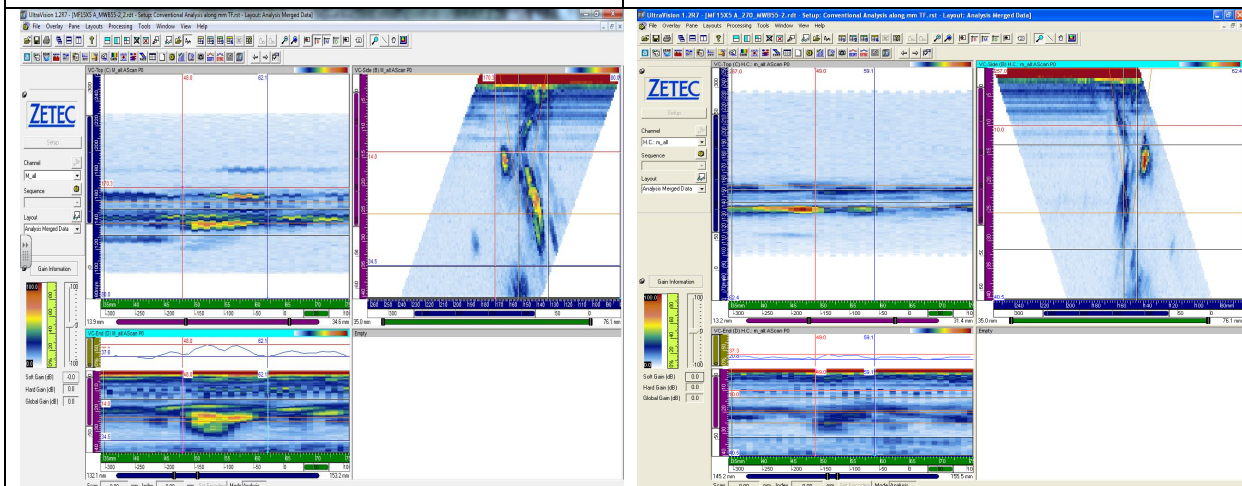
## APPENDIX 1. CONVENTIONAL ULTRASONIC TESTING SCREEN CAPTURES

### A1.1 MF 15X5 DEFECT A



MWB 45-2 90 near side. Above left: volume-corrected C-scan (top view), above right: volume-corrected B-scan (side view) and below: volume-corrected D-scan (end view),

MWB 45-2 270 far side



MWB 55-2 90 near side

MWB 55-2 270 far side

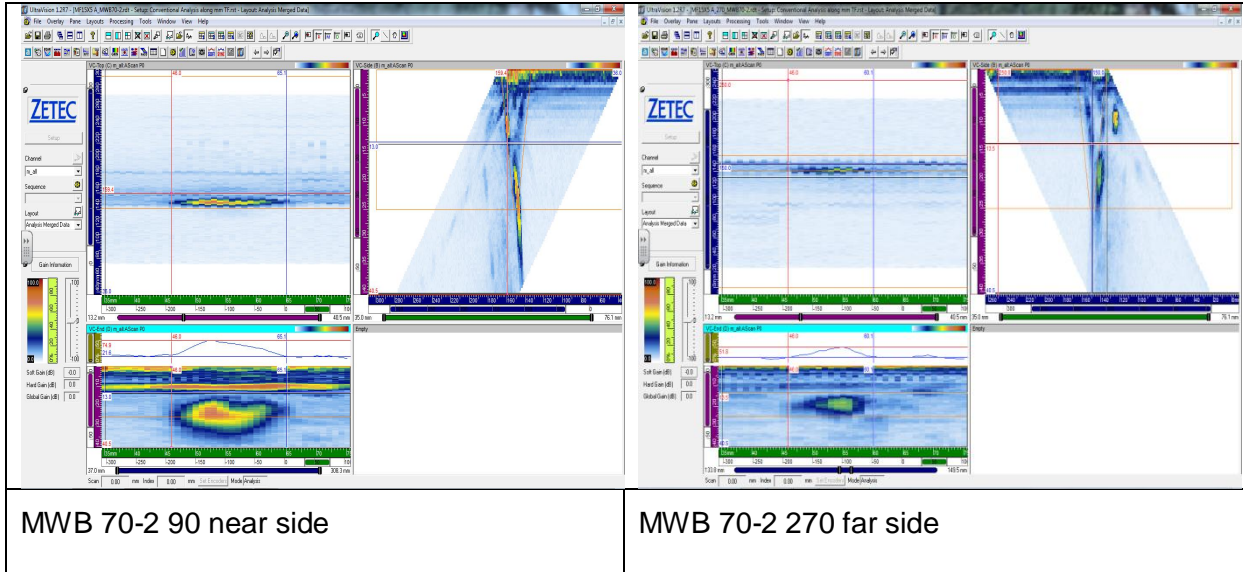
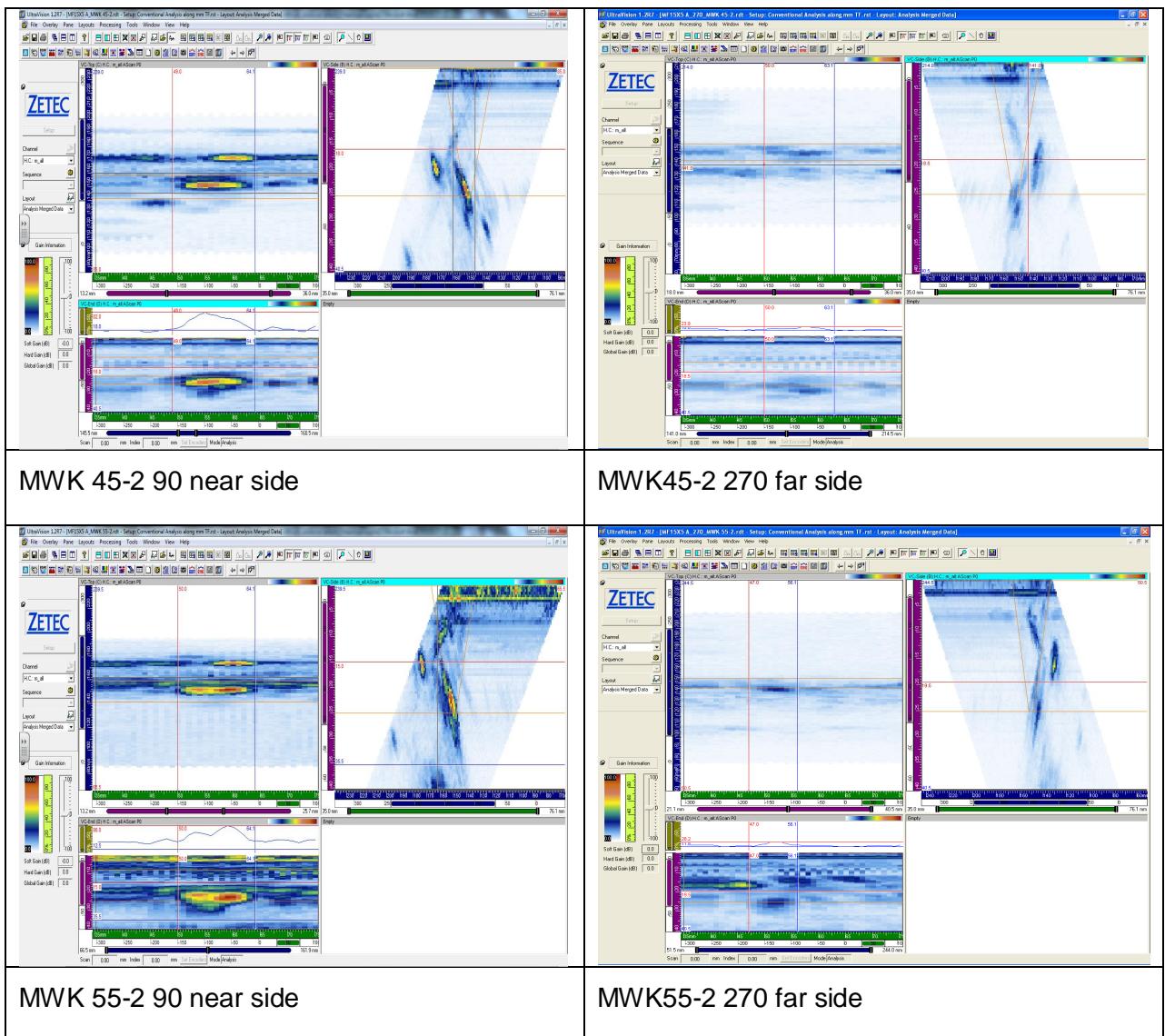


Figure 1. Screen captures of defect MF15X5 A inspection with MWB probes.





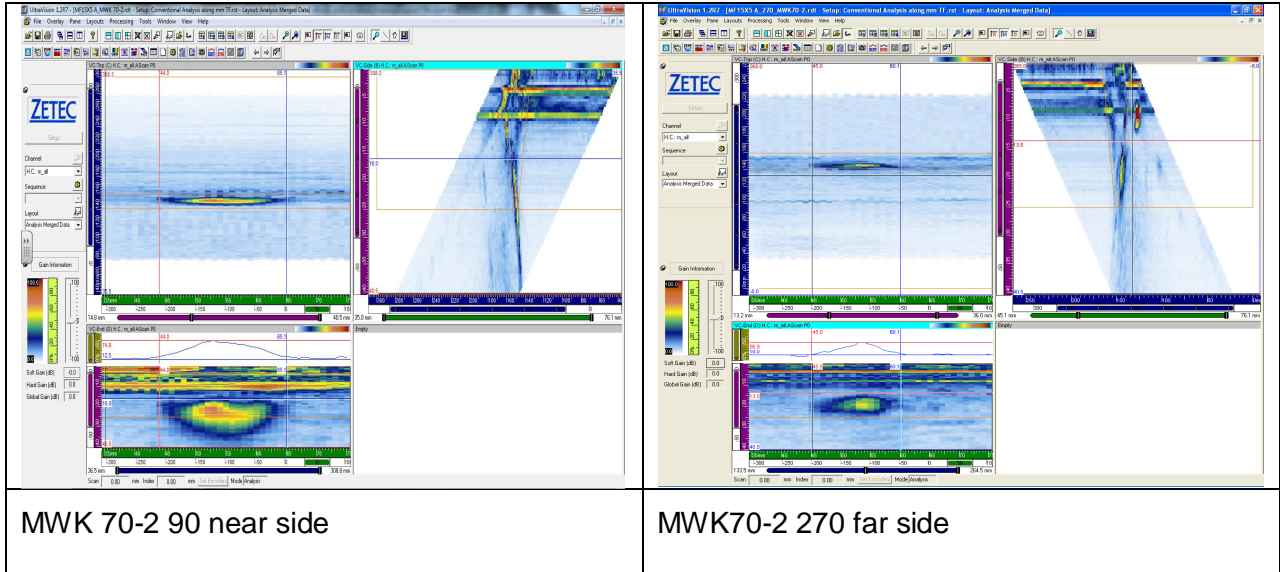
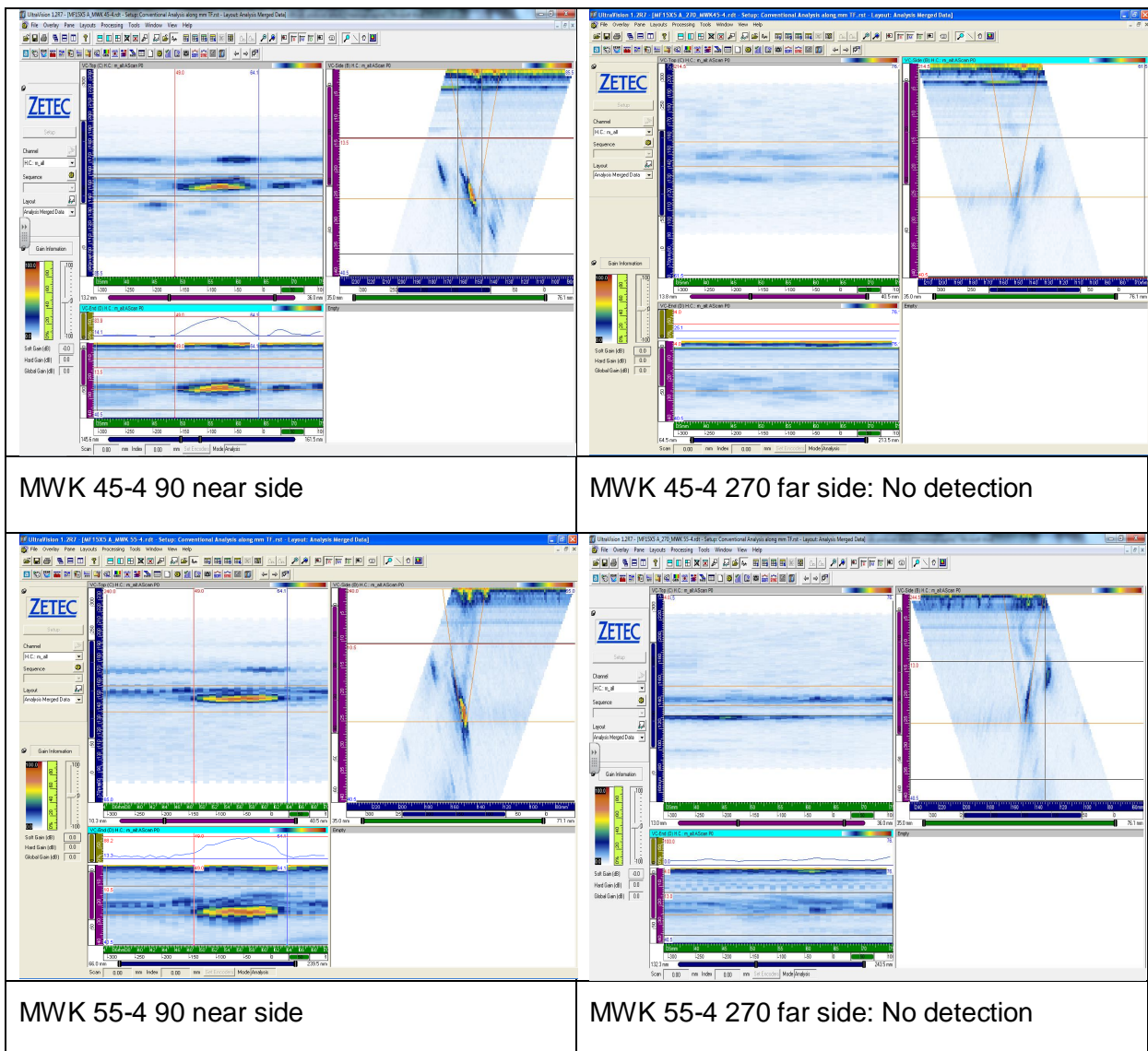


Figure 2. Screen captures of defect MF15X5 A inspection with 2 MHz MWK probes.



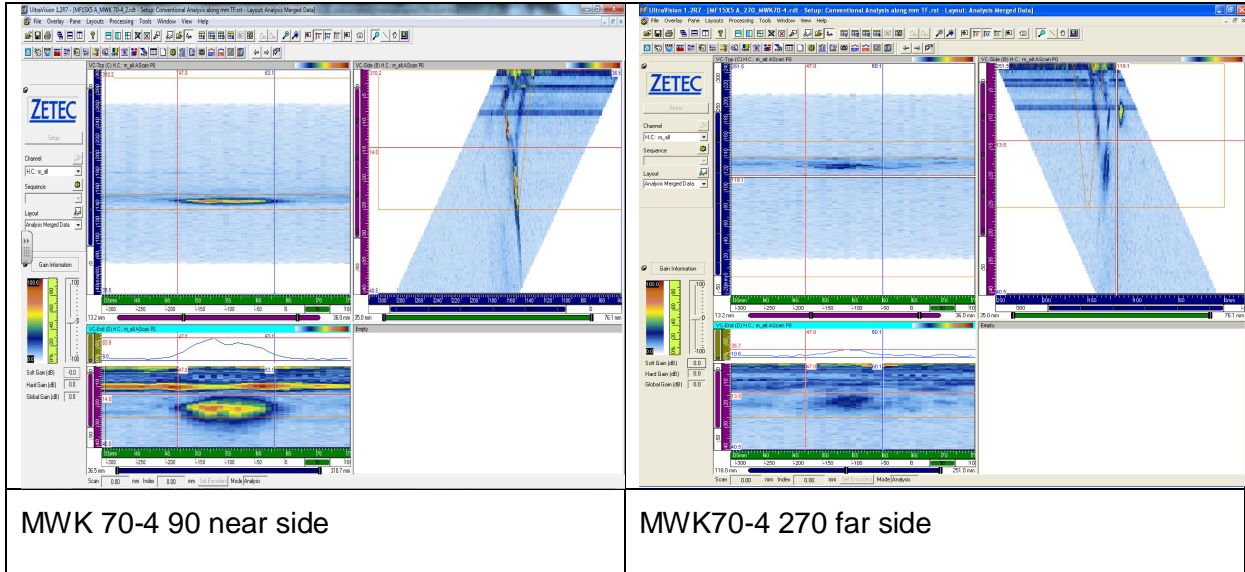
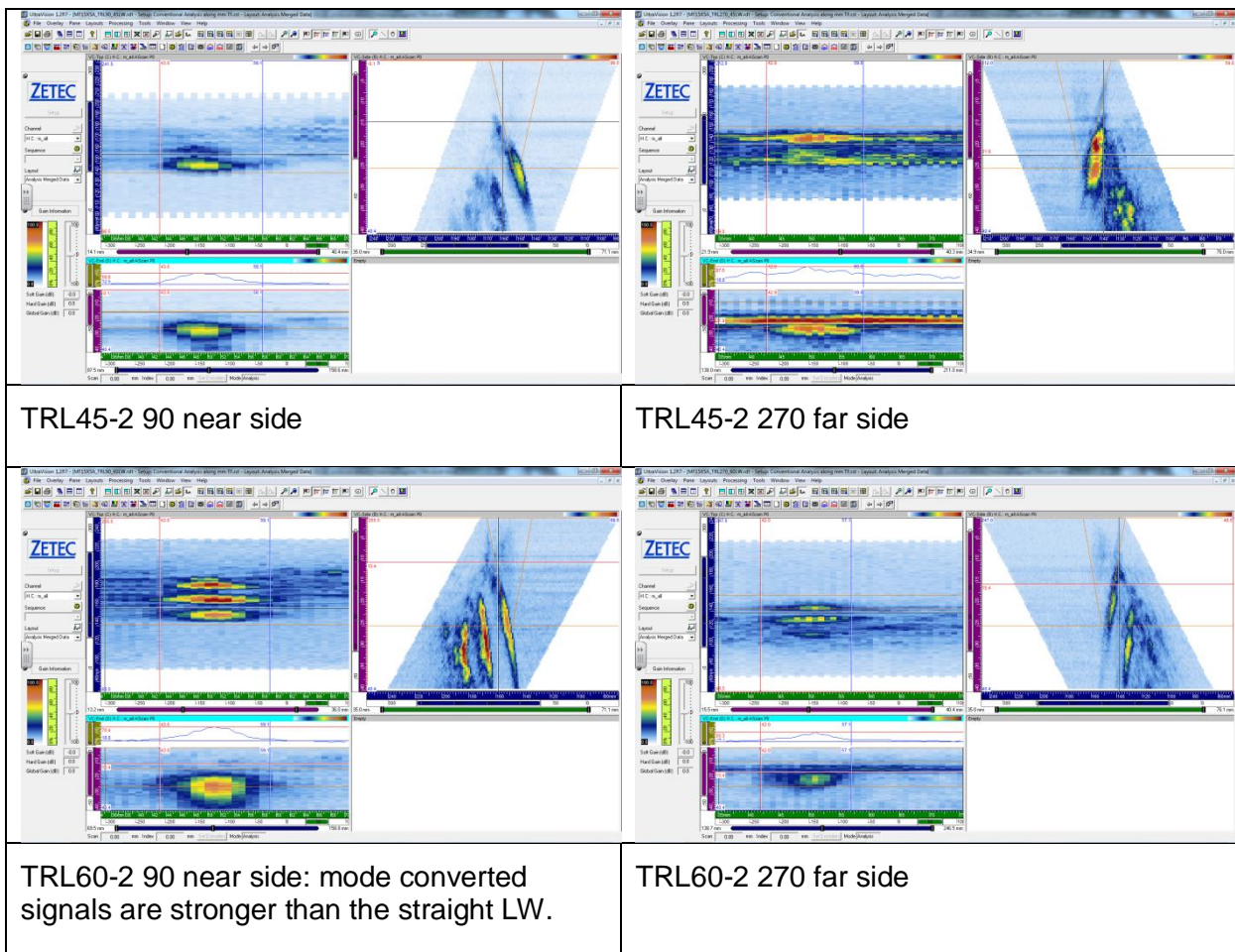


Figure 3. Screen captures of defect MF15X5 A inspection with 4 MHz MWK probes.



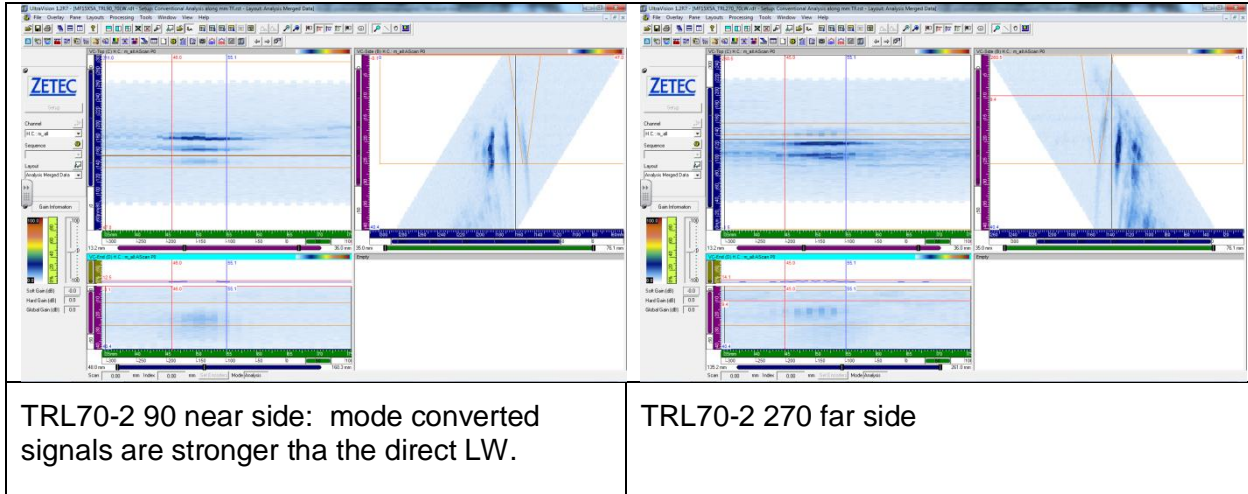
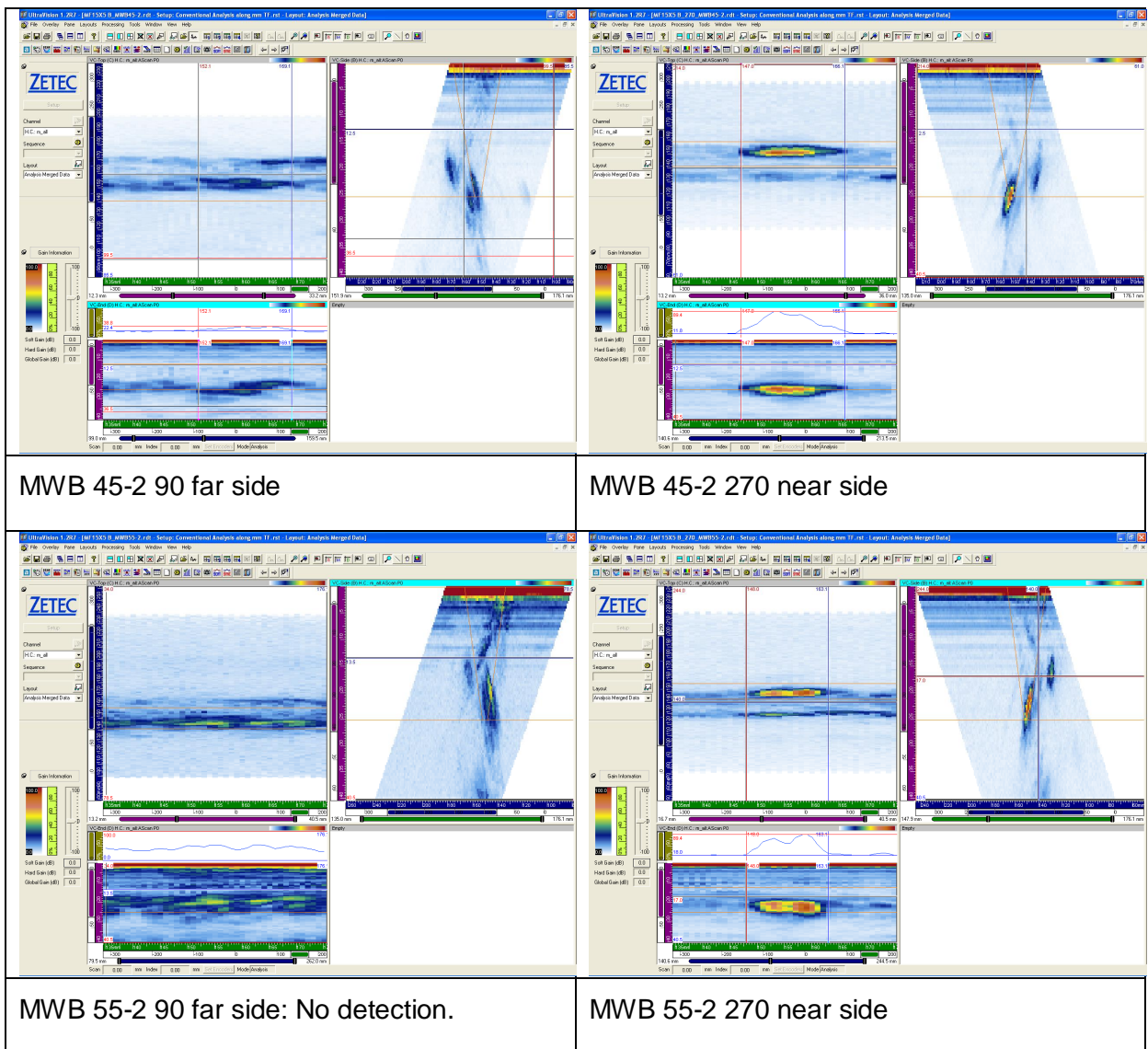


Figure 4. Screen captures of defect MF15X5 A inspection with TRL probes.

## A1.2 MF 15X5 DEFECT B



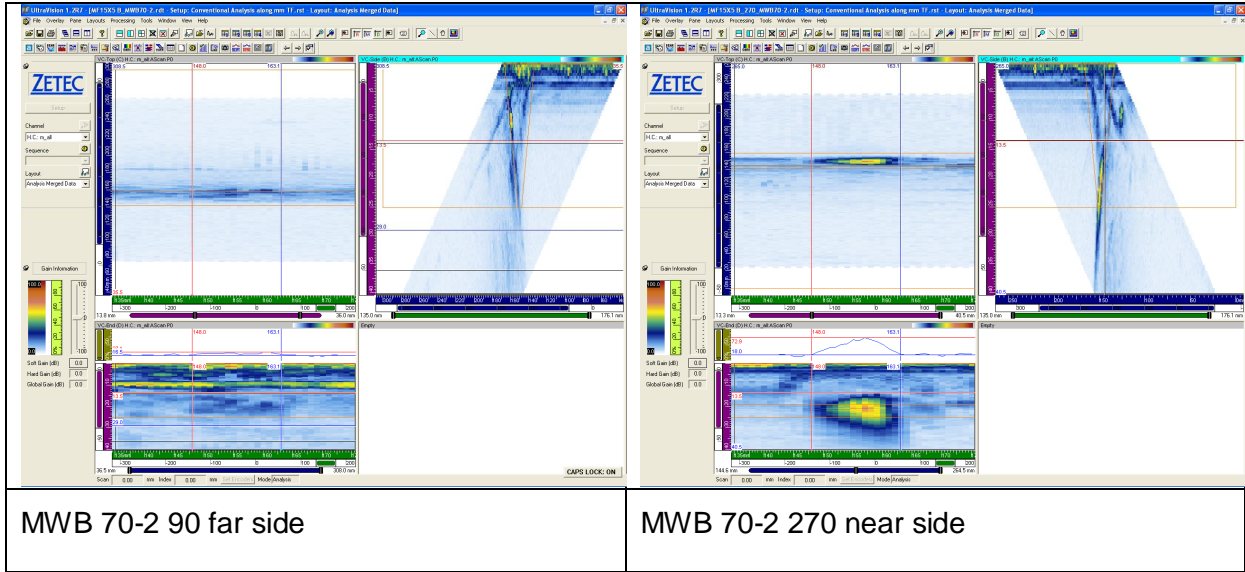
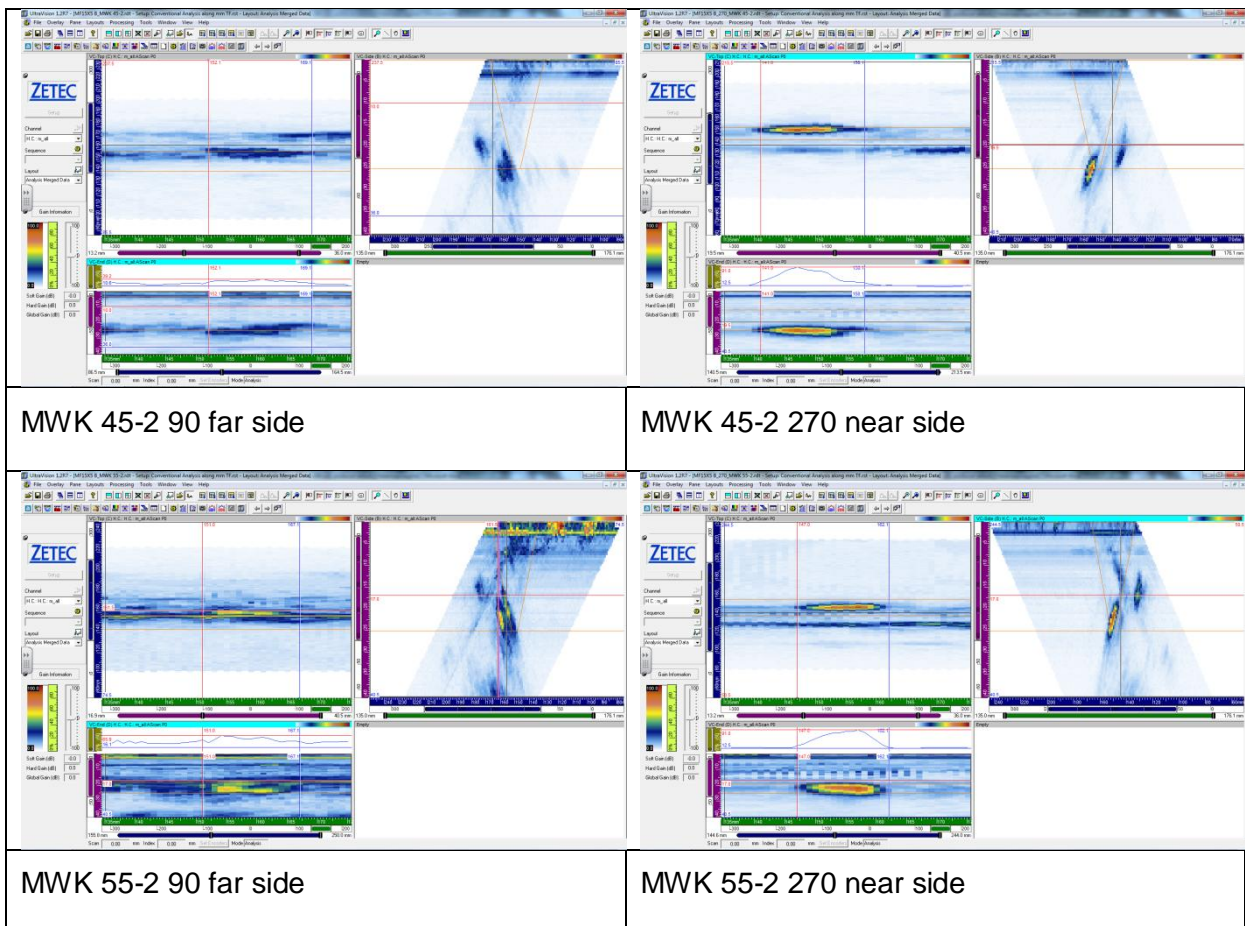


Figure 5. Screen captures of defect MF15X5 B inspection with MWB probes.



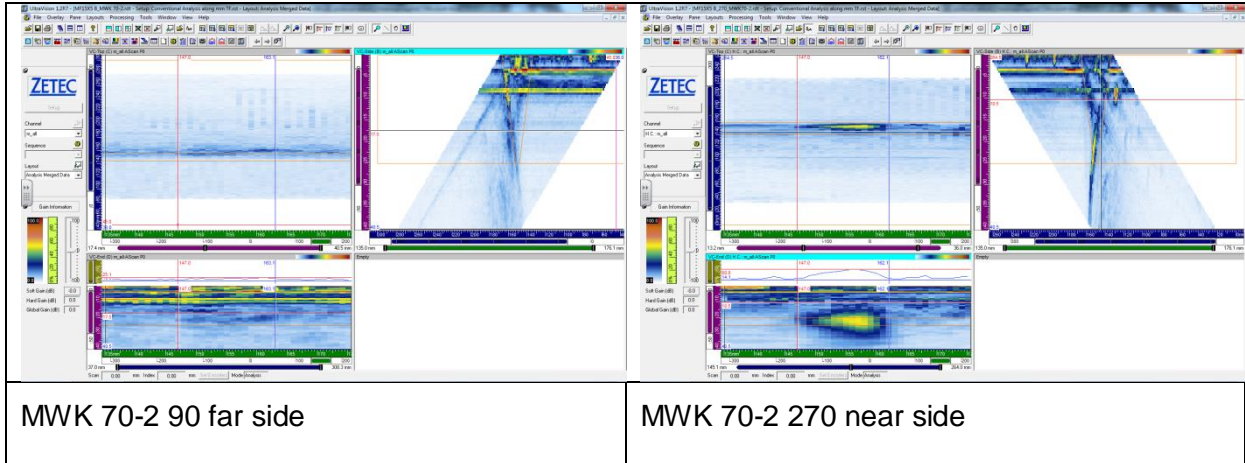
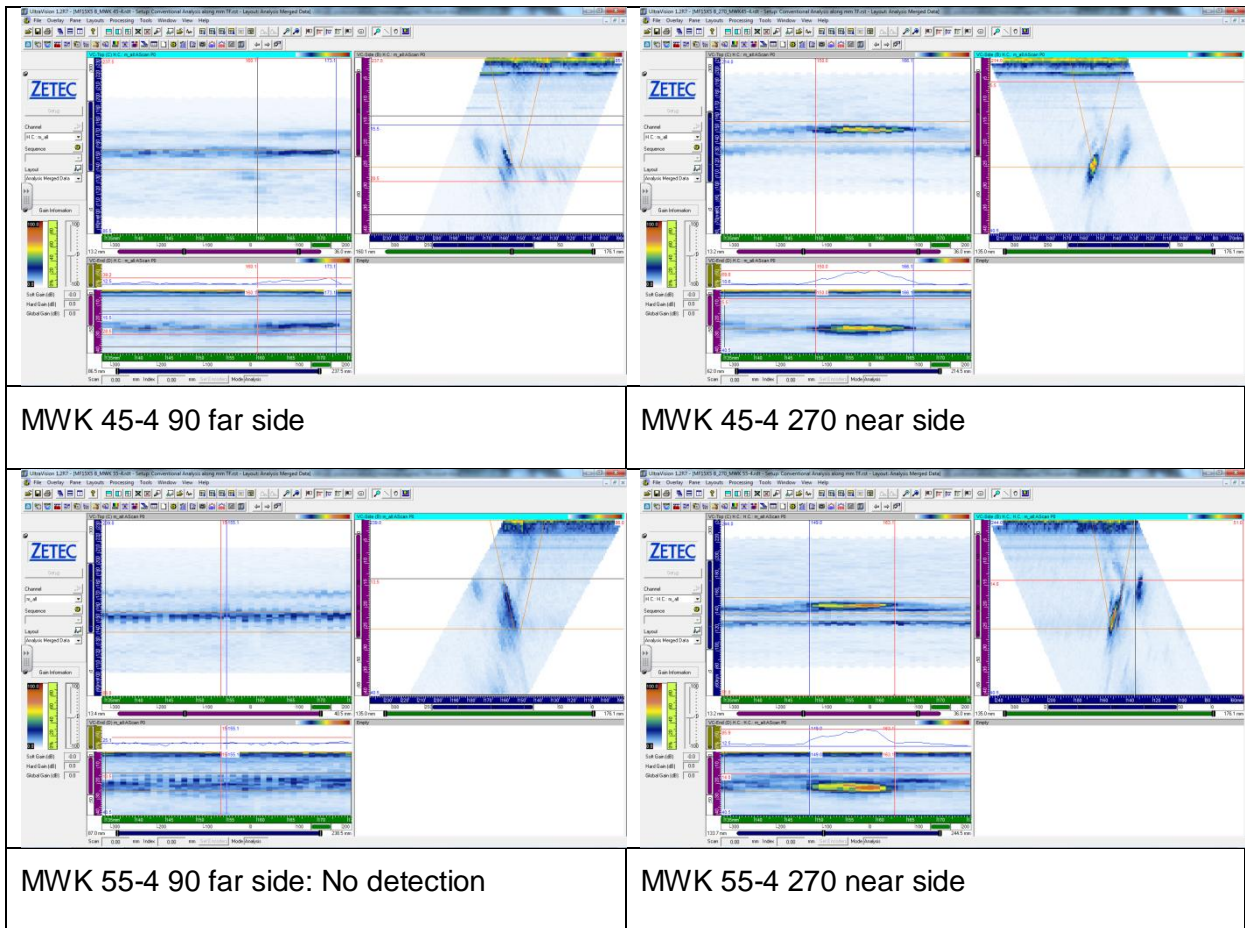


Figure 6. Screen captures of defect MF15X5 B inspection with 2 MHz MWK probes.



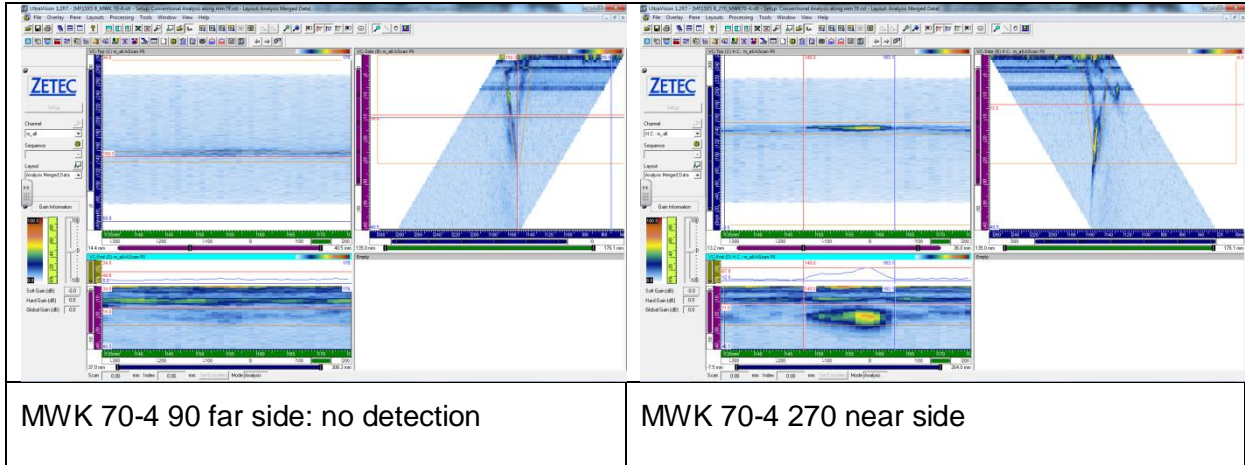
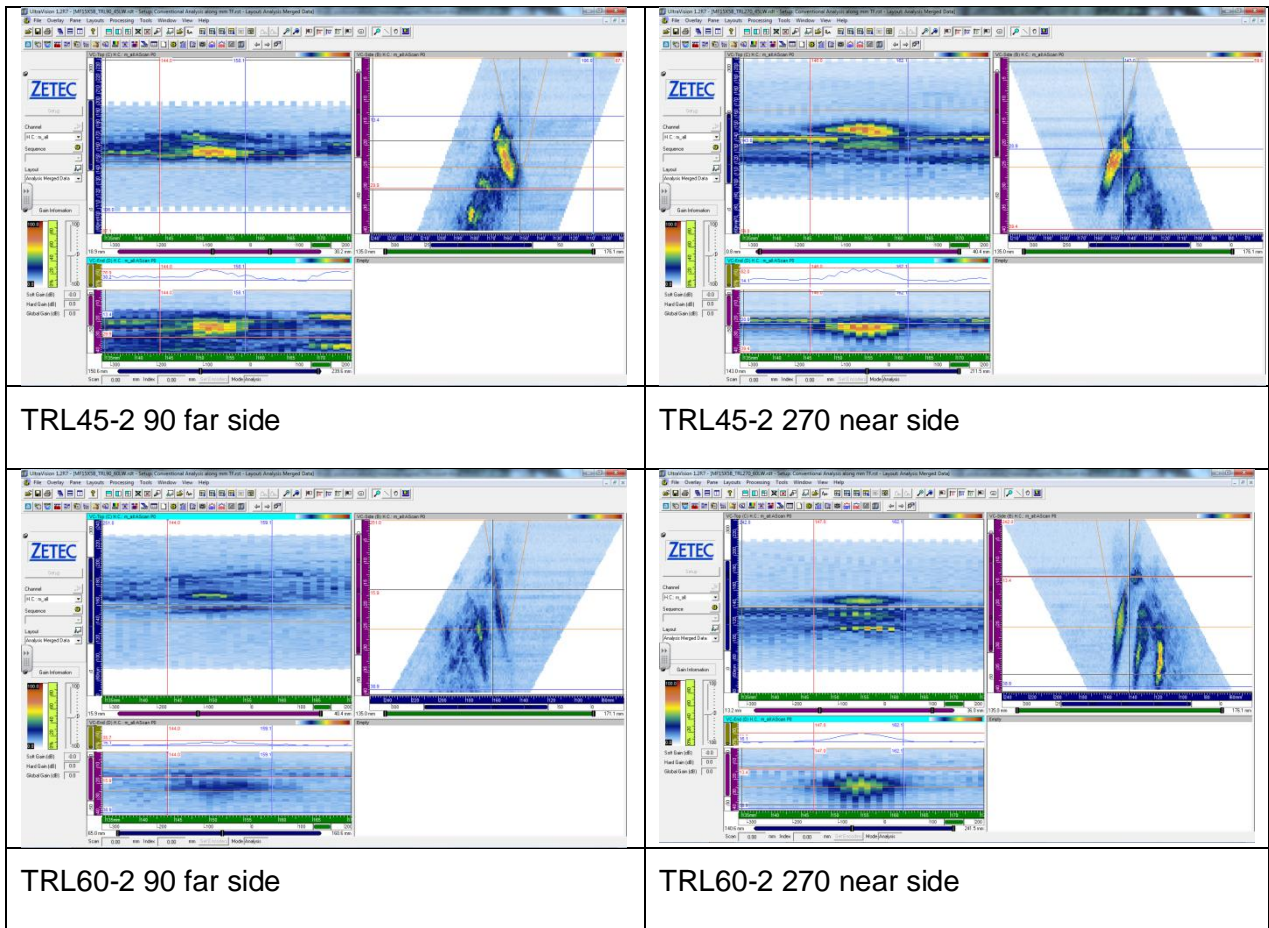


Figure 7. Screen captures of defect MF15X5 B inspection with 4 MHz MWK probes.



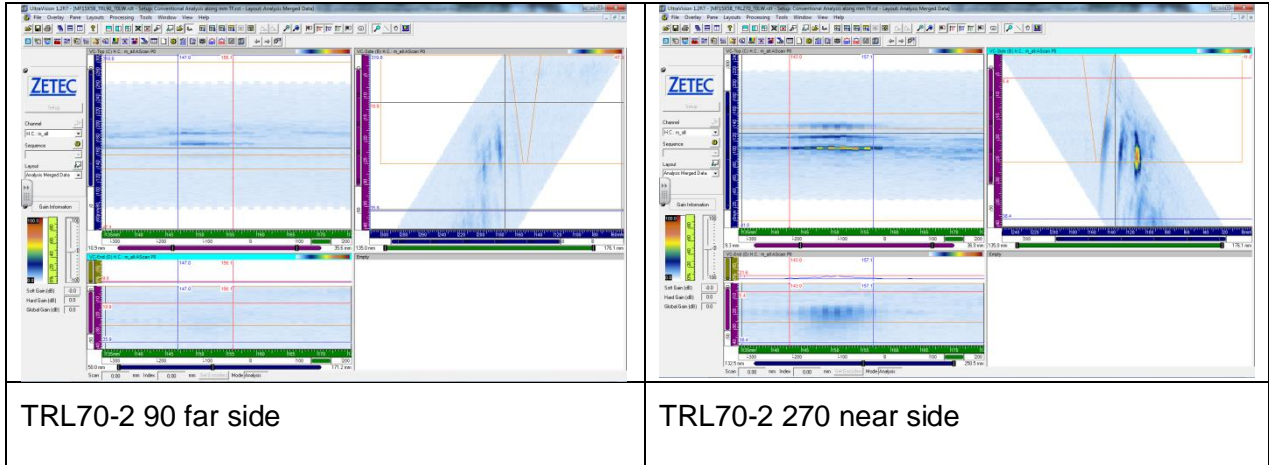
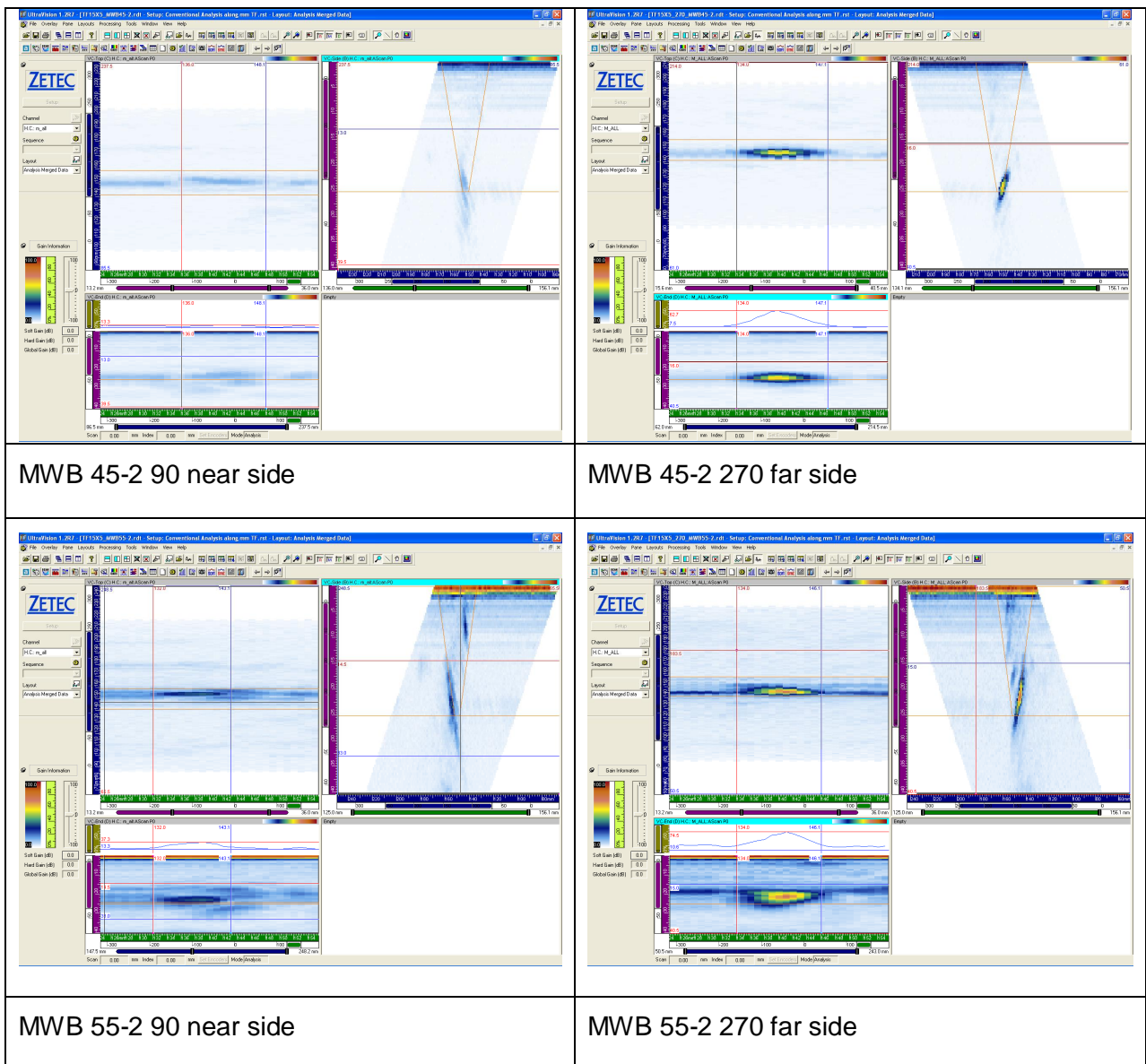


Figure 8. Screen captures of defect MF15X5 B inspection with TRL probes.

### A1.3 DEFECT TF15X5



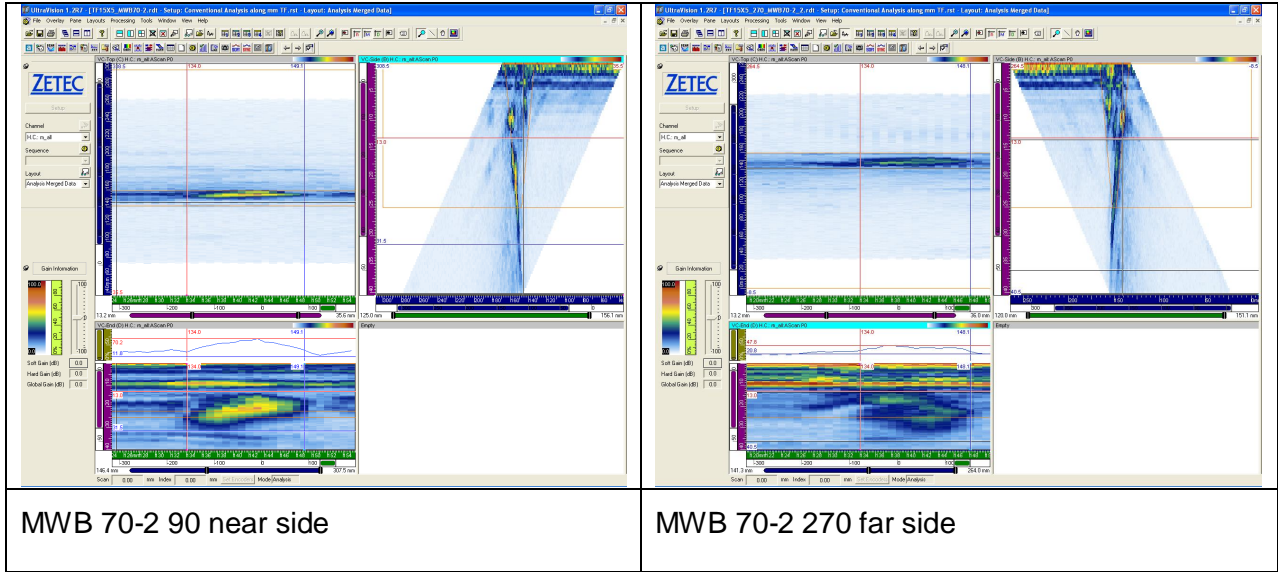
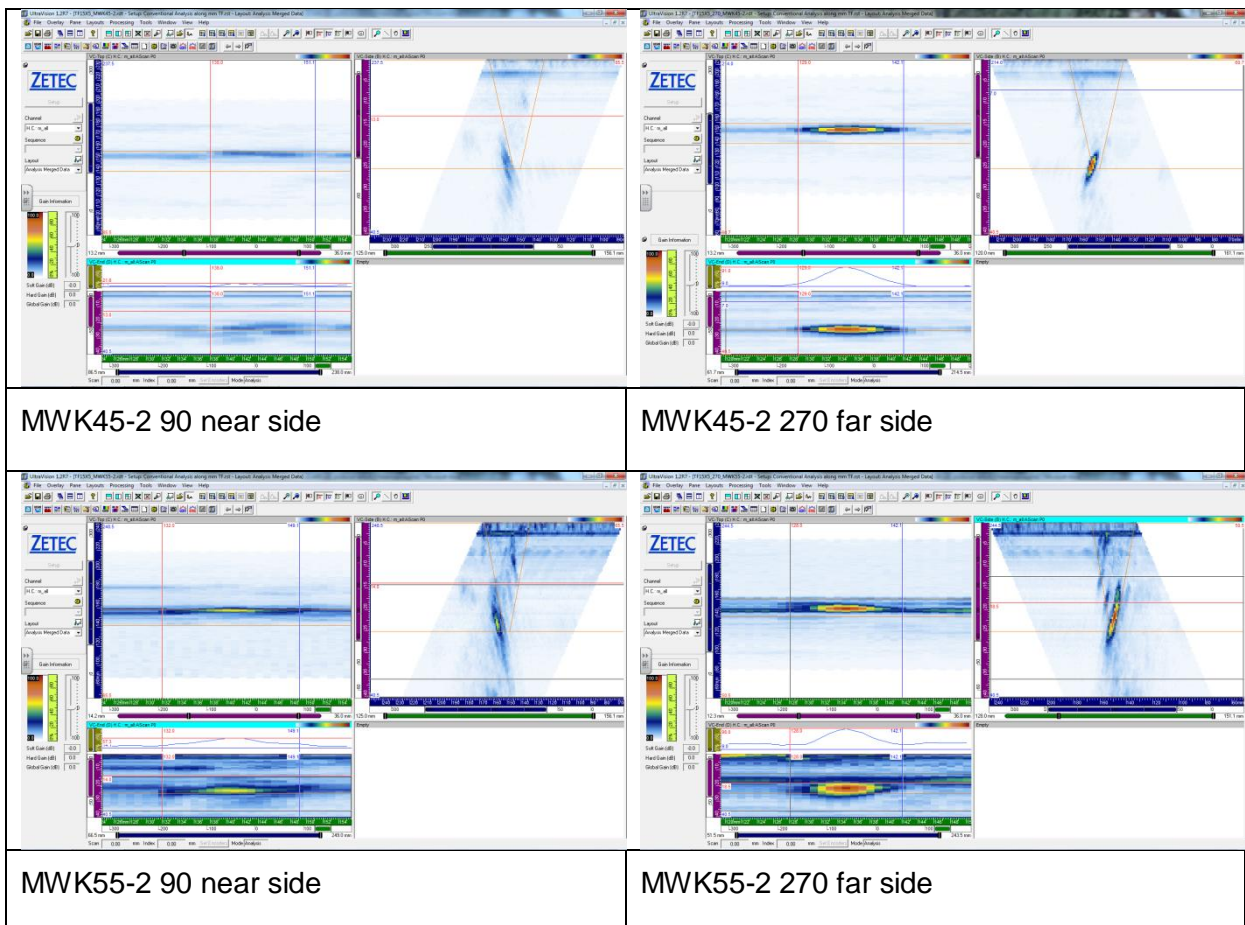


Figure 9. Screen captures of defect TF15X5 inspection with MWB probes.





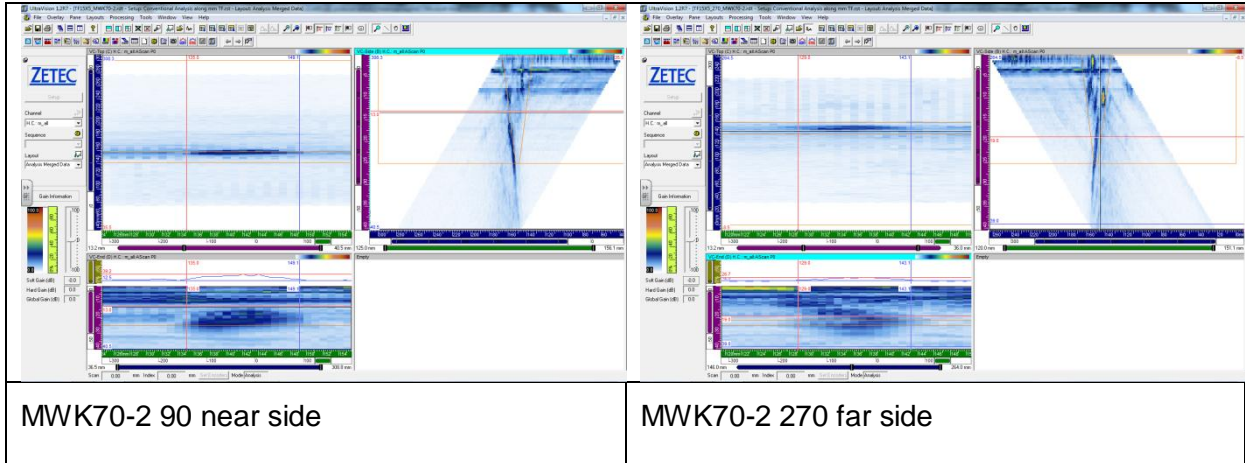
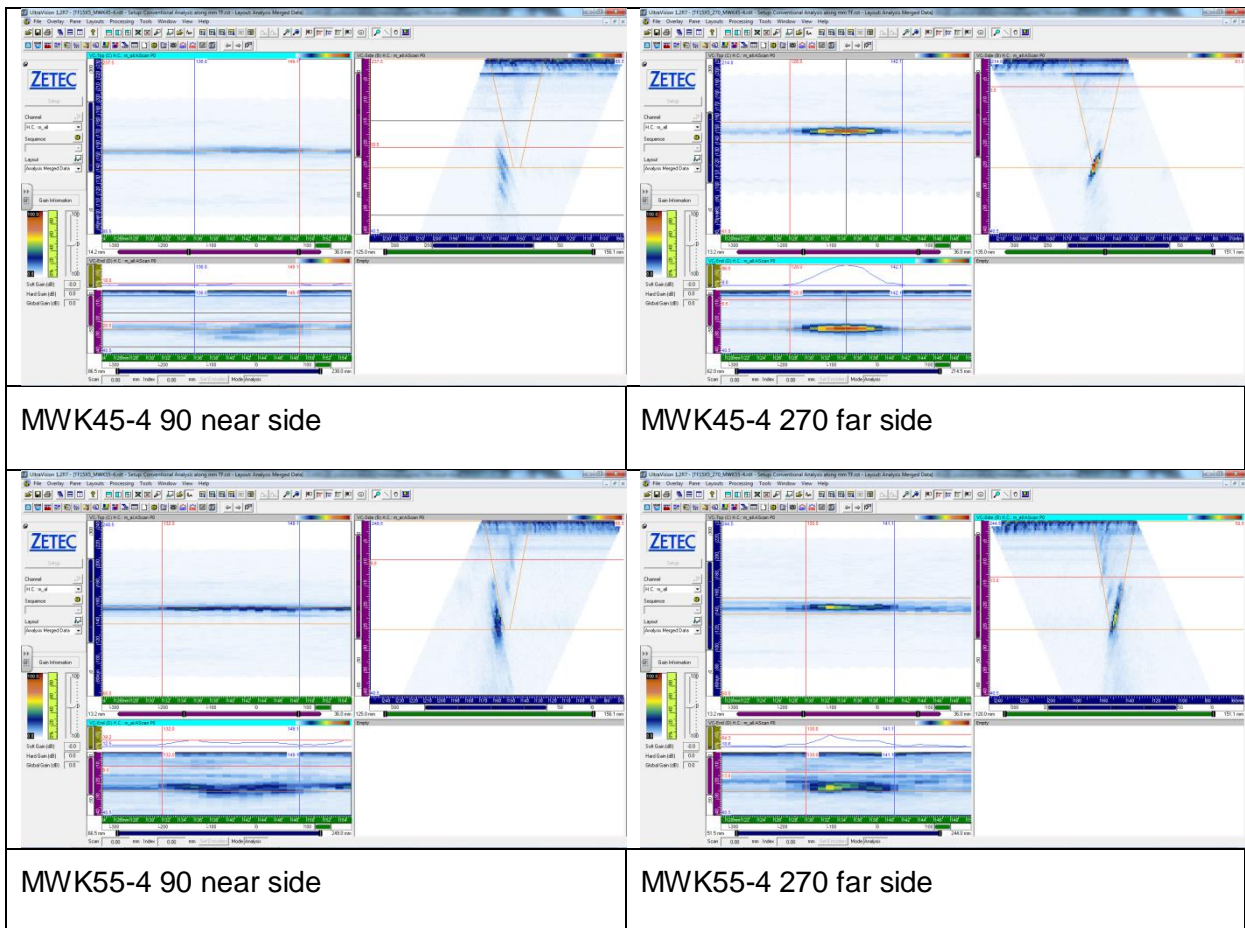


Figure 10. Screen captures of defect TF15X5 inspection with 2 MHz MWK probes.



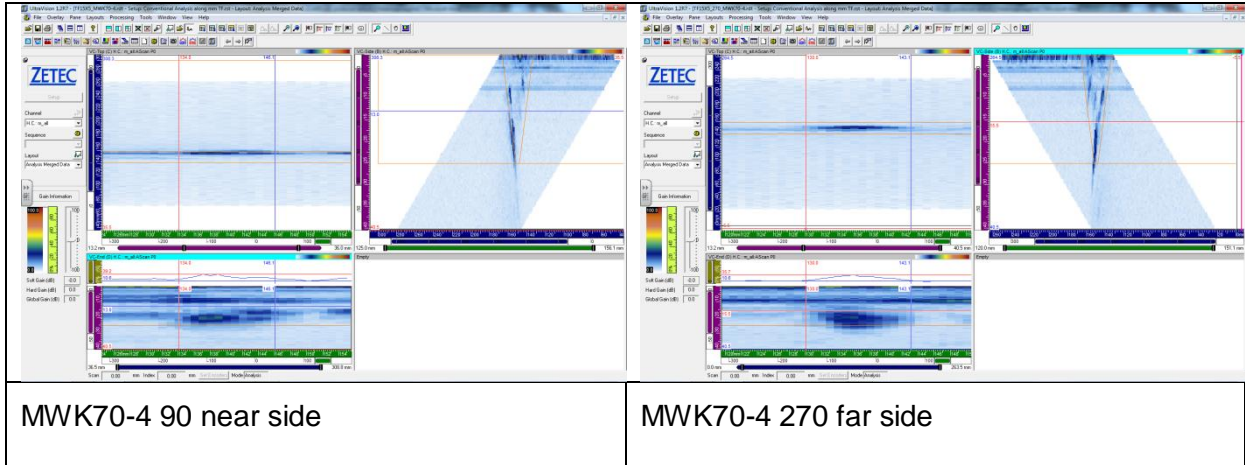
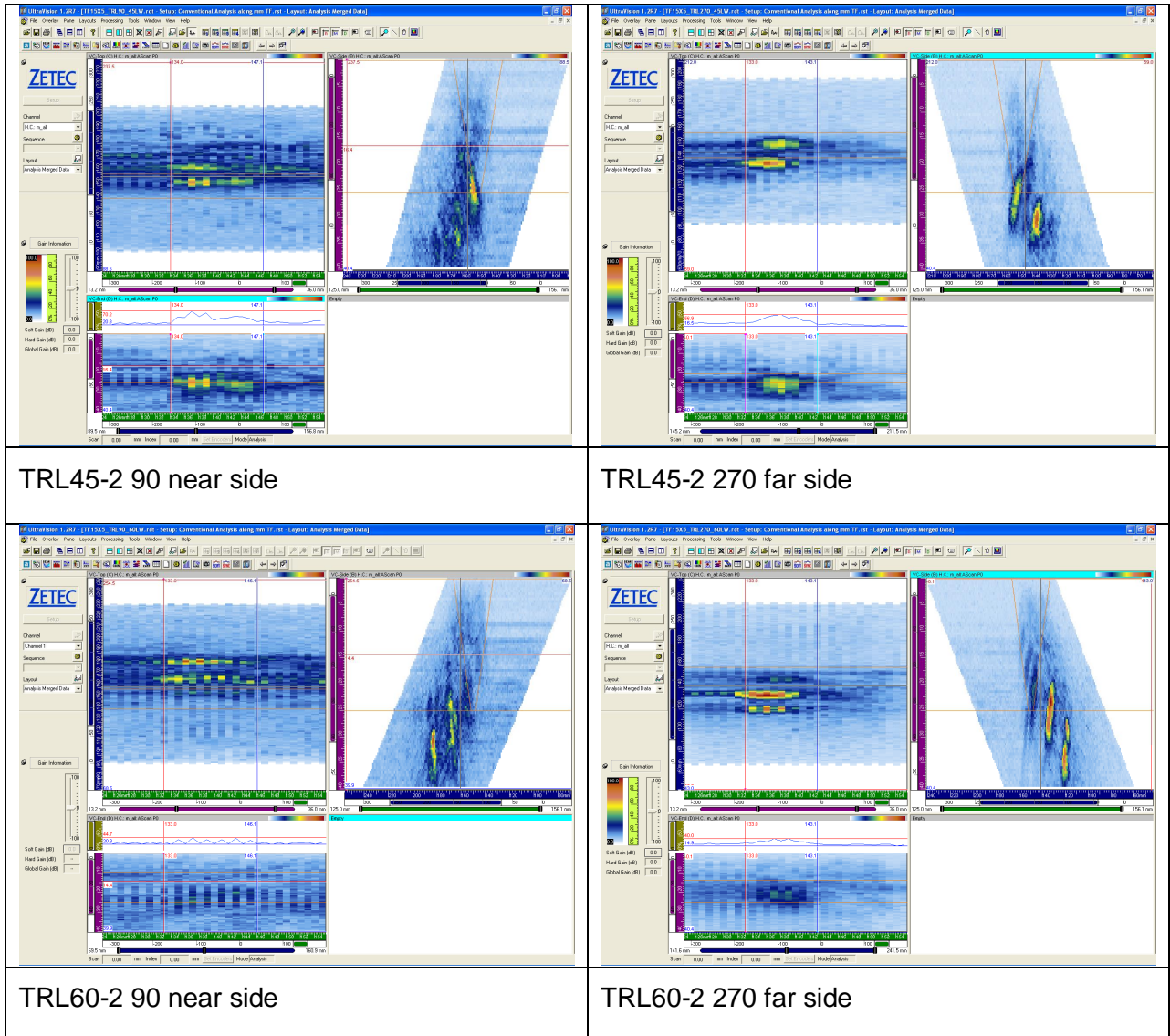


Figure 11. Screen captures of defect TF15X5 inspection with 4 MHz MWK probes.



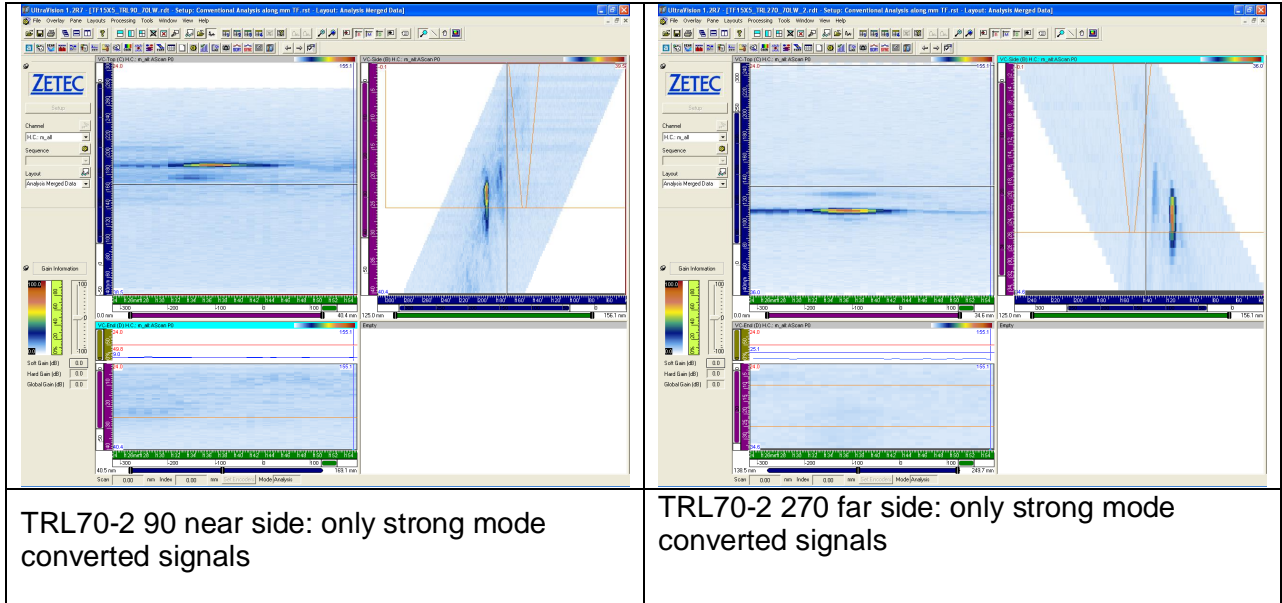


Figure 12. Screen captures of defect TF15X5 inspection with TRL probes.

## APPENDIX 2. PHASED ARRAY TESTING SCREEN CAPTURES

### A2.1 TECHNIQUE PA-1

#### A2.1.1 WELD MF

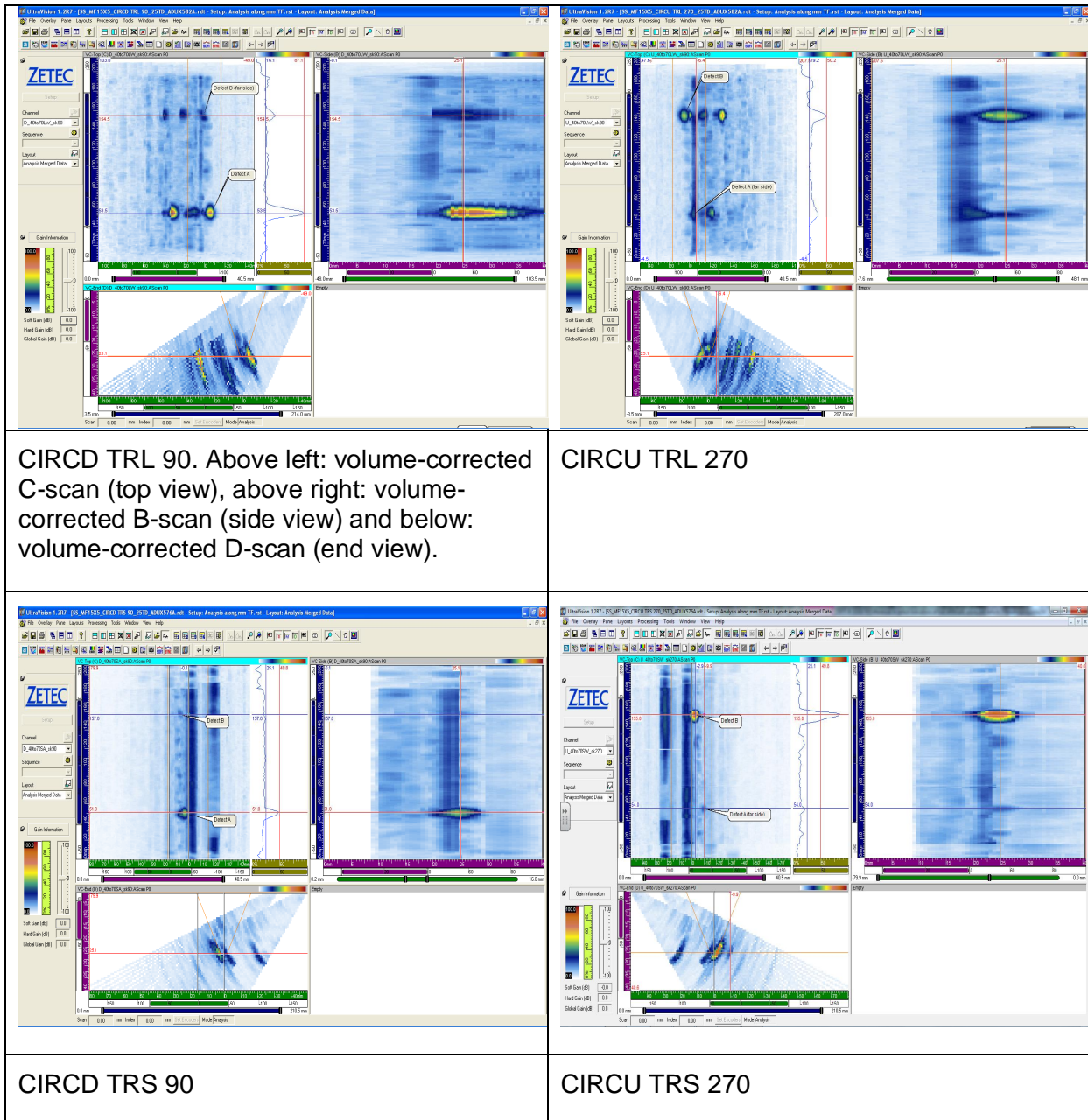


Figure 1. General views of weld MF scanned with technique PA-1.

## A2.1.2 MF15X5 DEFECT A

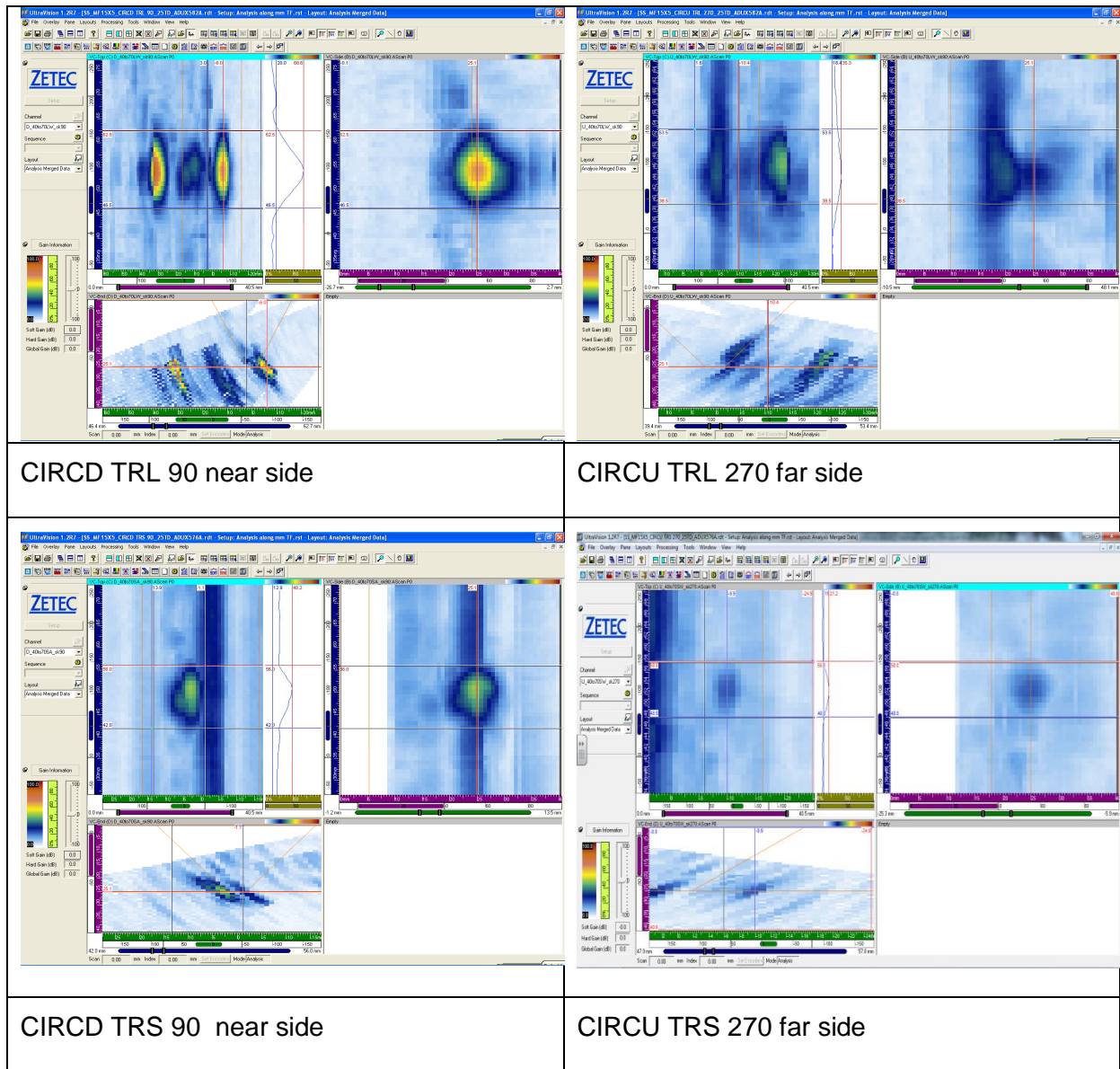


Figure 2. Screen captures of defect MF15X5 A inspected with technique PA-1.

### A2.1.3 MF15X5 DEFECT B

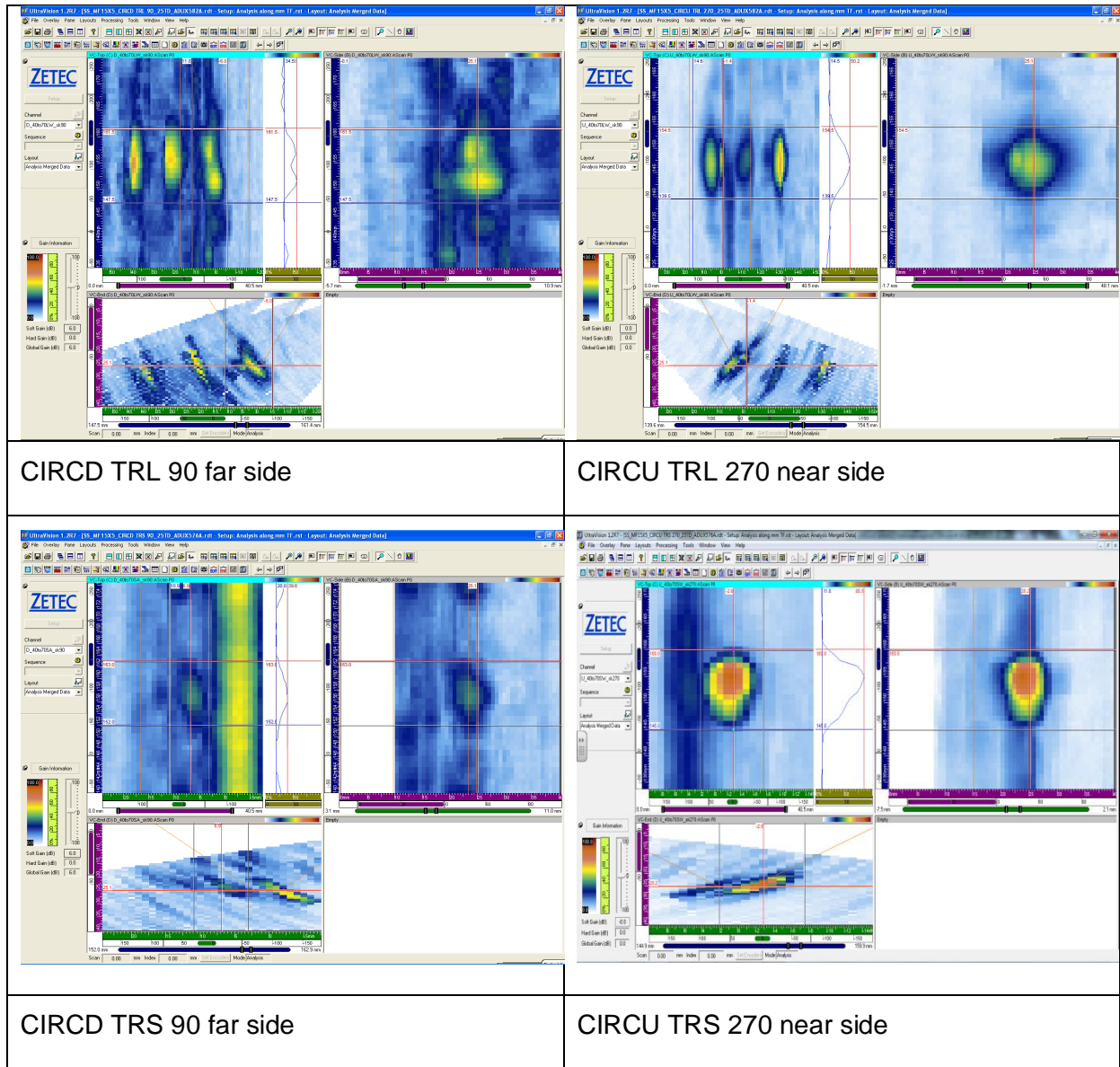


Figure 3. Screen captures of defect MF15X5 B inspected with technique PA-1.

## A2.1.4 WELDTF

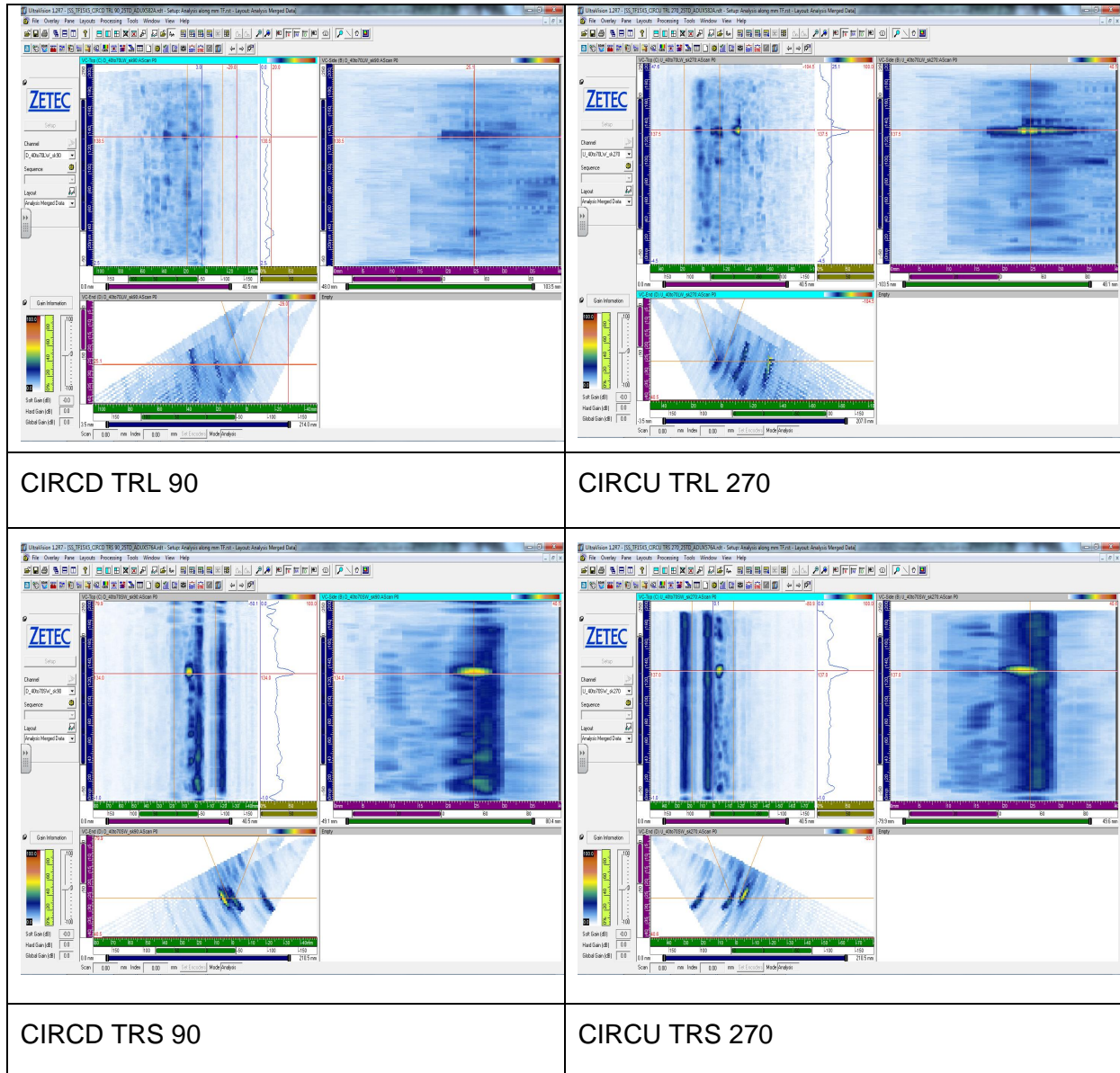


Figure 4. General views of weld MF scanned with technique PA-1.

## A2.1.5 DEFECT TF15X5

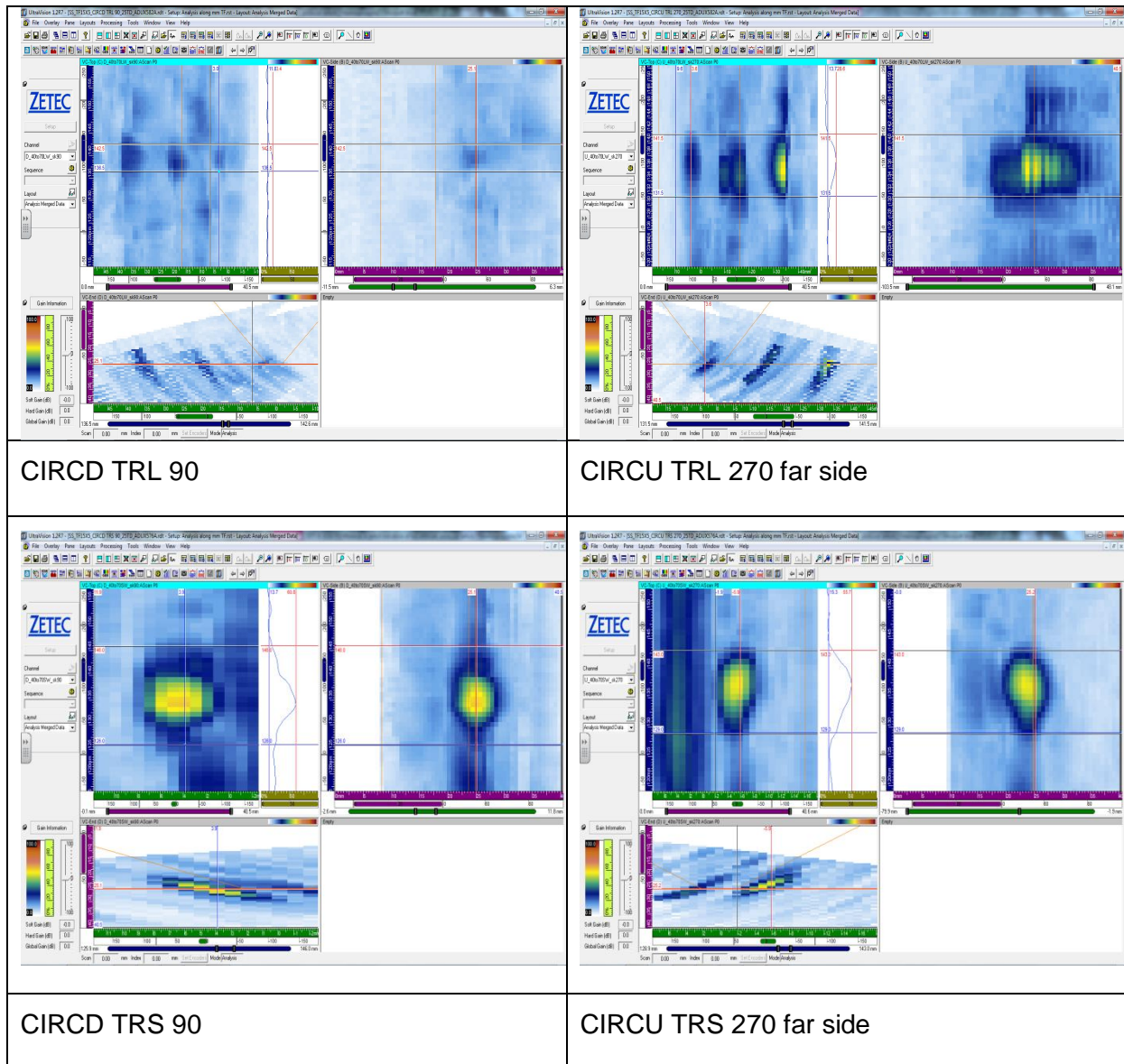


Figure 5. Screen captures of defect TF15X5 inspected with technique PA-1.



## A2.2 TECHNIQUE PA-2

### A2.2.1 WELD MF

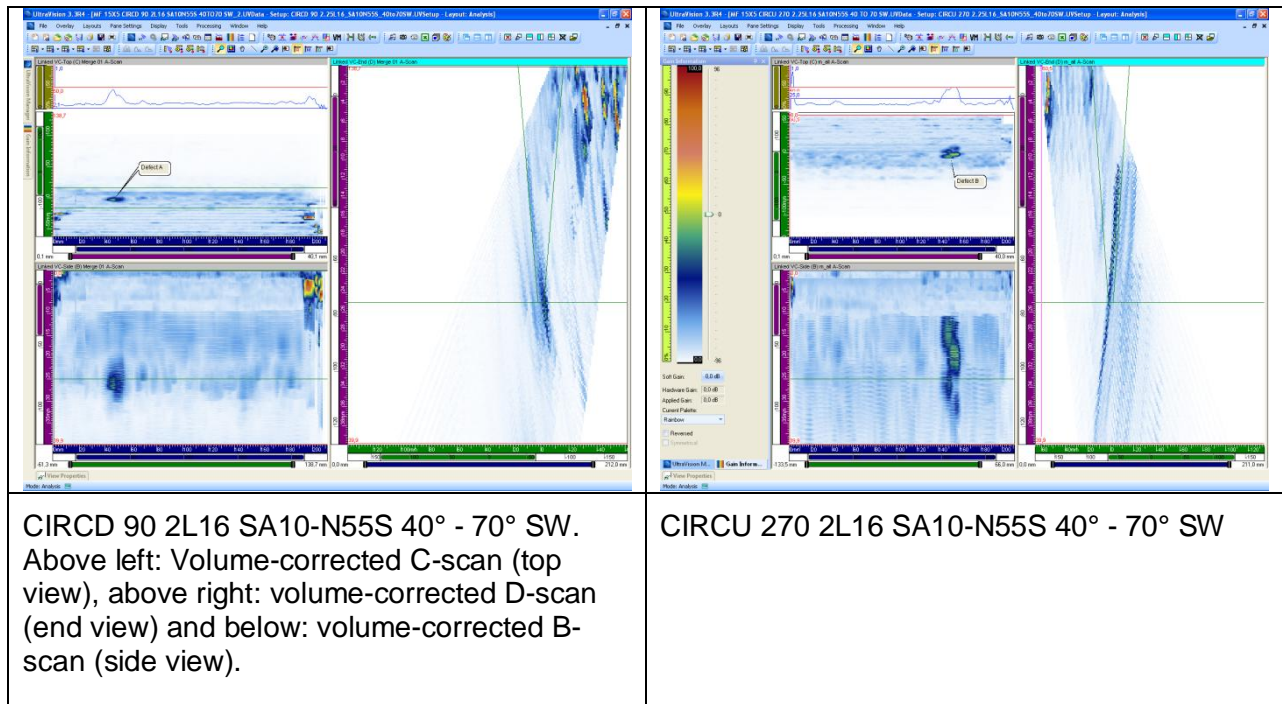


Figure 1. General views of weld MF scanned with technique PA-2 using 2 MHz probe.

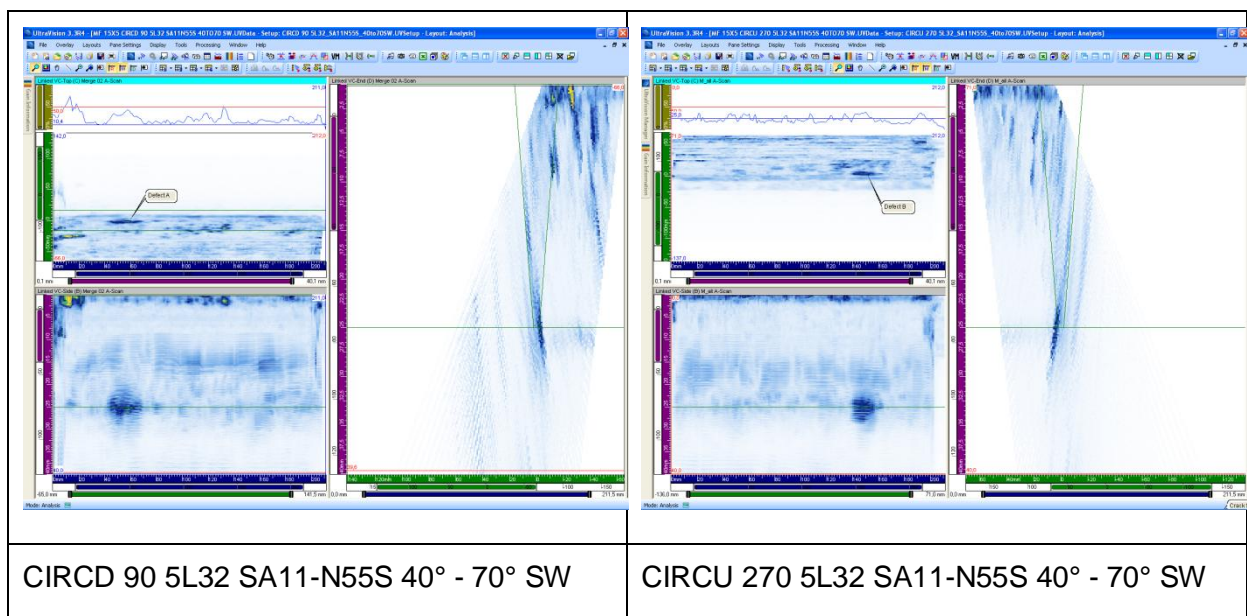


Figure 2. General views of weld MF scanned with technique PA-2 using 5 MHz probe.

## A2.2.2 MF15X5 DEFECT A

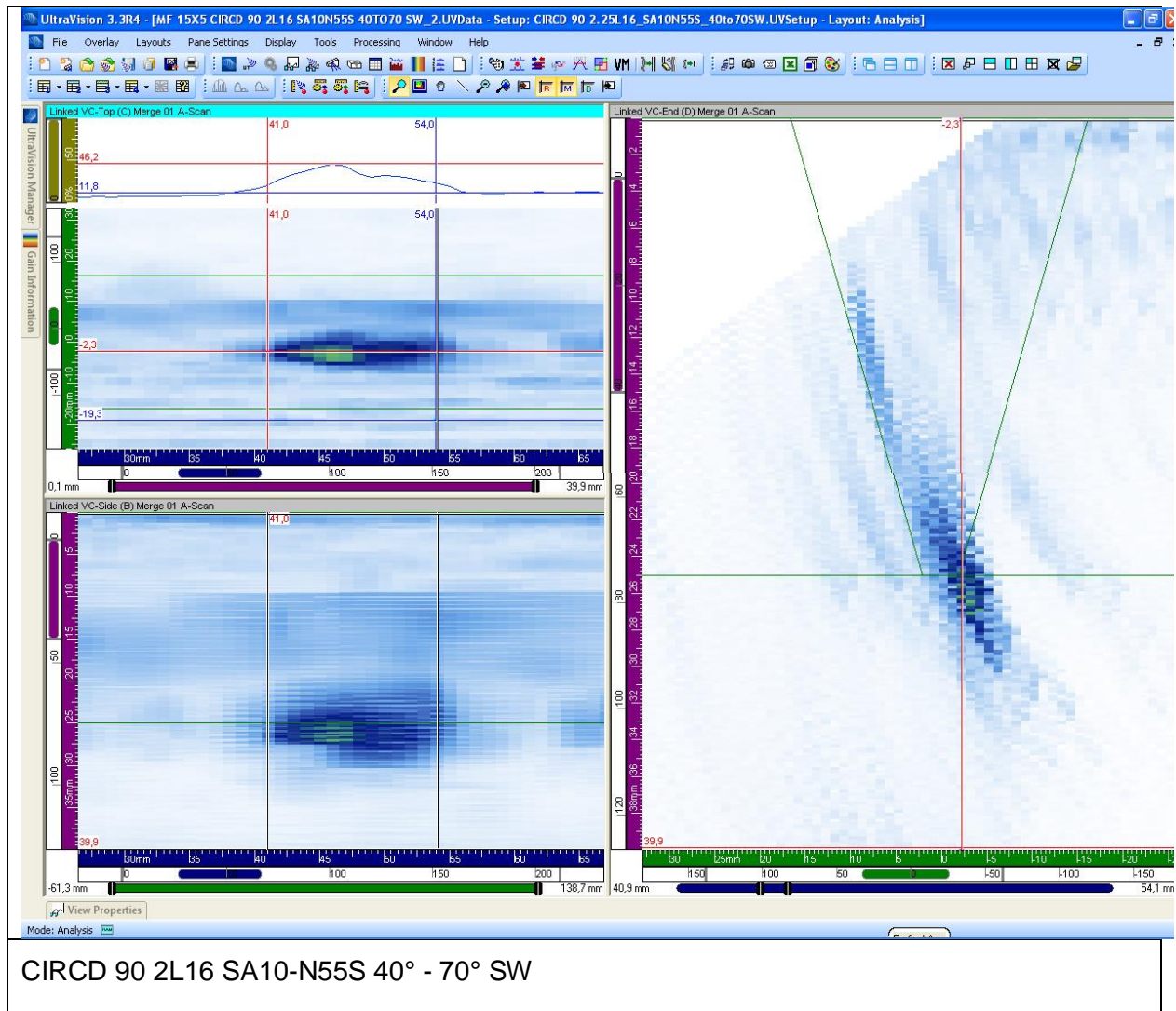


Figure 3. Screen capture of defect MF15X5A scanned with technique PA-2 using 2 MHz probe. Defect was detected only from near side.

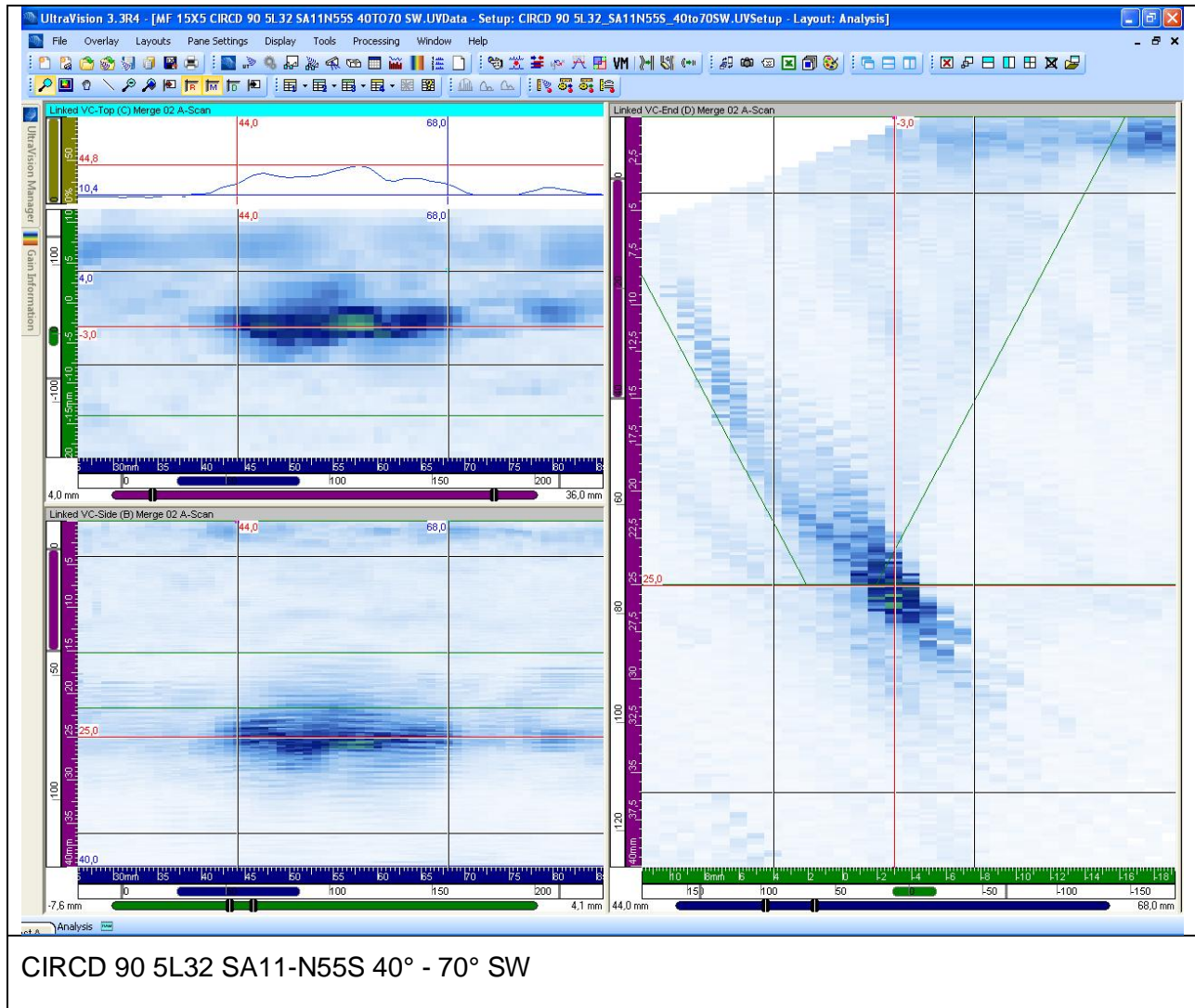


Figure 4. Screen capture of defect MF15X5A scanned with technique PA-2 using 5 MHz probe. Defect was detected only from near side.

### A2.2.3 MF15X5 DEFECT B

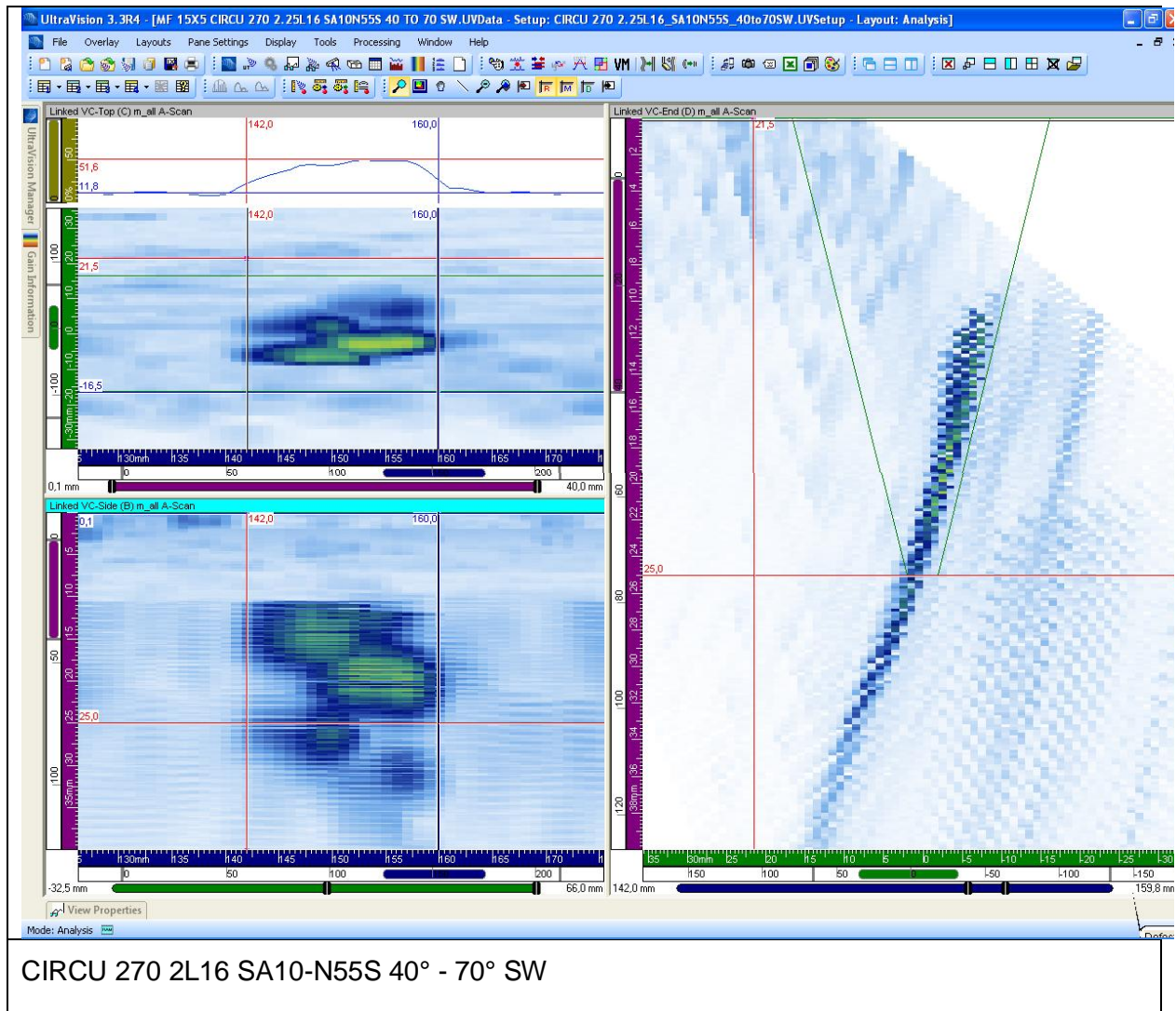


Figure 5. Screen capture of defect MF15X5B scanned with technique PA-2 using 2 MHz probe. Defect was detected only from near side.

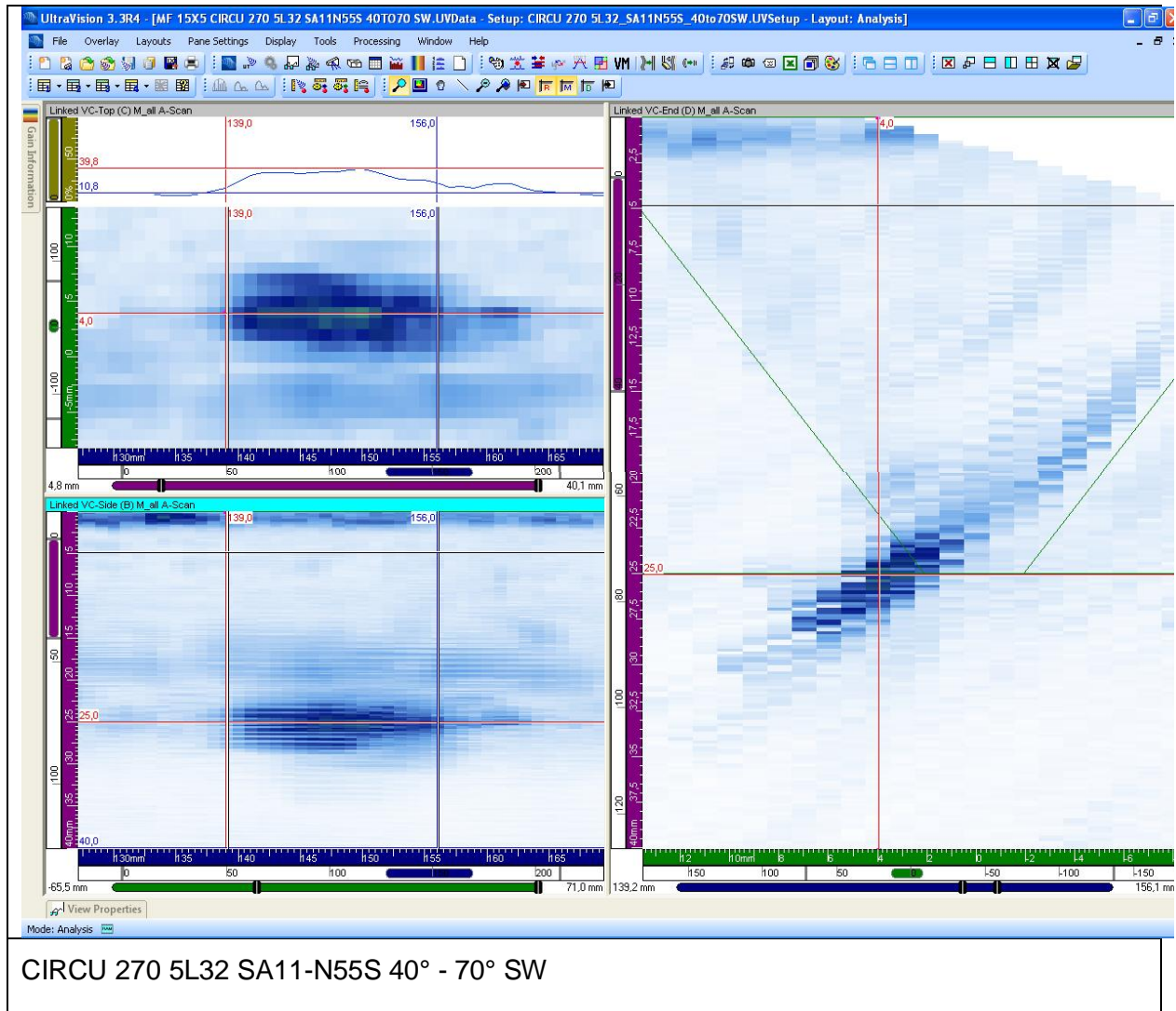


Figure 6. Screen capture of defect MF15X5B scanned with technique PA-2 using 5 MHz probe. Defect was detected only from near side.

## A2.2.4 WELD TF

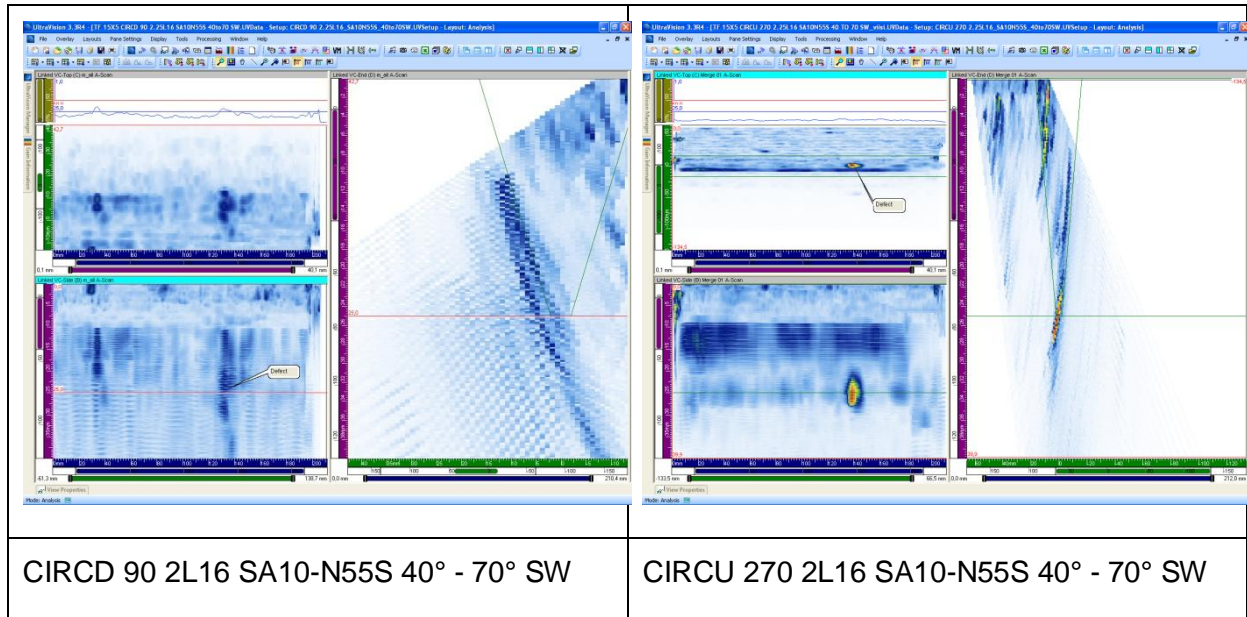


Figure 7. General views of weld TF scanned with technique PA-2 using 2 MHz probe.

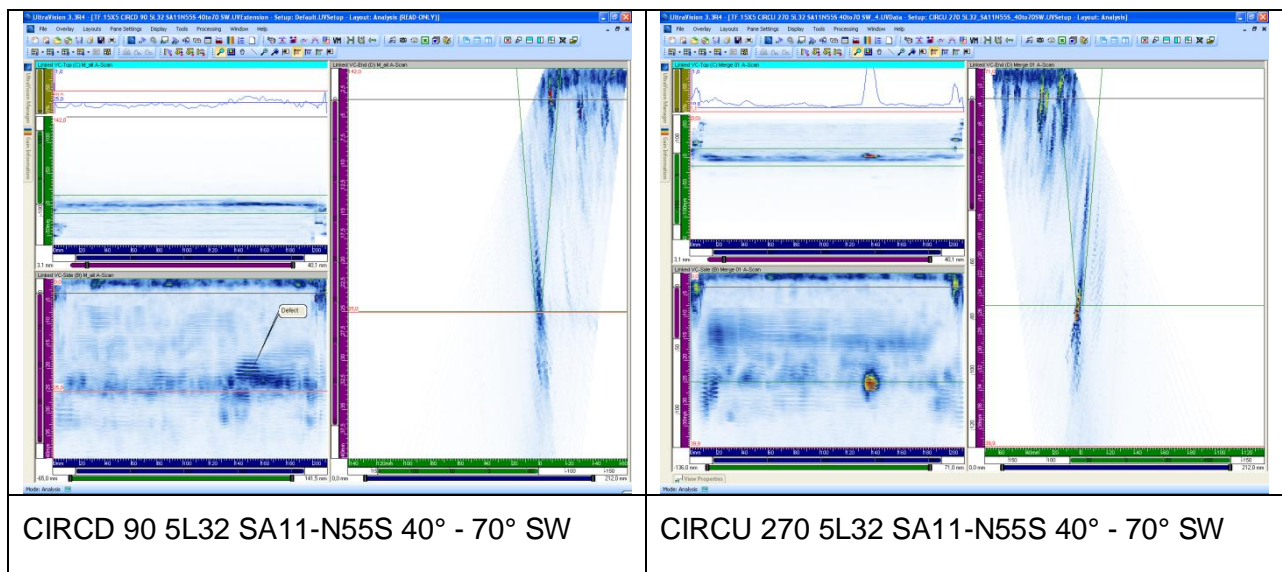


Figure 8. General views of weld TF scanned with technique PA-2 using 5 MHz probe.

## A2.2.5 DEFECT TF15X5

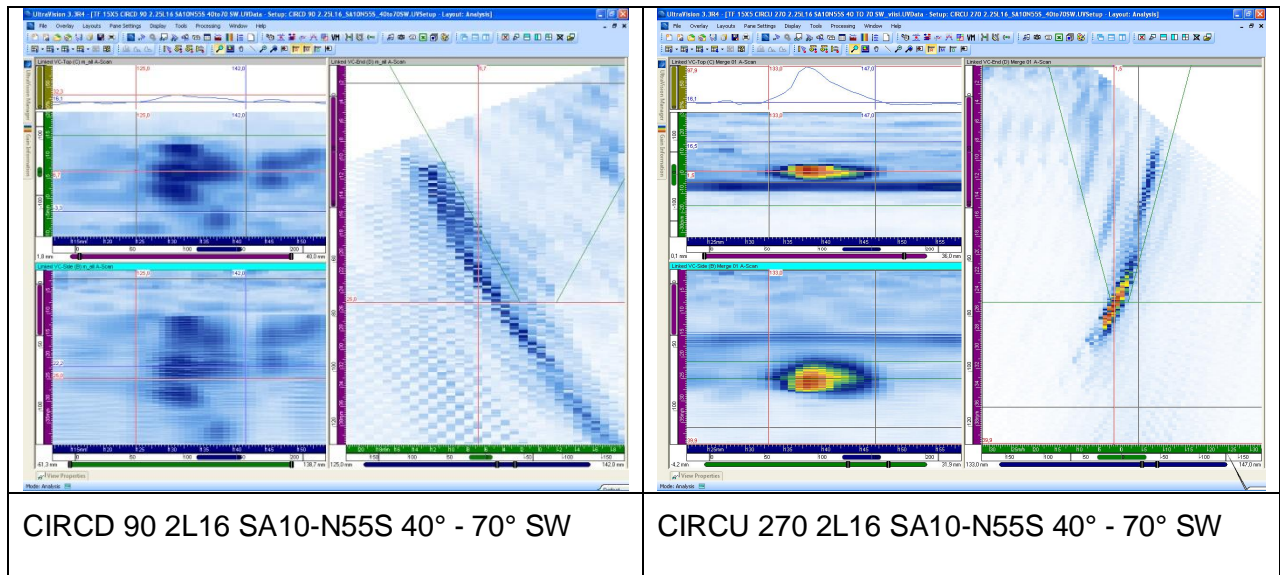


Figure 9. Screen captures of defect TF15X5 scanned with technique PA-2 using 2 MHz probe.

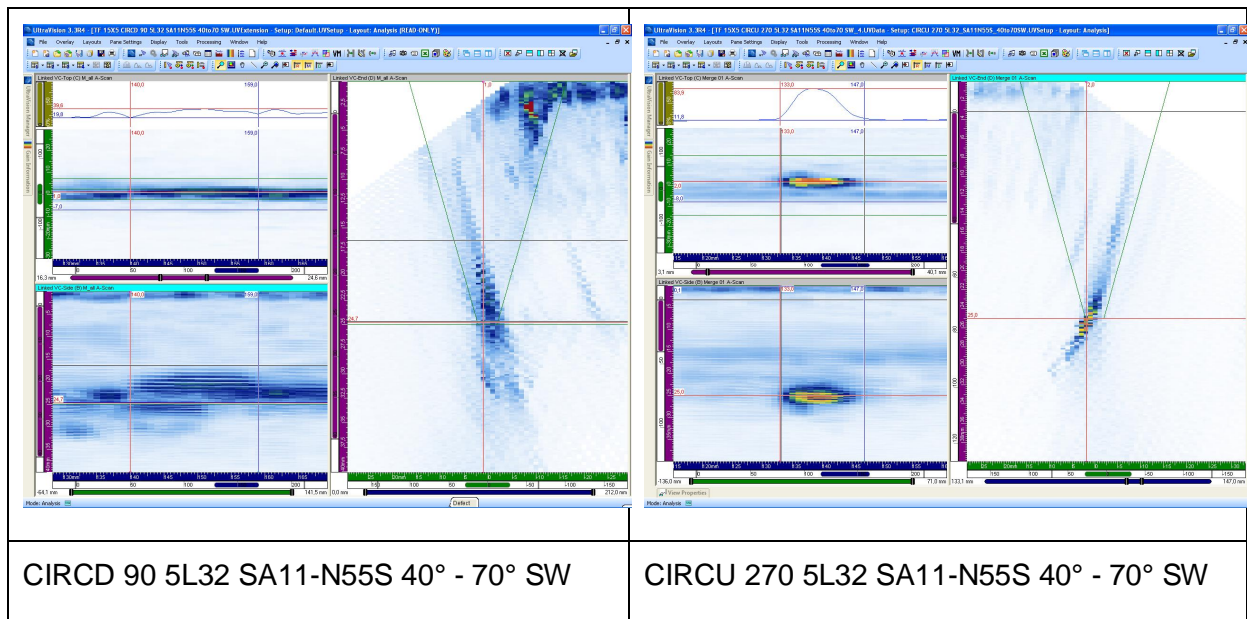


Figure 10. Screen captures of defect TF15X5 scanned with technique PA-2 using 5 MHz probe.

## A2.3 TECHNIQUE PA-3

### A2.3.1 WELD MF

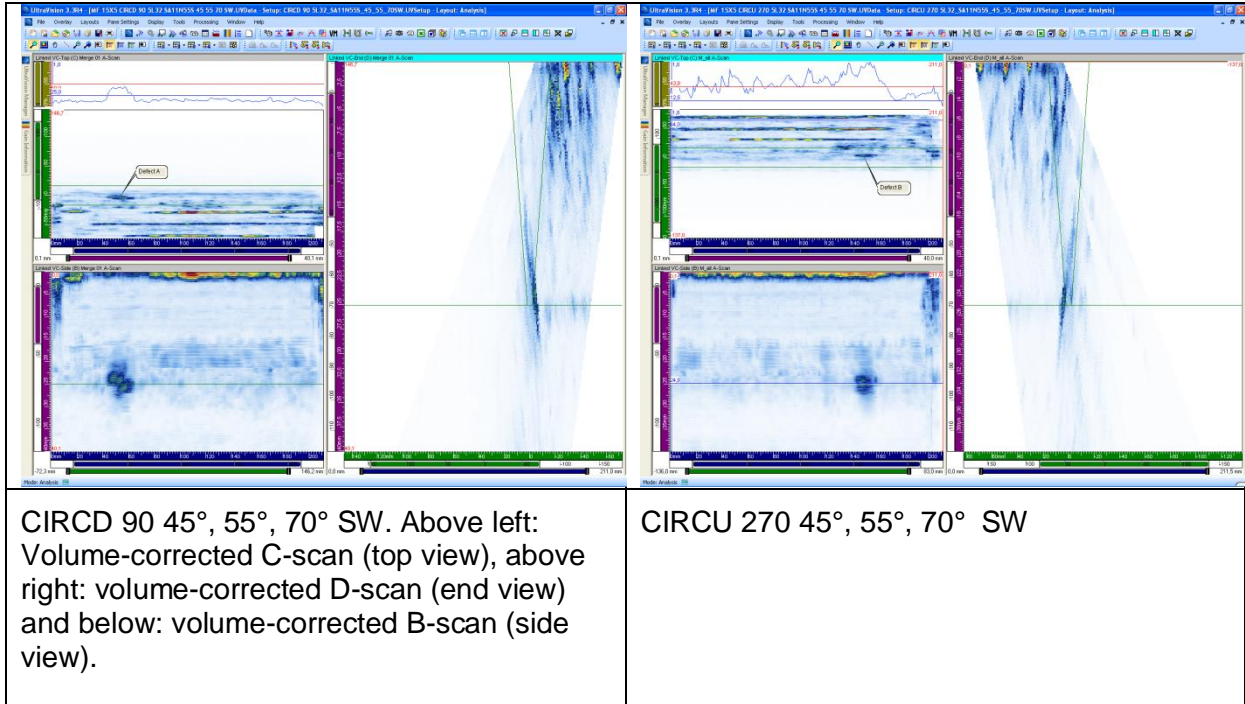
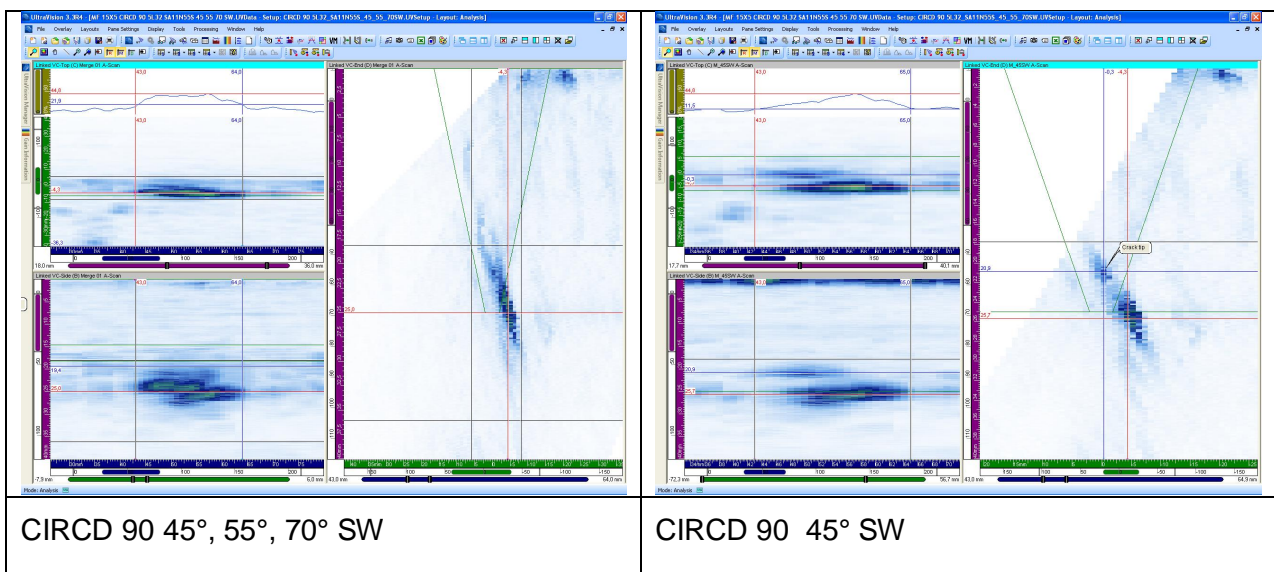


Figure 11. General views of weld MF scanned with technique PA-3.

### A2.3.2 MF15X5 DEFECT A





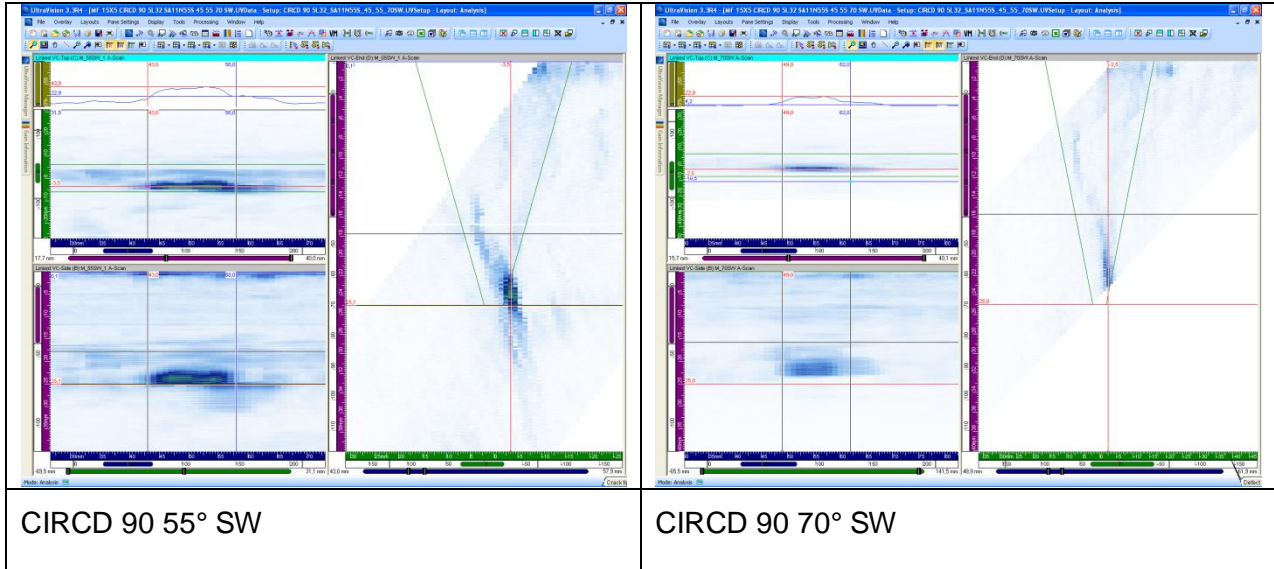
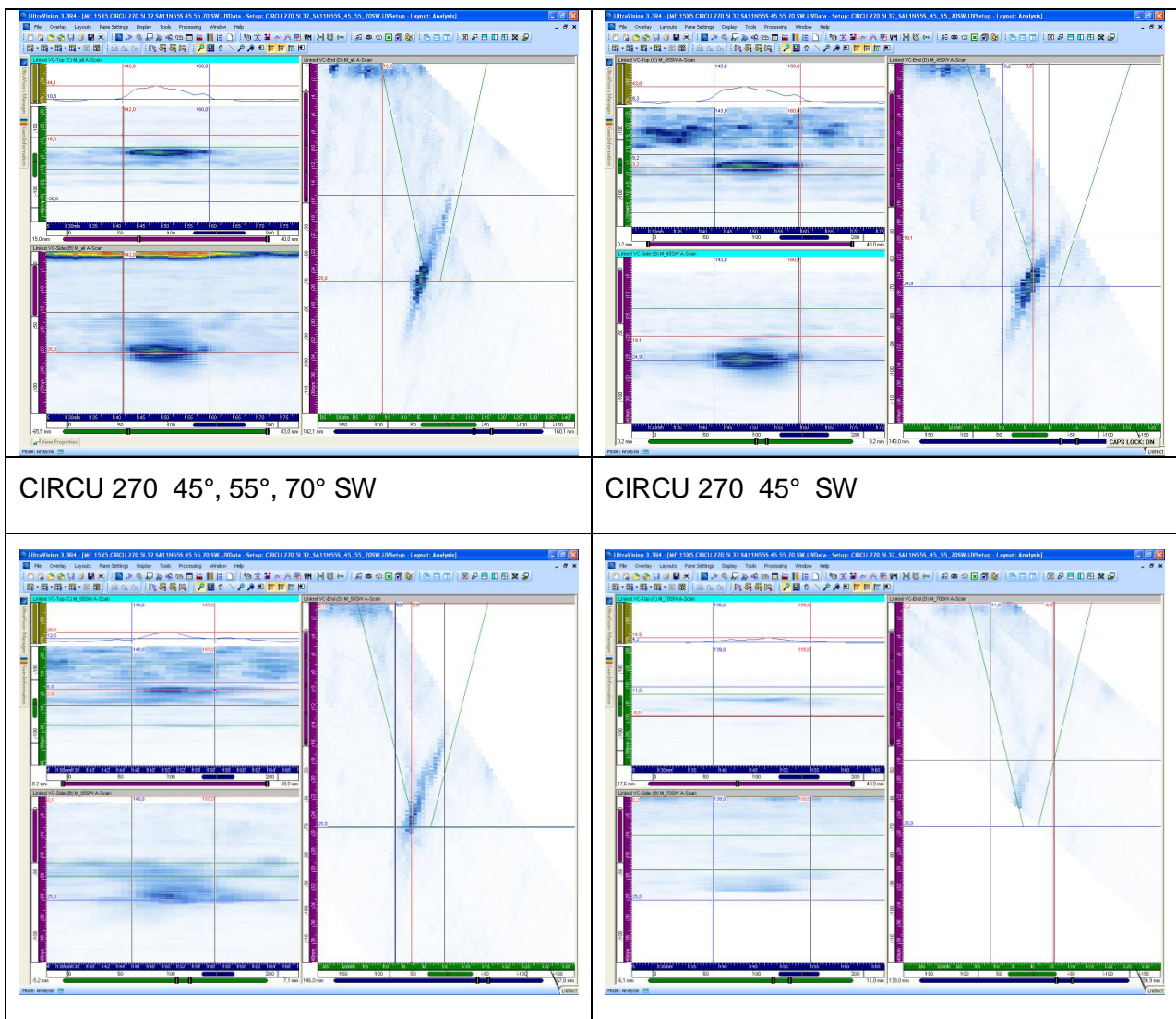


Figure 12. Screen captures of defect MF15X5A scanned with technique PA-3.

### A2.3.3 MF15X5 DEFECT B



CIRCU 270 55° SW	CIRCU 270 70° SW
------------------	------------------

Figure 13. Screen captures of defect MF15X5B scanned with technique PA-3.

### A2.3.4 WELD TF

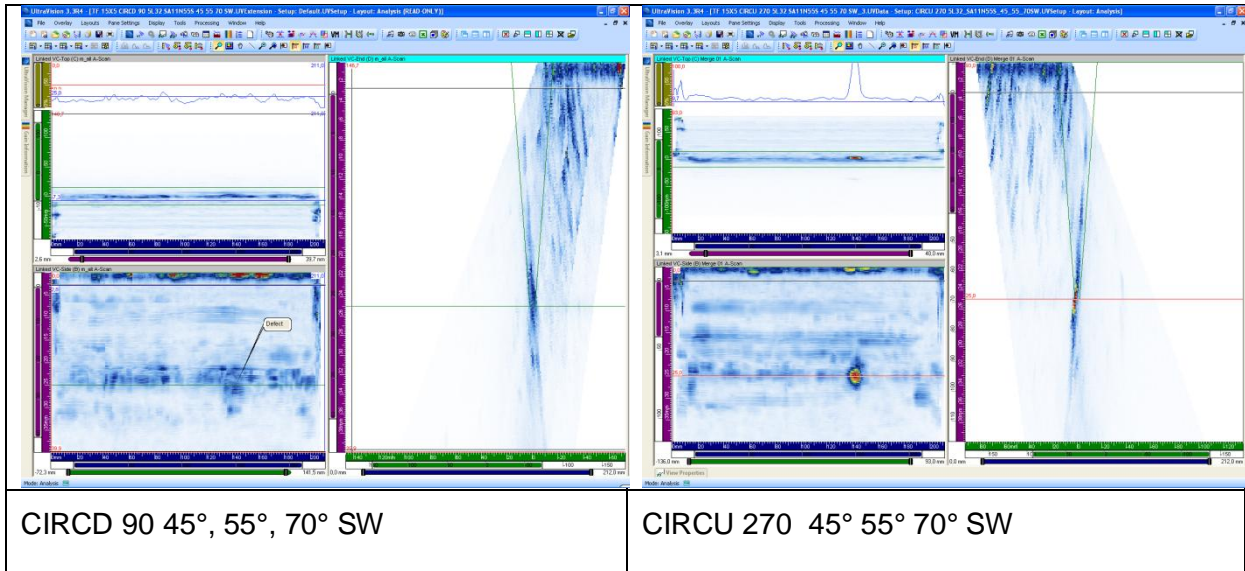
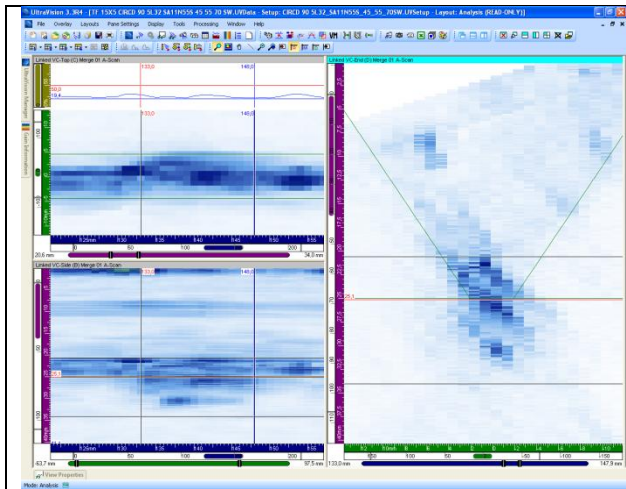
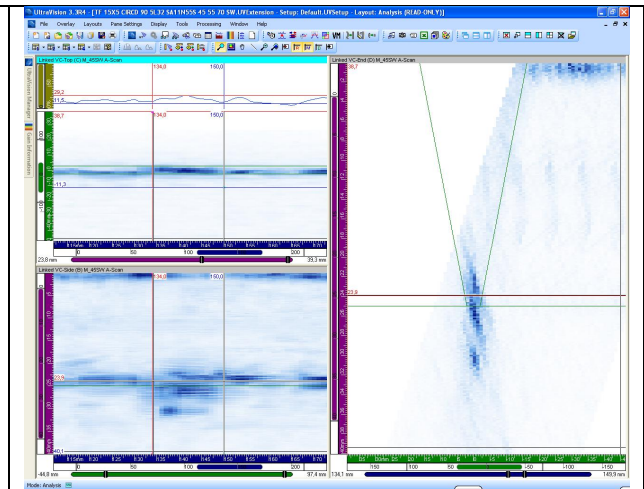


Figure 14. General views of weld TF scanned with technique PA-3.

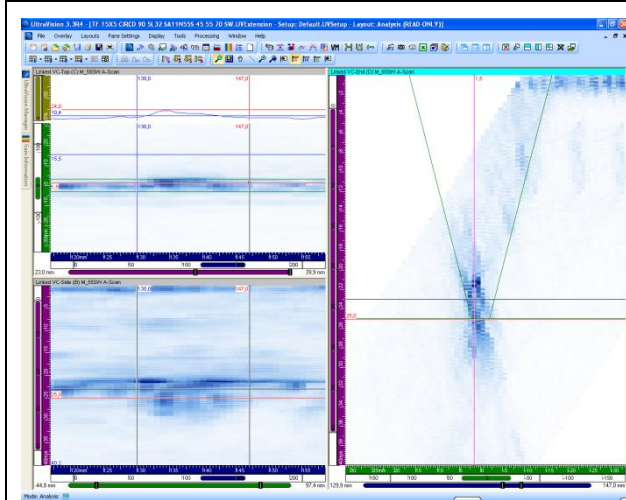
### A2.3.5 DEFECT TF 15X5



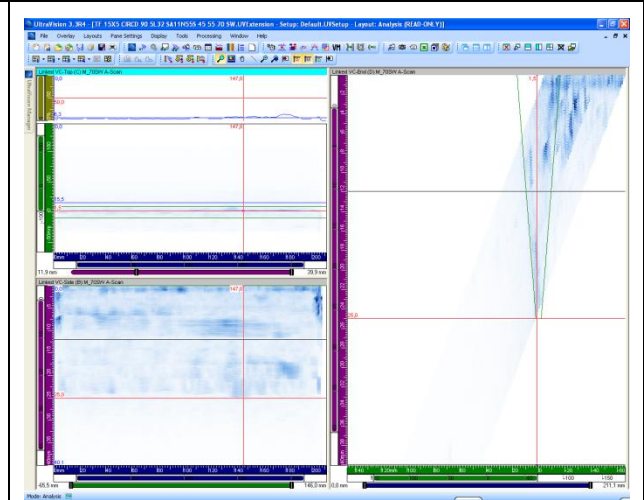
CIRCD 90 45°, 55°, 70° SW



CIRCD 90 45° SW



CIRCD 90 55° SW



CIRCD 90 70° SW: no detection

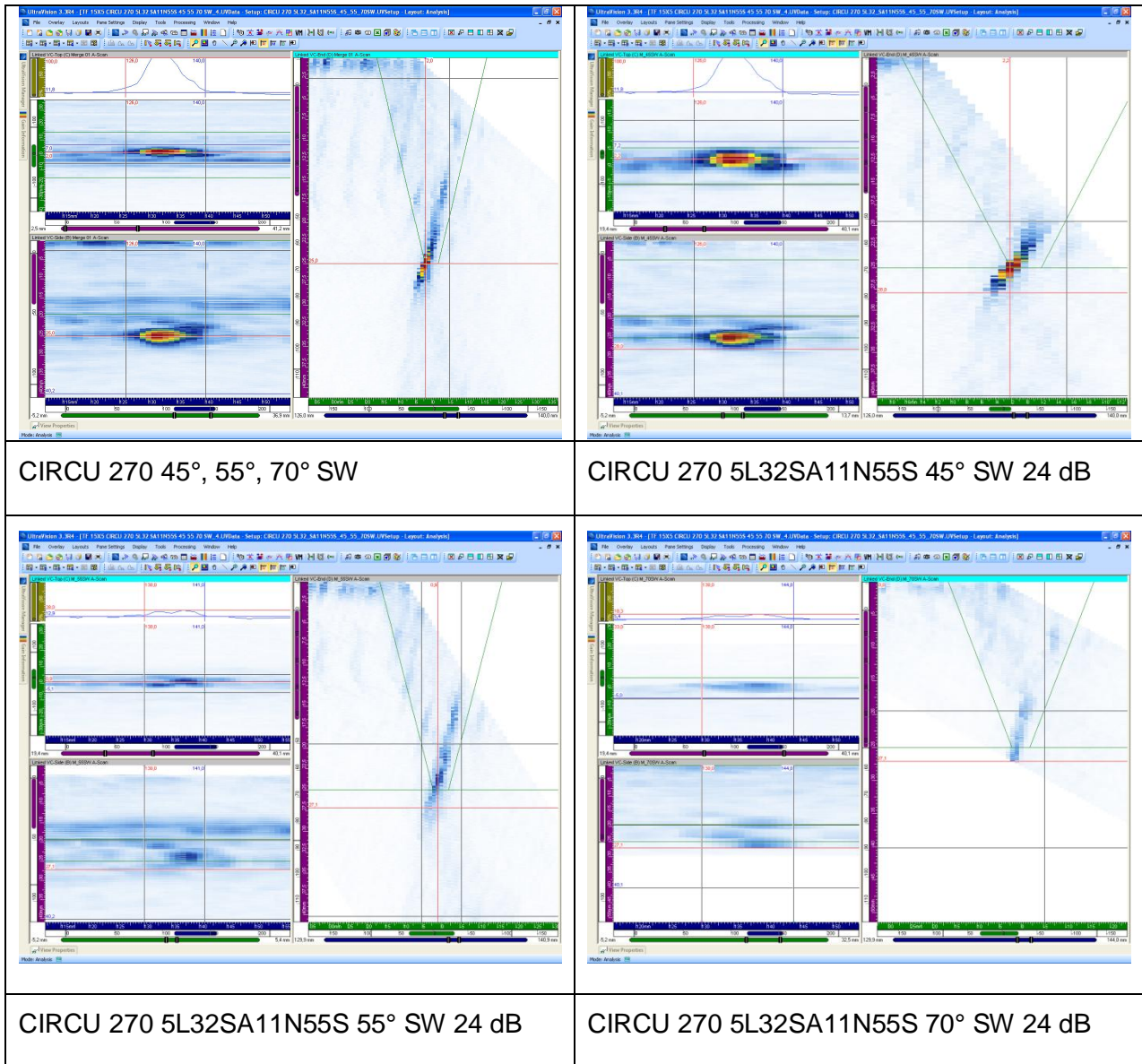


Figure 15. Screen captures of defect TF15X5 scanned with technique PA-3.

## A2.4 TECHNIQUE PA-4

### A2.4.1 WELD MF

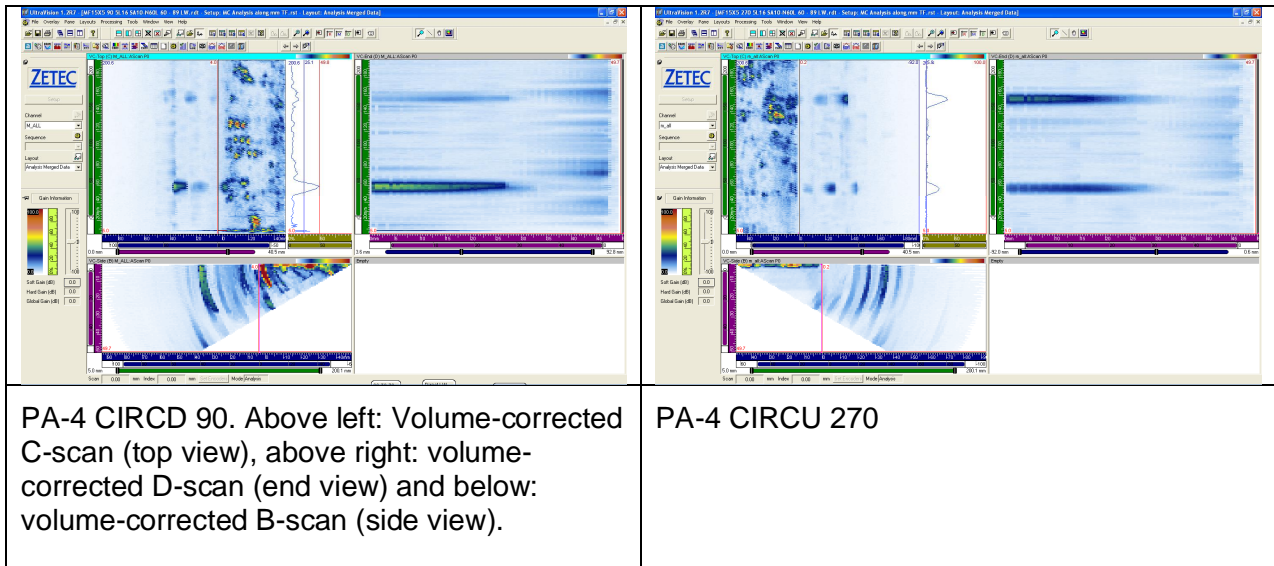


Figure 16. General views of weld TF scanned with technique PA-4.

### A2.4.2 MF15X5 DEFECT A

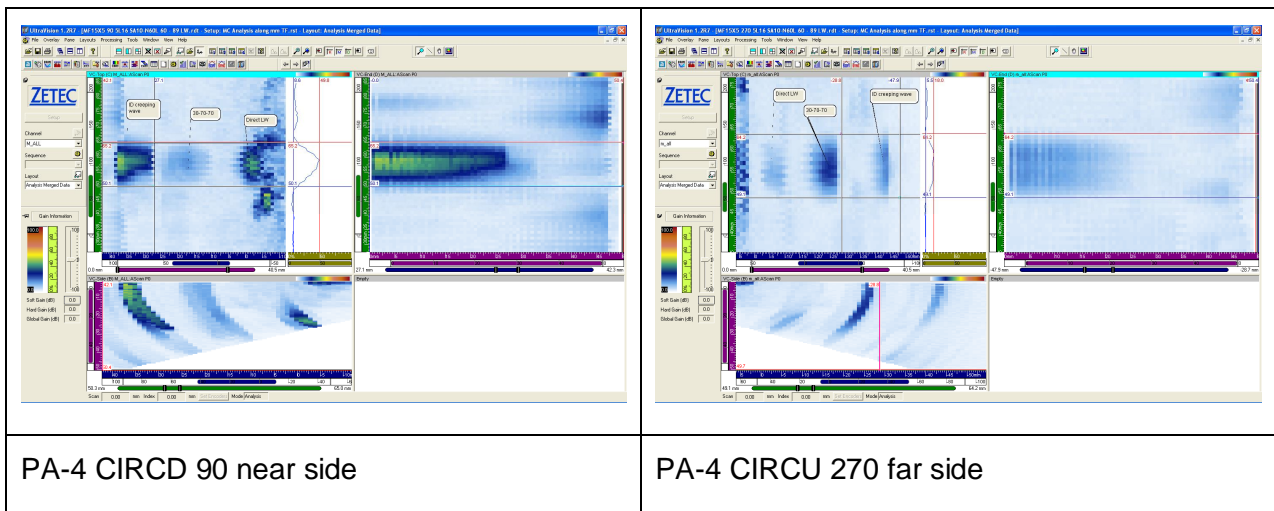


Figure 17. Screen captures of defect MF15X5A scanned with technique PA-4.

### A2.4.3 MF15X5 DEFECT B

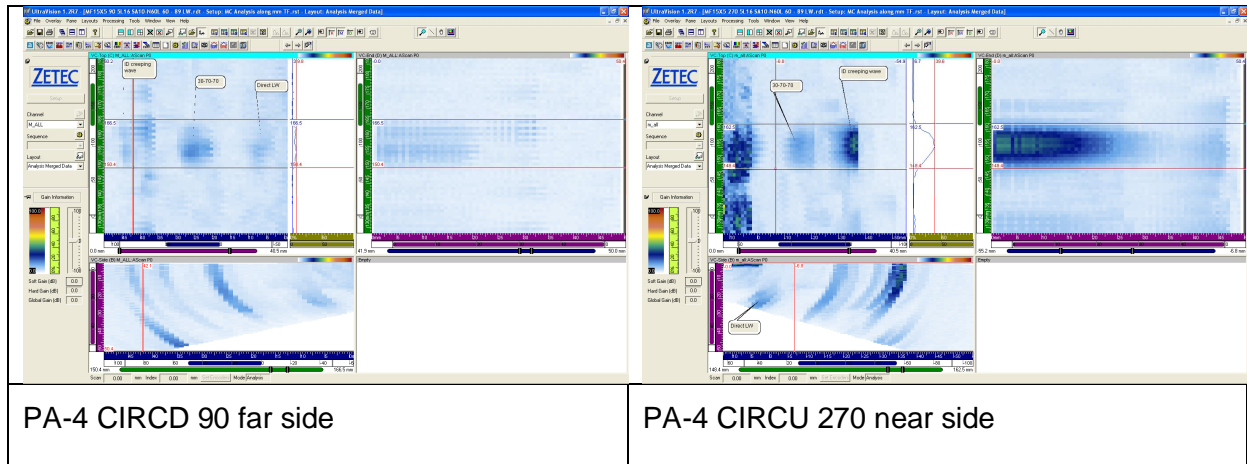


Figure 18. Screen captures of defect MF15X5B scanned with technique PA-4.

### A2.4.4 WELD TF

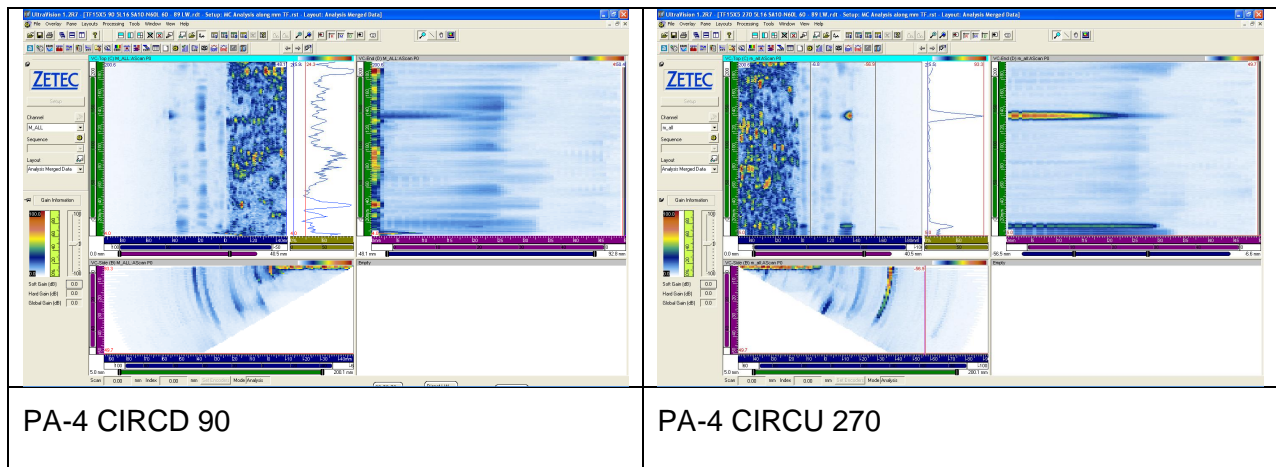


Figure 19. General views of weld TF scanned with technique PA-4.

## A2.4.5 TF15X5

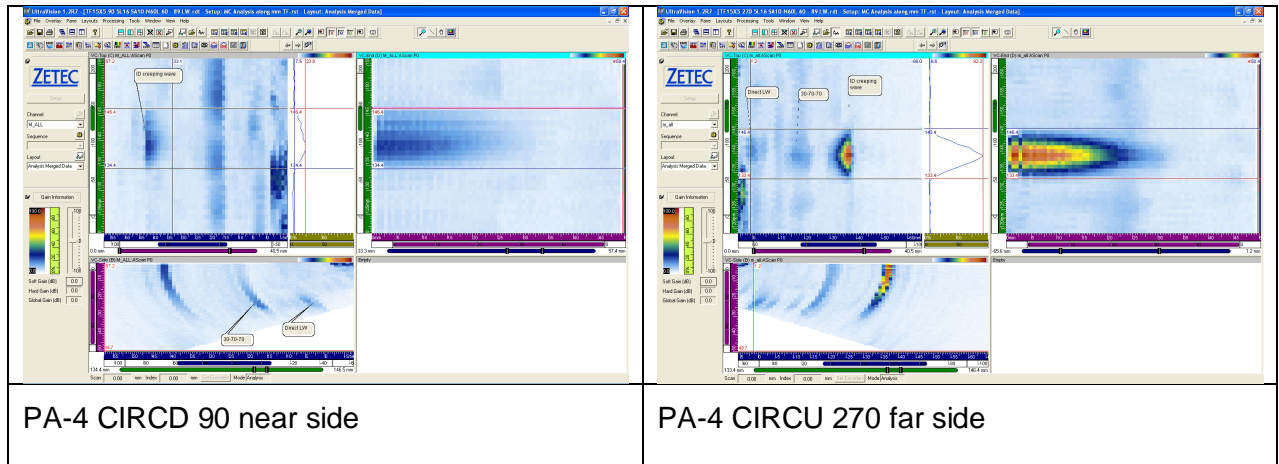


Figure 20. Screen captures of defect TF15X5 scanned with technique PA-4.